Thijs van Herwerden

Fatigue life prediction of composite marine propellers

Master of Science Thesis
March 2023

TU Delft

FATIGUE LIFE PREDICTION OF COMPOSITE MARINE PROPELLERS

by

Thijs VAN HERWERDEN

to obtain the degree of Master of Science in Marine Technology
at the Delft University of Technology,
to be defended publicly on Wednesday March 29, 2023 at 10:00 AM.

Thesis committee:	Prof. dr. ir. C. Kassapoglou,	TU Delft, supervisor
	Dr. ir. P. L. Pahlavan,	TU Delft, supervisor (Comittee chair)
	Dr. ir. J. H. Den Besten,	TU Delft
	Ir. A. J. Huijer,	TU Delft, supervisor
Student number:	4303296	

This thesis MT.22/23.029.M is classified as confidential in accordance with the general conditions for projects performed by the TUDelft.

An electronic version of this thesis is available at http://repository.tudelft.nl/.

TU Delft

CONTENTS

SUMMARY

Fiber reinforced composites have been increasingly used in the aerospace and automotive industry, due to their potential advantages for designing flexible, strong and lightweight structures. More recently they are also being considered for the manufacturing of marine propellers. Since they have the potential to lower the weight, lower the maintenance costs, increase the efficiency at off-design conditions, improve cavitation inception speed and minimize acoustic signatures. Exploiting the full potential of composite propellers however requires that they need to be cost-effective and to do so it is required that the lifetime of the blade is sufficient. To determine the lifetime of the blade it is crucial to determine how the composite blade will respond to a wide variety of environmental and loading conditions that it will experience over its life. Basically one needs to determine what effects fatigue will have on the material properties of the blade.

The main objective of this thesis is to estimate the fatigue lifetime of composite marine propellers subjected to a pressure distribution determined by a Fluid-Structure Interaction (FSI) model with the use of a progressive damage model integrated into a Finite Element Model (FEM). The fluid structure interaction model to determine the pressure distribution has already been created Maljaars (2019). Currently the mostly used and most reliable approach is to use an experimental approach in order to estimate the fatigue life. However, for custom designs such as marine propellers this is a long and costly process. Modelling fatigue the fatigue performance in an earlier stage of the design cycle will result in significant cost and time savings.

A carbon-epoxy composite propeller motivated by the Greenprop propeller design has been considered in this research. The fatigue lifetime of the composite marine propeller is estimated using a progressive damage model integrated into a FEM that determines the loss in strength and stiffness properties as a function of the applied stress and cycles. Where propeller failure is defined as when the structure is no longer capable of carrying the pressure load or when the propeller deflection is greater than the maximum allowed. It was chosen to use a progressive damage model that is a continuum damage model to achieve high resolution in modelling the distributed damage process without the need for computationally expensive micro-mechanics models that focus on each individual defect. The progressive damage model is integrated into the FEM environment using a set of user subroutines to run the code efficiently. The progressive damage model includes:

1. A fatigue life model that uses a strain energy density based fatigue criterion. The model is used to estimate the fatigue life of each individual ply.

2. A Hashin failure criteria to indicate if a ply has failed and what type of failure has occurred.

3. An immediate degradation model reduces the material properties suddenly in the case where one or more failure criteria are triggered.

4. A gradual degradation model that describes the degradation of the materials in prior to the failure of the ply indicated by the failure criteria.

The validation study has indicated that the progressive damage model gives mostly conservative results, however it also indicates that for an increasing number of cycles the sensitivity of the model with respect to the fatigue life parameters is increased. This indicates that for high fatigue cycle ranges it is more important to carefully determine these parameters. The expected fatigue lifetime of the composite marine propeller is concluded to be at least 10^{12} cycles under the considered loading condition. If the propeller would rotate at 600 rpm for 24 hours per day this would translate to over 3000 years. The reason behind this large number is that the combination of the applied pressure load and the strength of the carbon fiber propeller is such that the stresses in each ply are very low. These low stresses create almost no damage throughout the propeller blade even for ultra high cycles. If the pressure load was increased by a factor of 3, the damage in the propeller became more pronounced below 10^{12} cycles. The damage initiated due to transverse matrix cracks in the plies near the stress hot-spot locations on the blade near the leading and trailing edge. From there matrix cracks start to form in neighbouring plies spreading outwards. The effect on the propeller blade tip deflection remains limited since the affected plies are oriented at roughly 90° to the main radial direction and the highest loads are carried by the plies at a 0° orientation. The highest loads are carried by the elements near the root of the propeller however they remain largely unaffected by the fatigue loads.

1

INTRODUCTION

1.1. BACKGROUND AND MOTIVATION

Over the years, fiber reinforced composites have been increasingly used in the aerospace and automotive industry, due to their potential advantages for designing flexible, strong and lightweight structures. More recently they are also being considered for the manufacturing of marine propellers, with the ambition to lower the weight, lower the maintenance costs, increase the efficiency at off-design conditions, improve cavitation inception speed and reduce acoustic signatures.

The potential of these advantages have led to increased research effort into composite marine propellers. There have been studies into the Fluid-Structure Interaction (FSI) of these composite propellers interacting with the surrounding water [1]. This has led to insight in how to increase the efficiency at off-design conditions, cavitation performance and improving vibration performance. Even though this research has revealed promising results, it is also clear that a more thorough understanding is required on the mechanical aspect of composite propeller design. This is especially the case considering that the propellers are submerged in a seawater environment which can detrimentally affect the mechanical performance. To be a viable design option the composite propeller needs to be cost-effective and to do so it is required that the lifetime of the blade is sufficient. To determine the lifetime of the blade it is crucial to determine how the composite blade will respond to a wide variety of environmental and loading conditions that it will experience over its life. Basically one needs to determine what effects fatigue will have on the material properties of the blade.

In fatigue of fiber reinforced composites there are numerous types of damage, including matrix cracks, fiber-matrix interface debonding, fiber breakage, delamination among others. In composites these damages start early, they grow steadily and they can change depending on the stress distribution. Due to the deteriorating effect of the gradual increase in damage, the stiffness and strength of the material changes. This then results in a stress redistribution throughout the composite. This can cause the stress concentration locations to change over the life as well as the type of damage that occurs

there. This means that to completely describe the fatigue life of a composite structure, it is required to simulate the complete path of these successive damages throughout the laminate. This in the end will yield the time, the location and the type of damage causing final failure [2]. A multitude of models have been developed to establish the fatigue life of a composite with a specific stacking sequence, boundary condition, subjected to uni-axial constant amplitude loading at a certain frequency. However this is difficult if not impossible to extrapolate to real composite structures that have a varying layup and a more complex variation in loading. This means that significant research effort has to be put into fatigue life prediction of composites if a model that applies for a more generalized loading condition is to be developed. The main challenges of developing such a generalized model are summarized [2]:

- The governing damage mechanism is not the same for all stress level states [3][4]. Failure patterns vary with cyclic stress level and even with number of cycles to failure.
- The load history is important. When block loading sequences are applied in different orders (i.e.low- to high order or in high- to low order), there can be a considerable difference in damage growth [5].
- The residual strength and fatigue life of composite laminates have been observed to decrease more rapidly when the loading sequence is repeatedly changed after only a few loading cycles [6]. This so-called cycle-mix effect shows that laminates that experience small cycle blocks, have reduced average fatigue lives as compared to laminates that are subjected to large cycle blocks, although the total number of cycles they have been subjected to, is the same for both laminates at the end of the experiment.
- Most experiments are performed in uniaxial stress conditions (eg, uniaxial tension/compression), although these stress states are rather exceptional in real structures.
- The frequency can have a major impact on the fatigue life. Especially for matrix dominated laminates and loading conditions, frequency becomes important because of the general sensitivity of the matrix to the loading rate and because of the internal heat generation and associated temperature rise [7].

In the past research, the fatigue performance of a composite marine propeller was studied numerically and experimentally by Zhang [8]. As a case study, the Nautilus diving support vessel is considered in this research. It sails in a straight path in the calm water at the constant speed of 10.4 knots, with a four- blade composite propeller rotating at the constant speed of 600 rpm. The propeller experiences a non- uniform wakefield. In the first part of this research, the fatigue characteristics of such a composite propeller have been investigated. The propeller blade has a sandwich structure, where the blade faces at both the pressure and suction sides are made of carbon fiber reinforced composite laminates. The blade core is made of polymat/resin rich material. The approach was formulated in two steps: first, a numerical study was presented which aims to identify the critical areas of the composite marine propeller blade using the Tsai-Wu failure

criterion. Next, an experimental investigation on fatigue behaviour of the composite propeller was carried out based on the critical stress and moment resultants of the hot spot elements calculated in the numerical study.

1.2. AIM

Currently the mostly used and most reliable way to compute the fatigue life of composites marine propellers is to use an experimental approach. Such as the one proposed by Zhang [8]. However, this is a long and costly process. Modelling fatigue the fatigue performance in an earlier stage of the design cycle will result in significant cost and time savings. The main objective of this thesis is to determine the fatigue lifetime of composite marine propellers subjected to a pressure distribution determined by a Fluid-Structure Interaction (FSI) model with the use of a progressive damage model in combination with finite element analysis. Hence the research question is:

'What is the estimated fatigue lifetime of a composite marine propeller subjected to a predefined pressure load?'

The fatigue lifetime of the composite marine propeller is estimated using a progressive damage model in combination with a Finite Element Method (FEM) model that determines the loss in strength and stiffness properties as a function of the applied stress and cycles. Propeller failure is defined as the when the structure is no longer capable of carrying the pressure load or when the propeller deflection is greater than the maximum allowed by the hydrodynamics of the blade

1.3. STRUCTURAL DESCRIPTION

In order to answer the main question of this thesis, Chapter 2 firstly describes the methodology for creating the fatigue model, the physical reasoning behind the model and how it is implemented. This approach is motivated by analyzing the literature for comparable fatigue problems. Chapter 3 will explain the validation of these models with respect to experiments previously performed by Zhang [8] and in other literature. Chapter 4 highlights and discusses the results. The conclusion and recommendations for follow-up research are given in chapter 5. Furthermore, appendix 1 gives a more detailed description of different fatigue failure mechanisms to provide more background on the subject. Appendix 2 gives a description of the specimen scale FEM model that was created for the purpose of validation of the progressive damage model. Appendix 3 and 4 give a detailed explanation of the fatigue life model and the material degradation model as well as how they were chosen.

2

METHODOLOGY

This chapter will discuss the method used in this thesis to model the fatigue performance of the composite marine propeller. Section 2.1 will discuss the framework for fatigue damage progression modelling. Including the requirements and fundamentals of fatigue damage modelling. Section 2.3 will give an short summary on how the pressure load on the propeller is determined by giving a short summary on the Fluid Structure Interaction (FSI) model created by Maljaars [1]. Section 2.4 gives a schematic overview of the Finite Element Model (FEM) that is used in this thesis including a short description of each part of the model and how it is implemented. The subsequent sections 2.5, 2.6 and 2.7 will discuss the modelling techniques used in each part of the model in detail.

2.1. FRAMEWORK FOR MODELLING FATIGUE DAMAGE PROGRESSION

Considering the situation of the composite marine propeller blade, it is subjected to a constantly changing variable amplitude pressure load depending on the operating condition. Now consider a small material element of the propeller which is located in one of the layers, stresses will act on such an element along every axis and plane. Due to the varying nature of the pressure load, the stress tensor varies over time or cycles as well. The uniformly distributed pressure load induces a multi-axial stress state inside of the each element. Due to the complex geometry of the structure the stress will be non-uniformly distributed with different stress concentrations for each element. Thus, the varying pressure load on the global (structure) level, induces a multi-axial fatigue load on the local (element) level. Furthermore, due to the highly an-isotropic nature of composites together with the brittle nature of the fibers fatigue of composites is a highly stochastic process. Moreover, the large number of different material configurations resulting from the multitude of fibers, matrices, manufacturing methods, lamination stacking sequences, makes the development of a commonly accepted method to cover all these variances difficult[2][9][10][11][12]. In search for guidelines to a general approach for the fatigue failure mechanisms it was found that there are two kinds

of approaches: the micro-approach and the macro-approach [9]. The micro-approach is based on detailed local failure development, such as matrix cracking, fiber breakage, fiber-matrix interface debonding and delamination. The macro-approach is based on the assumption that failure is described by a macroscopic failure criterion, such as the maximum stress, Tsai-Wu and Tsai-Hill criteria. The influence on fatigue life of one or the other is strongly affected by a number of parameters, including material variables and testing conditions. Important parameters include environmental (temperature and moisture absorption) and loading conditions (stress ratio R, cycling frequency, etc.).

2.1.1. REQUIREMENTS

The model will be made with the following considerations: the model can determine the quality (location, type) and quantity (effect on properties) of the developing damage of the blade over it's lifespan until catastrophic failure occurs. Also, to be able validate the model with the AE sensor data and finally to use the combination of AE and model to determine in-situ the remaining life of the composite blade. However due to the limited amount of time available in my thesis the scope of the thesis will need to be limited to creating the model and validating this model with the use of experimental data acquired from literature and the test results of the coupon tests performed by Zhang [8].

One would ideally use a model that accurately models the experimentally observed damage accumulation, taking into consideration all material, loading and environmental variables. It describes the data for a large class of materials and permits the prediction of laminate fatigue behavior from lamina fatigue data. And, it should be extendable to spectrum fatigue loading and take into account data scatter. However there is no way to do this with the current micro-mechanical knowledge and modelling techniques. Even if this was known the computational effort to run such a model would be too great to make it a viable option. Therefore a compromise has to be made in accuracy and general applicability in order to get a reasonable answer. The best approach according to literature is to use a model that incorporates failure criterion that can be described as a macroscopic approach which is based on microscopic failure mechanics. This means that the criteria are chosen on the basis of observed failure modes in the material. This can be done using a progressive damage model (PDM), which describes the fatigue life of the structure on macroscopic scale as a function of damage on the microscopic scale.

2.1.2. FUNDAMENTALS OF PDM

Fatigue occurs due to a repeating and varying load that is applied to a structure. The cyclic stress σ can either have a Constant Amplitude (CA) or a Variable Amplitude (VA). Both types of fatigue loading are shown in 2.1. In case of real structures, fatigue loads are usually of the VA type. The figures shows that there are several parameter that are needed in order to fully describe the CA and VA cyclic stress behaviour. The CA stress can be described in terms of the the stress amplitude σ_a described in equation 2.1, the mean stress σ_m described by equation 2.2 and lastly the stress ratio R described by equation 2.3.

$$\sigma_a = \frac{\sigma_{max} - \sigma_{min}}{2} \tag{2.1}$$

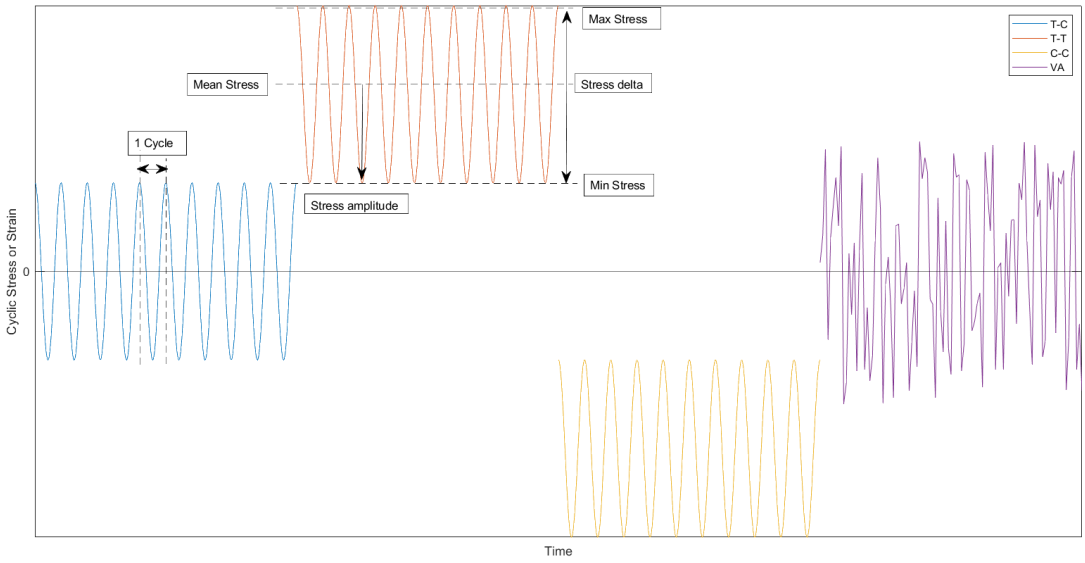

Figure 2.1: Fatigue terminology and loading patterns

$$\sigma_m = \frac{\sigma_{max} + \sigma_{min}}{2} \tag{2.2}$$

$$R = \frac{\sigma_{min}}{\sigma max} \tag{2.3}$$

In these equations, σ_{max} is the maximum applied stress and σ_{min} is the minimum applied stress. To simulate the VA stress, the stress divided into section with a certain applied stress, stress ratio for an amount of cycles δN. This approach will only give an approximation of the real VA loading spectrum, however simulating the stress history in its entirety is not feasible in practice. An example of a simplified VA stress histogram is shown in figure 2.2, where the VA cyclic stress is converted into a set of CA cyclic stress levels.

These so called loading blocks or cycle blocks can be used to determine, in discretized steps the accumulation damage of the composite due to applied stress and amount of cycles considered in that loading block. As is explained above the accumulation of fatigue damage can be modelled in two different ways. The main difference between the two methods is the used methodology to take into account damage initiation and/or progression. The macro-approach is based on the assumption that failure is described by a macroscopic failure criterion, such as the maximum stress, Tsai-Wu and Tsai-Hill criteria. However, physically the damage will be due to the formation of micro- and macrocracks which do not necessarily have a uniform distribution throughout the material. On the other hand these macro-scopic progressive damage models

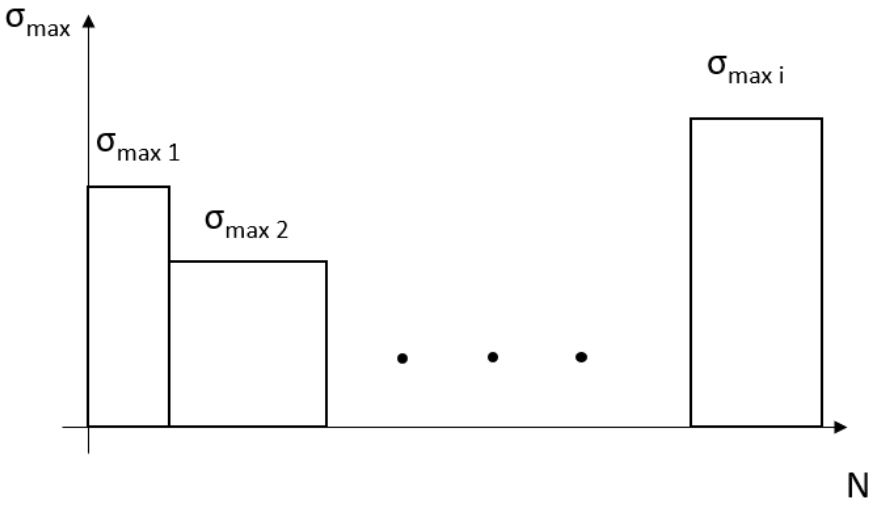

Figure 2.2: Simplified VA stress histogram

have shown to provide satisfactory predictions that can provide a good engineering estimate of the fatigue life and residual properties [13][14]

The micro-approach is based on detailed local failure development, such as matrix cracking, fiber breakage, fiber-matrix interface debonding and delamination. These models are concerned with modelling the fracture itself, taking into account the crack geometry and orientation. These models give a more detailed and accurate material degradation scheme and describe the experimentally observed damage accumulation more accurately. However there is no to do this with the current micro-mechanical knowledge and modelling techniques. Even if this was known the computational effort to run such a model would be too great to make it a viable option.

The aim of a progressive damage analysis is to not only predict the point of failure but also the degradation of the material properties in the structure throughout the loading history. The state-of-the-art progressive damage models use finite element method implementations to accurately predict the stress levels and stress distribution throughout the structure as damage progresses [13][14][15].

2.2. PROGRESSIVE DAMAGE MODEL OVERVIEW

Considering the situation of the composite marine propeller blade, it is subjected to a constantly changing variable amplitude pressure load depending on the operating condition. Now consider a small material element of the propeller which is located in one of the layer, stresses will act on such an element along every axis and plane. Due to the varying nature of the pressure load, the stress tensor varies over time or cycles as well. The uniformly distributed pressure load induces a multi-axial stress state inside of the material element. Determining this stress-state of a material element for a wide range of

applied pressure can be determined by the FEM analysis. However, for simplicity only one of the propellers operating conditions is considered. In light of the requirements discussed in previous sections, it is proposed that the complete simulation framework is implemented into the FEM environment. This leads to the framework shown in figure 2.3 which is based on the progressive fatigue damage methodology by Shokrieh and Lessard [16]. This section will also give a detailed explanation and comparison of different combinations of models that form the progressive damage analysis models. As is explained in the section above, the progressive damage models consist of 6 main parts. A flow diagram giving a simplified version of the communication between the 6 parts of the model is given in figure 2.3.

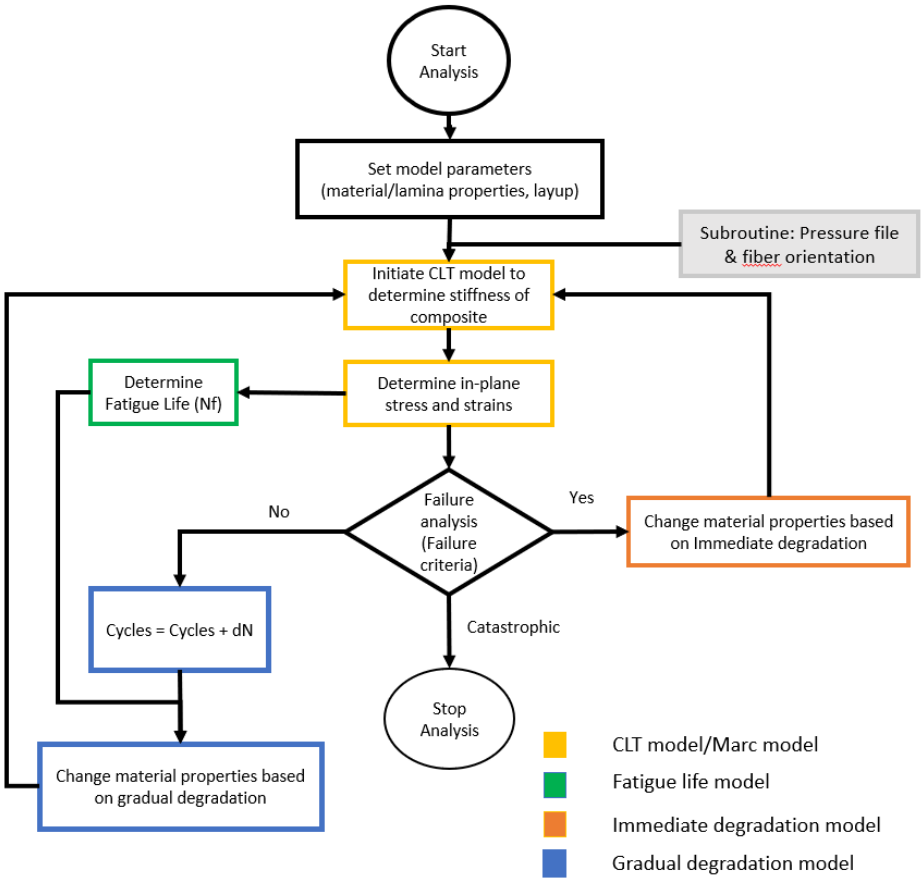

Figure 2.3: Simplified flow diagram of the progressive damage model

The PDM created in this thesis uses the FEM model in MarcMentat created by Maljaars [1] and Zhang [8] to calculate stresses and strains at each element. These stresses and strains are then transformed into stresses and strains in the local coordinate frame of each element at ply level, with the use of classical laminate theory (CLT). Using the

immediate and gradual degradation rules that are explained in more detail in appendix D, one can estimate the location, type and effect of the created damage. This is done using a combination of failure criteria and experimentally fitted phenomenological models for the immediate and gradual degradation respectively. The gradual degradation models require a residual lifetime estimate to determine how much it will degrade. Since the material degradation is a function of the fraction of applied cycles over residual life cycles. This combination of models is similar to approaches used in many different papers [15][16][17][18]. The next step is to recalculate stiffness of the composite at element level and implement this into the FEM model. The last step is to determine the redistribution of the stresses and strains throughout the composite blade. This is then repeated until the failure is catastrophic or the deflection of the blade has increased above a to be determined threshold. A flow diagram describing this model is given in figure 2.3.

2.3. PROPELLER LOADCASE

To analyse the hydrodynamic performance of the propeller blade a Fluid-Structure Interaction (FSI) model is used. A FSI model iteratively solves the hydrodynamic response to a change in deflection and the structural response to a change in pressure distribution in order to converge to a steady state solution. To solve the hydrodynamic response of the blade a boundary element methods (BEM) has been used. The main advantage of using the BEM for the composite propeller FSI model is that it requires less computational effort compared with higher fidelity methods. The Maritime Research Institute Netherlands (MARIN) developed BEM PROCAL was used. The Finite Element Method used is described in more detail in section 2.4. The flow chart of the BEM-FEM coupled FSI model is given in figure 2.4. The initial step in the simulation is a BEM calculation on the undeformed blade geometry, to get an initial pressure distribution. The pressure is then corrected to rectify the overestimation at the propeller tip. This correction smoothly degrades the pressure coefficient to zero from 95% propeller radius, which is a better representation of reality. The next step is to apply a viscous correction to include frictional losses. The skin frictional losses are determined by computing the viscous shear stresses introduced by the water on the blade. The tangential forces this introduces on the blade are calculated per element and imposed on the FEM model. Subsequently, the FEM model is used to solve structural problem with these new pressures and viscous forces. The next step is to use the newly determined propeller geometry to calculate a new pressure distribution. Finally, a convergence check is used to check if the solution is satisfactorily converged. If this is not the case, the iteration loop will start over [1].

The FSI interaction model is used to compute the load cases used in the fatigue analysis. These load cases have been determined for a unique scenario, a vessel sailing in a straight path in calm water with a constant speed of 10.4 knots. The propeller experiences a non-uniform wakefield behind the ship due to the shear stresses the ships hull introduces into the water. This non-uniform wakefield is shown in figure 2.5. It shows an increasing flow velocity from near the hull of the ship to the free stream flow. This non-uniform wakefield introduces a constant amplitude fatigue load on the propeller blades. Furthermore, the propeller rotates at a constant speed of 600 rpm. The full revolution of the blade is divided into 60 equally large time steps. Finally, the pressure distribution over the blade's surface is converted to nodal forces acting through the centroid of the

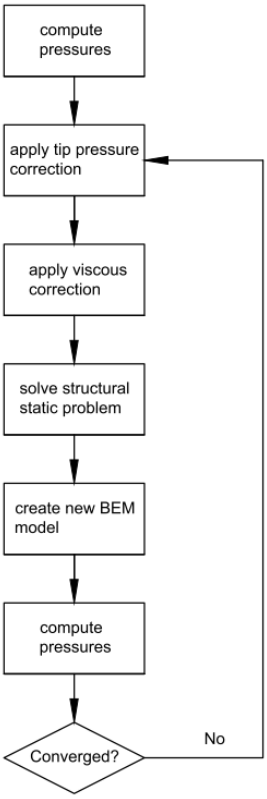

Figure 2.4: Flow chart of BEM-FEM coupling [1]

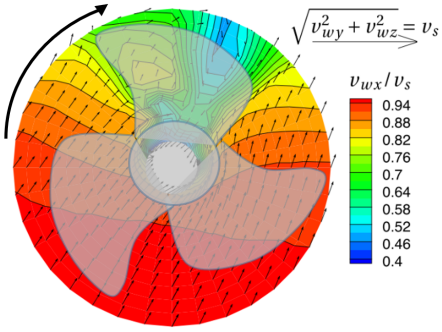

Figure 2.5: Propeller rotating through a nominal wakefield at the portside propeller plane [1]

surface elements [8]. This pressure distribution is the only one considered for the fatigue analysis of the composite propeller blade in order to decrease the complexity and reduce

the amount of variables that need to be verified.

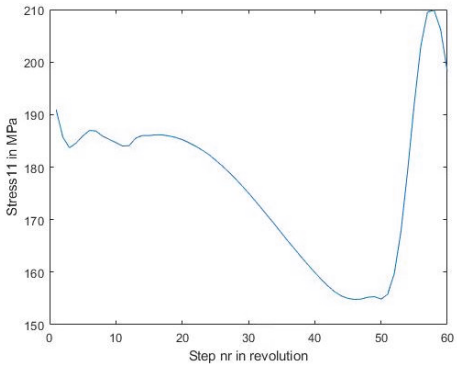

Figure 2.6: Fatigue loading caused by the propeller rotating through the non-uniform wakefield

The propeller rotating through this non-uniform wakefield creates a fatigue loading on the propeller blade as can be seen in figure 2.6. This figures shows the fatigue loading caused in one of the elements in the longitudinal direction of the fiber. The stress reaches its maximum at step 59 and minimum at step 46 with an R ratio of approximately 0.74. In order to simplify the analysis the progressive damage model only uses the maximum stress at cycle 59 and the R ratio determined for each of the elements. This is a simplification of the problem, however it is deemed necessary to complete the analysis within a reasonable time span.

2.4. FEM MODEL

To simulate the mechanical behaviour of complex structures, FEM has shown to be a powerful tool. Implementing it into the fatigue analysis gives a means to accurately simulate the damage evolution throughout the structure. However, the difficulty with implementing a finite element analysis is that the quality of the output is only as good as the input. The accuracy depends on the underlying models for simulating the behaviour of the materials.

On an important note, for this research only commercial FEM software is considered. Which is largely motivated by the author's experience with these types of environments and the easy of integration of more complex geometries. However, this is purely based on the author's experience with Abaqus[1] and Ansys[2]. On a more practical note, Marc[3], the software used in this work is selected due to the previously completed works regarding the FSI model and the quasi-static fatigue analysis by Maljaars [1] and Zhang [8] respectively. Marc provides highly advanced solving capability for non-linear systems. The choice for Marc as the commercial FEM environment is not deemed to be a of the present work, because it provides quite some freedom in using self-developed subroutines and the concept strategy can be reused for other types of frameworks. Another

[1] https://www.3ds.com/products-services/simulia/products/abaqus/
[2] https://www.ansys.com/products/ansys-workbench
[3] https://hexagon.com/products/marc

benefit of using Marc as a solver is that it comes with an integrated visualization software package called Mentat[4].

2.4.1. ORIGINAL MODEL

The FEM model was first created by Maljaars [1] for the research into the fluid-structure interaction of the GFRP composite propeller behind a nonuniform wakefield. It was then adapted by Zhang [8] to find the critical hot-spot locations on a CFRP blade to check its short-term fatigue life. The FEM model consists of a single propeller blade without the hub. The stiffness contribution of the propeller hub is represented by fully clamping the blade at the blade-hub interface. The reasoning being that the stiffness of the hub is significantly higher than that of the blade. The blade is discretised using quadratic solid elements. Solid elements to better capture the interlaminar stresses, the quadratic elements in order to accurately model the bending dominated blade response. Maljaars, performed a convergency study to find the required number of elements in chordwise, radial and through thickness direction. The results show a 29×30×4 element distribution. Furthermore, Maljaars [1] showed the importance of material orientation for doubly curved structures. An erroneous material orientation can lead to a false prediction of the structural stiffness of the blade. To correct the material orientation of each element, a user-defined subroutine was used. In this subroutine, the through-thickness direction and the projection of the transverse laminate (90°)-direction on the element surface are used to establish the material orientation per element [1]. The determination of the correct material orientations are shown in figure 2.7.

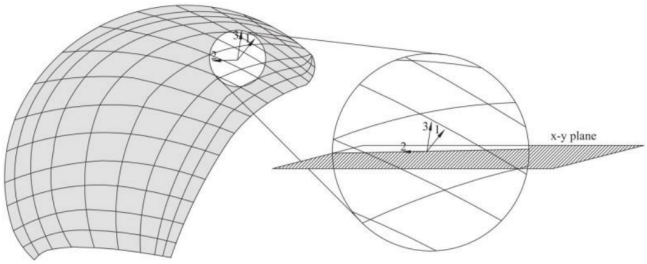

Figure 2.7: Determination of the material orientations for one element [1]

To apply the pressure loads extracted from the FSI model another user-defined subroutine was used. This subroutine allowed Maljaars [1], to apply the pressure loads to the correct nodes. Zhang [8] subsequently altered the FEM model by changing the material properties, whilst keeping the layup the same. The laminate consist of an outerskin and a blade core. The outerskin is made of one outer ply of woven CFRP and multiple plies of unidirectional CFRP. The woven ply is used to minimise the damage created by impacts on the blade. The core is made of a resin rich material called polymat, with a density of around 1200 kg/m3. See table 2.1 for the elastic and strength properties of the CFRP lamina and see figure 2.8b for the solid model of the propeller blade. The $*$ in table 2.1

[4]https://hexagon.com/products/mentat

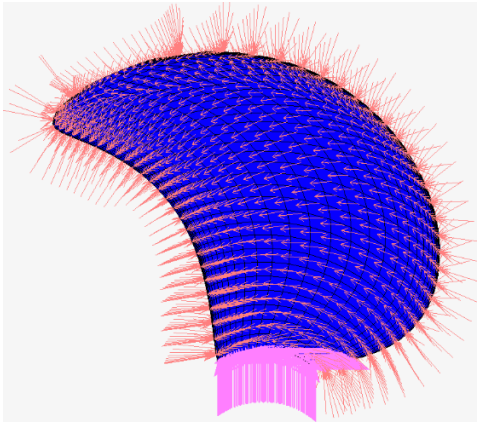

(a)

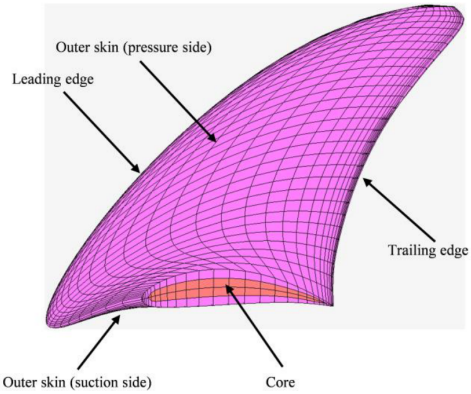

(b)

Figure 2.8: a) The boundary conditions and pressure load applied to the propeller blade and b) FE model of the composite marine propeller blade and cross-sectional view: blade faces (magenta) and core (orange) [8]

denotes a correction in this property with respect to the source data. This same layup and material properties are also applied to the current fatigue analysis.

Table 2.1: Elastic and strength properties of the polymat, the woven and the UD CFRP materials [8]

	Parameters	Polymat	Woven CFRP lamina	UD CFRP lamina
Elastic Properties	t [mm]	Variable	0.19	0.15
	E_L, E_T, E_H [GPa]	4	70, 70, 11.2	140, 11.9, 11.9
	ν_{LT}, ν_{TH}, ν_{HL} [-]	0.3	0.05, 0.4, 0.064*	0.29, 0.4, 0.0247*
	G_{LT}, G_{TH}, G_{HL} [GPa]	1.538	4.9, 3.92, 3.92	4.9, 4.17, 4.9
Strength Properties	S_L^t, S_T^t, S_H^t [MPa]	N/A	910, 910, 70	2100, 84, 84
	S_L^c, S_T^c, S_H^c [MPa]	N/A	665, 665, 70	1540, 280, 266
	S_{LT}, S_{TH}, S_{HL} [MPa]	N/A	126, 84, 112	126, 119, 126

2.4.2. FEM IMPLEMENTATION STRATEGIES

Two different modelling strategies can be distinguished for implementing a FEM into the fatigue analysis namely, the joint and disjoint implementations. Joint implementations perform the complete simulation process inside the FEM environment. The joint implementations have some inherent limitations. First, to simulate the complete simulation within the FEM environment the whole model needs to be specifically tailored to that environment. Which will make it complicated to change the simulation to another FEM environment, because then the model needs to be remade. Another limitation is that the complexity of the progressive damage model can be limited due to the lack in flexibility of the FEM environment. Most widely used FEM environments provide subroutines which can be used to implement user-defined functionalities. However the flexibility is often limited and there is a lack of access to the source of the FEM environment.

Disjoint implementations run parts of the simulation outside of the FEM environment. In the context of this thesis, the parts of the simulation run outside of the FEM environment refer to the modelling of the fatigue behaviour. The benefit of doing a disjoint implementation is that it uses the high-fidelity capabilities of FEM but it also has the flexibility of self-developed source code. Unlike the joint implementation which inherently limited in its flexibility by the FEM environment. However, the flexibility is not limitless since the FEA environment is still used for part of the analysis. Another inherent drawback of disjoint implementation is that it may experience issues related to computational inefficiency due to the communication between the different environments. This inefficiency leads to slower overall solving of the simulation. In practice this inefficiency is mostly due to the required pre- and post-processing of the FEA environment every time a cycles is run.

Considering the discussion presented in the section above, the joint approach is selected as the best concept for the progressive damage analysis of the composite marine propeller subjected to fatigue loading.

- Due to the preceding research performed by Maljaars [1] on the FSI model integration with Marc, the model can simulate an entire cycle without having to change the input file. Doing so outside of the FEA environment is not trivial and may not be possible within the limited time frame.
- The joint implementation strategy will reduce the computational effort considerably. Which will reduce the time it takes to solve the fatigue analysis considerably.
- The implementation of the joint strategy reduces the flexibility of the PDA, in comparison to programming the PDA outside of this environment.
- One of the most powerful aspect of Marc is that it provides the user with *user subroutines* capabilities, which adds increased flexibility in solving non-standard problems [19].
- The joint implementation cannot achieve direct compatibility with different commercially available FEM environments.

The major advantage of using the joint implementation is that the solving time is significantly lower. This is because in the course of the execution of a Marc program, most of the time is spent to deal with the input and output operations. Whereas the the arithmetic and the memory access operations of a program are fast procedures [19]. Running the fatigue analysis inside the FEM environment reduces the number of times that the input and output need to read and altered with an alternate programming language. Reading of the output, computing the created damage using the PDA and subsequently creating a new input file also require significant computational effort. The required computational effort is important, because in order to predict the damage evolution within the propeller blade, it is important to simulate the propeller mechanical behaviour over a one complete revolution for a high number of cycles. Which will require considerable computational effort. Although concepts such as cycle jumping can be used to alleviate some of this computational effort.

2.4.3. CYCLE JUMPING

Progressive damage analysis models can be used to determine damage on a cycle by cycle basis. When these models are applied to full-scale structures with complex geometries, subjected to multi-axial loads, they are able to determine the stiffness degradation and subsequential stress redistribution for each element within the structure. However running this simulation for each subsequent cycle will be near impossible due to the required computational effort. Especially for structures that last up to very high cycle fatigue ranges. Because of this the simulation should be run for a well chosen set of fatigue cycles so that the overall prediction of stiffness degradation and stress redistribution are sufficiently accurate. A range of cycle jump methods have been developed to do the progressive damage simulations more efficiently [20]. In general the step size which can be used for the cycle jumps depends greatly on the stress introduced into the structure.

- The stress-state of elements that are loaded with a very low stress level will remain almost constant, making it safe to jump over a large amount of cycles without leading to wrong estimations of the damage distribution.
- Elements in the structure that are loaded with high stresses, damage is growing more quickly for each subsequent load cycle. This makes that the stress-state is continuously changing, because the damaged zones are no longer able to sustain the applied load. The cycle number that can be jumped in such an element will be small, or the estimation of the damage distribution will be inaccurate.

So the amount of cycles that can be jumped is indirectly limited by the stress-state to which the element is subjected. However one way to make sure the amount of cycles jumped is not too great, is to limit the increase in damage over the amount of cycles jumped. This can be done by using the Euler explicit integration formula 2.4. Where $njump1$ is the local cycle jump and D is the damage variable going from 0 for undamaged till 1 for failure. Using this equation and limiting the growth in damage $\frac{dD}{dN}$ to a certain value, it is possible to determine the amount of cycles jumped. In figure 2.9 a maximum damage growth of 0.1 is allowed, leading to approximately 23000 cycles to jump.

$$D_{N+NJUMP1} = D_N + \frac{dD}{dN}|_N * NJUMP1 \tag{2.4}$$

Because of this relation between stress-state and change in damage variable, it would ideally be possible to set a cycle jump size for each element separately. However, this will defeat the purpose of making a realistic simulation. Therefore a global cycle jump value needs to be determined which is equal for all elements and nodes. A simple choice would be to pick the lowest of the local values, this will give a realistic solution albeit an inefficient approach to jump cycles. Because at any given cycle there will be a node with a rapidly increasing damage variable. Another approach is to equally divide the number of cycles to jump in groups (i.e. groups of 1000 cycles) and check the relative frequency of appearance of these groups to create the probability distribution function. Next step is to make the cumulative distribution function of this frequency. This will give the probability that the number of cycles jumped is less than a selected number of cycles.

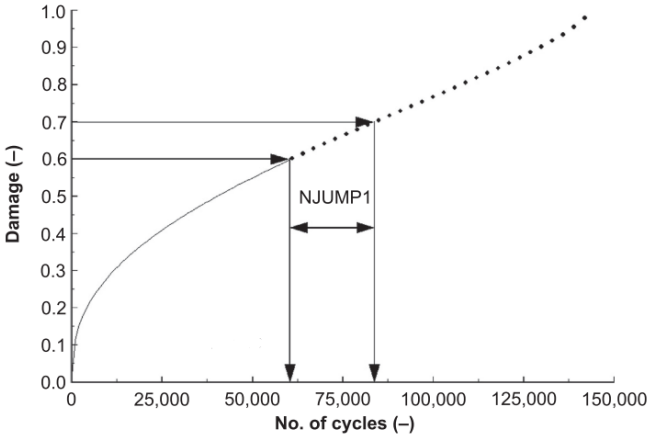

Figure 2.9: Example for calculation of the amount of jumped cycles NJUMP1 [20]

This can be used to set a statistical limit to make sure that most of the number of cycles jumped is equal or greater than chosen cycle jump. For example the 10th percentile is used as a lower limit, gives a certain cycle jump.

2.4.4. NEW FEM MODEL

There is a multitude of ways to communicate with the Marc solver to get it to run a progressive damage model. However, the most efficient method is by using the user subroutines that can be read by the solver. In order to run these subroutines in the Marc/Mentat environment they need to be compiled into an executable file. First the subroutines are written in Fortran programming language and compiled using the Intel oneAPI Fortran compiler [5]. This is schematically represented in figure 2.11. The flow diagram of these subroutines is given in figure 2.10. The first step of the progressive damage model is the setup of the FEM model. This includes writing the input file for the Marc model containing the geometry, the material properties, the layup, the boundary conditions, the loading type and the expected number of cycles. The next step is to make sure the fiber angles are correctly oriented with respect to the blade, this is done using the ORIENT2 subroutine. Then the distributed pressure load can be applied to the blade surface using the FORCEM subroutine. Subsequently, the finite element solver can determine the stress-state of the propeller blade elements. Next, run the subroutines for the first cycle to determine (for each node) if failure occurs using the UFAIL subroutine. This subroutine contains the Hashin failure criteria that can determine fiber tension and compression failure and also matrix tension and compression failure. If the failure criteria indicate failure then the UPROGFAIL subroutine reduce the material properties of that node using the immediate degradation rules. If there is no failure indicated then the UPROGFAIL subroutine will use the gradual degradation rules to reduce the material properties of the nodes. After all of the elements and nodes have been analysed. The

[5] https://www.intel.com/content/www/us/en/developer/tools/oneapi/fortran-compiler.html

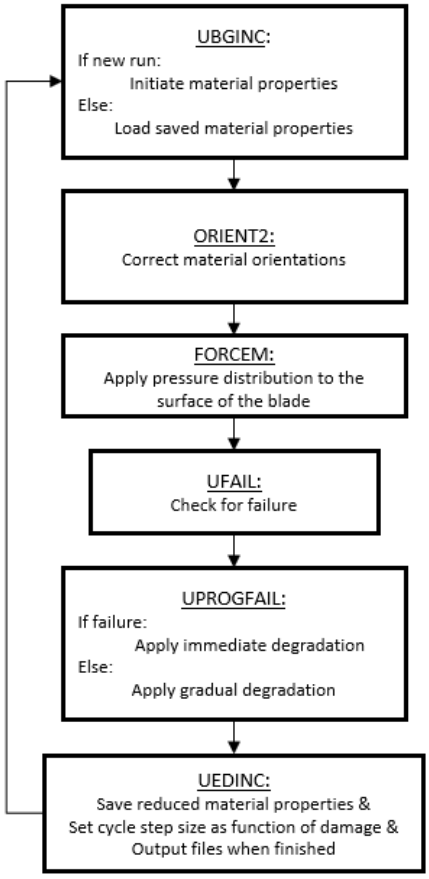

Figure 2.10: Flow diagram of subroutines used in the new FEM model

new properties will then be saved to the next cycle using the UEDINC subroutine. The UEDINC subroutine is also used to set the cycle step size of the next loading block as a function of the amount of damage created during the previous cycle. Lastly it is used to write information to a file for post-processing in Matlab.

Next to this some slight changes were made to the original FEM model in order to correct for some mistakes. These changes lead to a slightly different stress distribution which in turn led to new failure indices as can be seen in figure 2.12. The figure shows the maximum Tsai-Wu failure indices for static loading. The maxima are the highest failure indices through the thickness of the skin of the propeller. For some elements this will be in layer 2 whilst for others this could be in layer 10. If the results from this FEM analysis are compared to the results from Zhang [8]. The maximum failure index have only increased slightly from 3.169 to 3.26 and it is still at the same 1421 element.

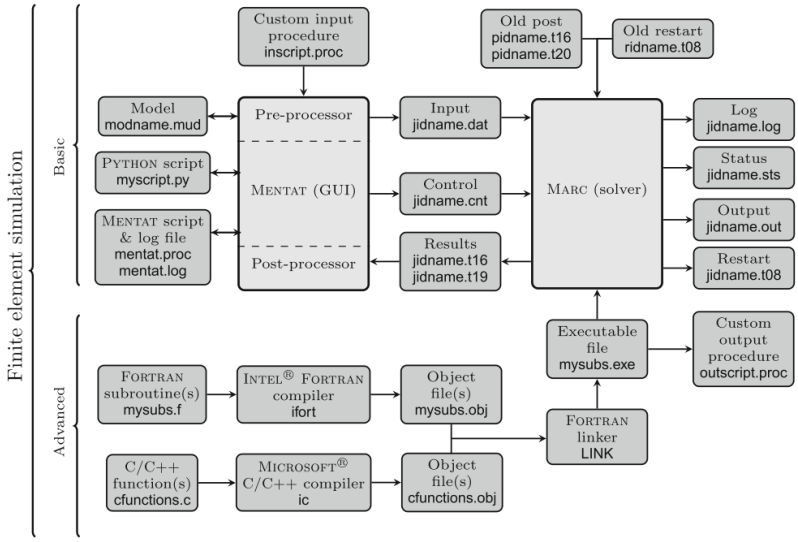

Figure 2.11: Marc/Mentat interaction flow diagram [19]

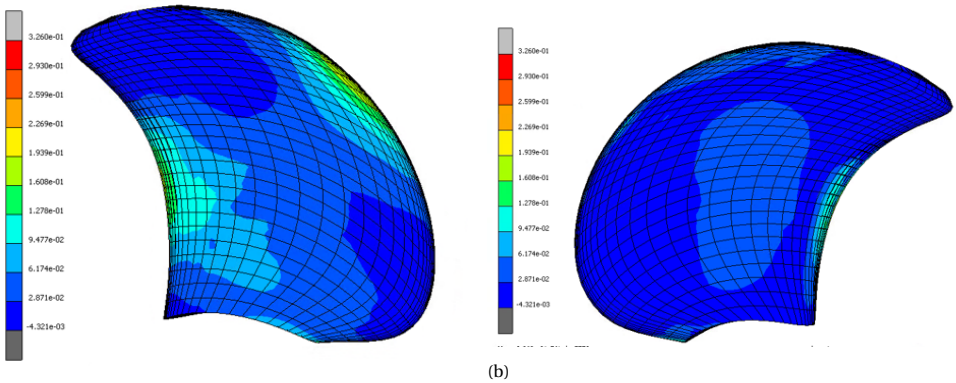

(a) (b)

Figure 2.12: Maximum Tsai-Wu failure indices of the composite propeller blade for the new FEM model

2.5. FATIGUE LIFE MODELS

The fatigue life model gives an estimation of the fatigue life of a ply subjected to a fixed constant amplitude loading by using curve fitting parameters. The fatigue life model uses a strain energy density based fatigue criterion and introduces the criterion into analysis and subsequently fitted to S-N curve data. Using this fatigue criterion the model can be fitted to for certain fiber orientations and stress ratios without the need to test it for all of these directions. This reduces the amount of testing required to fit them. The model does not take into account damage accumulation, but predicts the number of cycles at which fatigue failure occurs under fixed loading conditions. A detailed explanation of how the fatigue life model is selected and how it works is given in appendices C. Figure 2.13 gives the flow diagram of the fatigue life model with the required model inputs and the outputs. This is than included into the progressive damage model as shown in the progressive damage model flow diagram 2.3. It is important to note that the fatigue life for the longitudinal, transverse and shear directions are given separately. The appendices show that there are a few different models considered for the fatigue life analysis. However there is only 2 models that are able to estimate the fatigue life to within a reasonably degree for all stress ratios. Because the progressive damage model aims to determine the decrease in material properties in longitudinal, transverse and shear direction separately in the end only one model is considered.

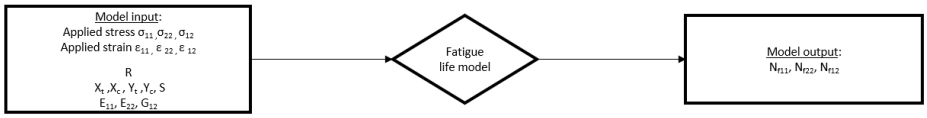

Figure 2.13: Flow diagram of the fatigue life model

2.6. GRADUAL DEGRADATION MODELS

When the laminate is subjected to a cyclic stress that does not initiate failure the properties are degraded using the gradual degradation models. The gradual degradation model and how it is selected is discussed in more detail in appendix D. The input and output of the gradual degradation models can be summarised into figure 2.14. This part of the model is included into the progressive damage model as is shown in the flow diagram 2.3. In the case of a ply subjected to state of cyclic (fatigue) stress prior to the onset of sudden material failure, there is some prior gradual material property degradation. For the a certain ply subjected to cyclic loading, the strength of the plies can be greater, at first, than the applied stress, Due to the gradual increase of the number of loading cycles and corresponding increase of the loading history, the material properties of the individual plies are slowly degraded. Finally, after a certain number of loading cycles, the mechanical properties of the plies eventually hit a threshold value activating some (or all) of the failure criteria. After this point the immediate material degradation model is applied.

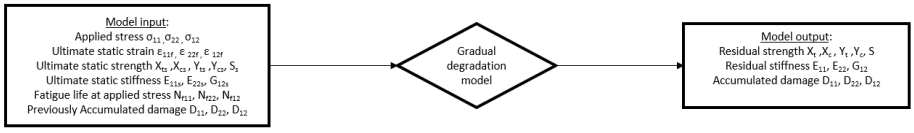

Figure 2.14: Gradual degradation model flow diagram

2.7. IMMEDIATE DEGRADATION MODEL

In the case when the laminate is subjected to a cyclic stress that does initiate failure the properties are degraded using the immediate degradation model. The immediate degradation model and how it is selected is discussed in more detail in appendix D. The flow diagram of the immediate degradation model is shown in figure 2.15. It can be included into the progressive damage analysis scheme as is shown in figure 2.3. The immediate degradation model is triggered if the mechanical properties of the individual plies are reduced to a threshold that triggers the failure criteria to activate. If this happens the material properties are degraded to a 1% of their initial value.

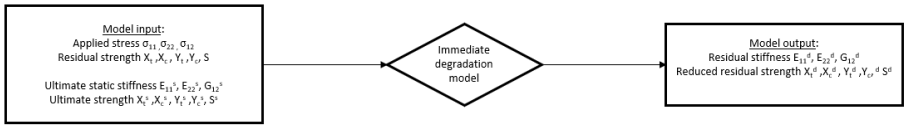

Figure 2.15: Immediate degradation model flow diagram

3

VALIDATION STUDY

This section describes the validation study of the progressive damage model on specimen scale. The model is validated by comparing the lifetime and material degradation with experimental data gathered from literature. In order to validate the model, the progressive damage model is applied to a smaller scale FEM model which is explained in more detail in appendixB. First the progressive damage model's predicted degradation of material properties is compared to experimental data in section 3.1. Then the models fatigue lifetime predictions are compared to experimental results in section 3.2. In section 3.3 the sensitivity of the model with respect to the curve fitting parameters is explained as well as a strain energy density correction factor to reduce the underestimation of the results.

3.1. VALIDATION STUDY OF STIFFNESS DEGRADATION

3.1.1. COMPARISON WITH IM7/8552 [38/ − 52/ − 7/ − 52/38] LAMINATE STIFFNESS DEGRADATION TESTS

The stiffness degradation of an IM7/8552 carbon fiber epoxy laminate was determined experimentally by Zhang [8]. He performed this test to determine the short term structural health of the propeller blade to which the specimen and loading conditions were equivalent. The layup of the specimen is [38/−52/−7/−52/38]. This layup was made unbalanced on purpose, because this allowed the author to perform uni axial fatigue tests which would reproduce an equivalent multi-directional load on the specimen. The stiffness of the specimens was measured first without applying any fatigue load to find the static ultimate stiffness of the specimen. Subsequently the stiffness was measured after applying 10^4 cycles and 10^6 cycles. He performed experiments both with and without extensometers to test the stiffness of the specimens. For the experiments without the extensometers he determined the stiffness by linearly fitting the data points from the experiments and converting them to a stress-strain relation. Then the stiffness was defined as the slope of these stress-strain curves. The stiffness was also measured using the extensometers for a set of specimens in order to find a more precise estimate. After com-

Property	Value [unit]
E_{11}	176.5 [GPa]
E_{22}	17.7 [GPa]
G_{12}	4.9 [GPa]
ν_{12}	0.29 [-]
X_T	2100 [MPa]
X_C	1540 [MPa]
Y_T	84 [MPa]
Y_C	280 [MPa]
S_{12}	126 [MPa]

Table 3.1: Material properties IM7/8552 [8]

paring the stiffness from the data fitting and the extensometers it was concluded that the testing machine had a significantly low stiffness. Such that it would act as a spring in series with the specimen and thus influencing the results. Using this knowledge the equivalent stiffness of each specimen was determined and the results are averaged. Table 3.1 gives the material properties of the specimens used in the experiments performed by Zhang [8]. These material properties are now used in the progressive damage model.

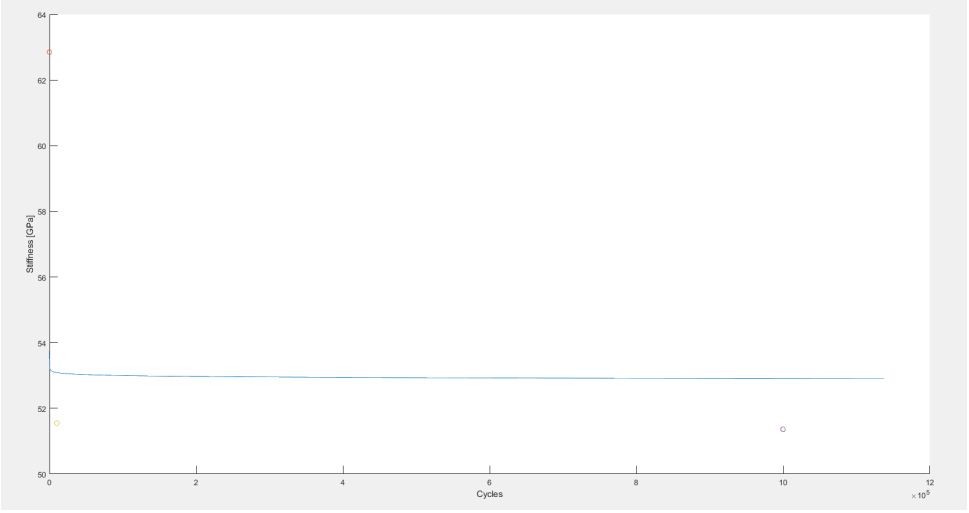

Figure 3.1: Stiffness degradation plotted against the number of applied cycles the prediction is plotted as the solid line and the dots are the averaged experimental results from [8]

Figure 3.1 shows that the initial stiffness drop exhibited by the experiments is greater than the stiffness drop calculated by the progressive damage model. The reasons for the difference can be explained by the fact that the model models the loss in stiffness of a certain element in all directions separately. In the cases where there is a the stresses in all directions are considerable the interaction effects between these loads will have a larger influence on the degradation of the material properties compared to when the loads are

unidirectional. In the case of this specimen where the layup is unbalanced there is a considerable multi-directional stress acting on the specimen due to the uni-axial load. This also shows in appendix C where it can be seen that the fatigue life model becomes less accurate when the plies are not loaded in the 0° and 90° directions. Furthermore, decrease in stiffness is modeled per element and the loss in stiffness is smeared over the entire volume of the element instead of cracks initiating leading to high local stress concentrations. Since these stress concentrations now still exist but are averaged over a larger volume this leads to a later failure of the matrix/fiber matrix interface. Another possible reason is that the fit of the degradation is model based on empircial data fitting process. All of these paramterers are fiber/matrix specific therefore never a perfect fit for all models. A small sensitivity study is performed in the section 3.3. Figures B.2, B.3 and B.4 show the increase in damage in the top and the middle layer after 1, 10^4 and 10^6 cycles respectively. According to these figures the damage increases steadily with applied cycles and increases more rapidly for the 38° layer than that of the −7° layer. Furthermore, the increase in damage is larger from the first to the 10^4 cycle than from the 10^4 cycle to the 10^6 cycle. It must also be noted however that for the 7° layer the point with the highest degradation lies on the node that is subjected to boundary condition. This creates a local stress concentration which might not be realistic and the predicted degradation for this ply is higher than it is in real life. The same analysis has also been performed for a mesh size of 1mm, figures B.5, B.6 and B.7 show the degradation of the top and middle layer. For the degradation of the middle −7° layer the results of the 5mm mesh size and 1mm mesh size are almost the same. The damage locations are comparable although for the finer mesh size the increase in damage over the amount of cycles is increased. For the top layer the damage locations are also comparable except for one hot spot near the fixed boundary condition in the 1 mm mesh size which is not present in the 5 mm mesh size. This interaction between the increase in damage with a decrease in mesh size is yet not fully understood and might therefore lead to skewed or even incorrect results.

3.1.2. COMPARISON WITH AS4/3501-6 $[0/90_2]_s$ LAMINATE STIFFNESS DEGRADATION TESTS

Daniel et al. [21] performed a set of longitudinal tensile fatigue tests on AS4/3501-6 $[0/90_2]_s$ laminates. They recorded the stiffness degradation as a function of the normalized applied cycles. The test were performed at three different cyclic stress levels: 28% of the ultimate static failure stress, 53% and 85%. The stiffness degradation curves were generated for each loading type. To be able to compare the model's prediction accuracy with respect to the experiments, it is necessary to know the fatigue life of the specimens. Because in the paper the authors give the stiffness degradation as a function of normalized applied cycles. Another paper written by the same authors [22] provide the fatigue life predictions for the AS4/3501-6 $[0/90_2]_s$ laminate. It is possible to estimate that an AS4/3501-6 [0/902]S laminates loaded with a maximum normalized cyclic stress of 85%, 53% and 28% of the ultimate static failure stress will have fatigues lives in the order of 10^4, 10^{10} and 10^{14} cycles respectively. Figure 3.2 shows the stiffness degradation at 85%, 53%, 28% of the ultimate failure load. The stiffness is normalized with respect to the initial static stiffness and the amount of cycles is log normalized with respect to the total amount of cycles. The curves follow the experimental values reasonably accurate espe-

cially in the later stages of the normalized fatigue life. For figures 3.2a and 3.2b the initial drop in stiffness is not well represented by the predictions. This is mainly because according to the predictions given in [22] the specimens should last around 10^4 and 10^{10} cycles and the predictions from the model give a lifetime of around 10^2, 10^5 respectively. If the data the amount of cycles applied is log normalized with respect to failure cycle the initial data point on the horizontal axis will be offset from the zero axis. Figure 3.2c gives the degradation curve at 28% of the ultimate static stress. Even though the experiments only give the data up until 0.4 of the log normalized cycles, the prediction matches them quite accurately. At 28% of the ultimate static stress the matrix does not fail instantly after the first cycle and therefore there is no sudden drop in stiffness in the initial stages. After about 20% of the log normalized life the matrix starts to fail at certain high stress locations up until around 50% when the matrix appears to have been saturated with matrix cracks and the stiffness remains approximately constant.

Property	**Value [unit]**
E_{11}	142 [GPa]
E_{22}	10.3 [GPa]
G_{12}	7.6 [GPa]
ν_{12}	0.27 [-]
X_T	2372 [MPa]
X_C	1197 [MPa]
Y_T	57.2 [MPa]
Y_C	204 [MPa]
S_{12}	71 [MPa]

Table 3.2: Material properties AS4/3501-6 [23]

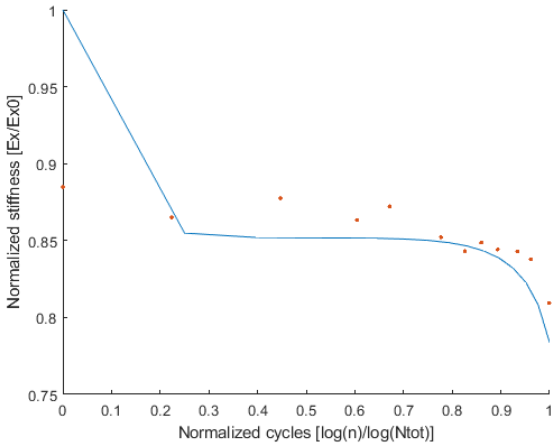

(a)

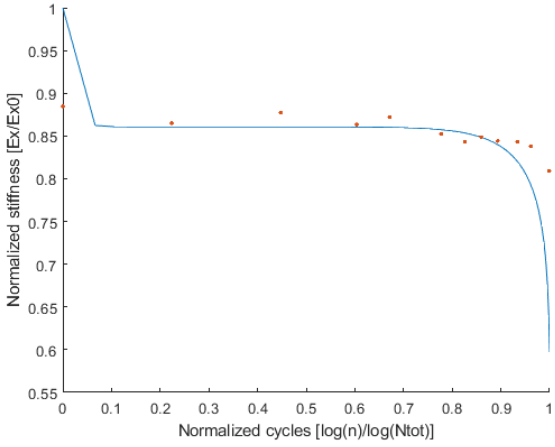

(b)

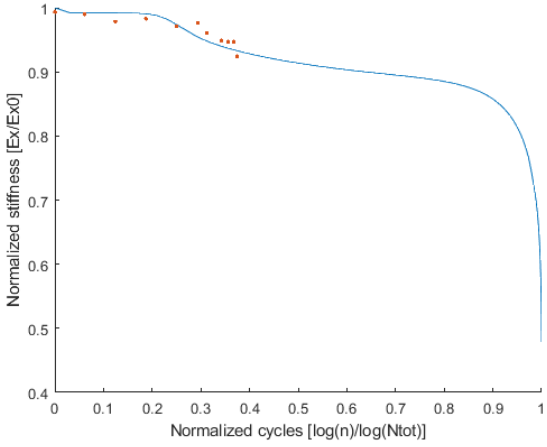

(c)

Figure 3.2: Stiffness degradation plotted against the number of applied cycles for an AS4/3501-6 laminate subjected to a) 85%, b) 53% and c) 28% of the ultimate load. The dots indicate the experimental parameters and line gives the predicted values. Data is take from [22]

3.2. VALIDATION STUDY OF LIFETIME ESTIMATION

3.2.1. COMPARISON WITH AS4/APC-2 $[-45/0/+45/0]_{2s}$ ORTHOTROPIC LAMINATE

Michel et al. [24] performed a set of high cycle longitudinal fatigue tests on AS4/APC-2 laminates. The idea was to quantify the S-N curve behaviour of AS4/APC-2 laminates for variety of different layups and loading conditions. In order to quantify this multiple $[-45/0/+45/0]_{2s}$ specimens were loaded in unidirectional tension fatigue at a range of different stresses. Because it is expensive and time consuming to test specimens above 10^6 cycles only a small number of samples was tested beyond this range, decreasing the confidence in the results. The results show some results for specimens tested up to 10^9 cycles. Table 3.3 shows the material properties of the unidirectional AS4/APC-2 plies used to calculate the fatigue life of the specimen.

Property	**Value [unit]**
E_{11}	138 [GPa]
E_{22}	10.2 [GPa]
G_{12}	5.7 [GPa]
ν_{12}	0.3 [-]
X_T	2068 [MPa]
X_C	1206 [MPa]
Y_T	86 [MPa]
Y_C	200 [MPa]
S_{12}	188 [MPa]

Table 3.3: Material properties AS4/APC-2 [24]

Table 3.4 shows the predicted fatigue lifetime using the progressive damage model compared to the experimental data from Michel et al. The results progressive damage model underestimates the performance of the orthotropic specimen for all of the applied stress levels. At the lower stress levels the prediction is approximately 2 orders of magnitude lower than the experimental results. However, the prediction of the fatigue life above for 10^6 cycles, becomes less conservative. Also, the experimental results are extracted from a small number of samples this means that the results could lie within the experimental scatter of the specimens.

Applied Stress [MPa]	**Experiments [cycles]** (Data from [24])	**Predicted [cycles]**
835	10^4	$3.3 * 10^2$
650	10^6	$2.60 * 10^4$
360	10^9	$7.65 * 10^8$

Table 3.4: Experimental versus predicted results for the fatigue life of AS4/APC-2 $[-45/0/+45/0]_{2s}$ specimens subjected to tension fatigue loading

3.2.2. COMPARISON WITH T800H/3631 $[45/0/-45/90]_s$ QUASI-ISOTROPIC LAMINATE

In a paper written by Hosoi et al. [25] a set of unidirectional fatigue life experiments has been performed on T800h/3631 laminates. They quantified the S-N curve behaviour of T800H/3631 laminates for variety of different layups and loading conditions. In order to determine this S-N curve behaviour the quasi-isotropic $[45/0/-45/90]_s$ specimens were loaded in unidirectional tension fatigue at a range of different stresses. Table 3.5 shows the material properties of the unidirectional T800H/3631 cfrp plies used to calculate the fatigue life of the specimen.

Property	**Value [unit]**
E_{11}	165 [GPa]
E_{22}	8.0 [GPa]
G_{12}	4.2 [GPa]
υ_{12}	0.32 [-]
X_T	2100 [MPa]
X_C	1540 [MPa]
Y_T	84 [MPa]
Y_C	280 [MPa]
S_{12}	126 [MPa]

Table 3.5: Material properties T800H/3631 [25]

The fatigue lifetime is predicted using the progressive damage model and compared to the experimental data from Hosoi et al. in table 3.6. The results show that the progressive damage model severely underestimates the performance of the quasi-isotropic specimens for all of the applied stress levels. It can be noted that with a decrease in stress level the predictions become more and more conservative. For a stress level of 625 and 585 MPa the experiments give a fatigue life that is between 1 and 2 orders of magnitude higher than the prediction. At the stress level of 540 MPa the difference between experiments and prediction becomes higher than 2 orders of magnitude. The expectation is that apart from the experimental scatter, this is also caused by an error in the picked fatigue life parameters. Section 3.3 shows that for increasingly higher fatigue lives the sensitivity with respect to the fatigue life parameters is increased.

Applied Stress [MPa]	**Experiments [cycles]** (Data from [25])	**Predicted [cycles]**
625	10^4	$4.6 * 10^2$
585	10^5	$9.9 * 10^2$
540	10^6	$6.0 * 10^3$

Table 3.6: Experimental versus predicted results for the fatigue life of T800H/3631 $[45/0/-45/90]_s$ specimens subjected to tension fatigue loading

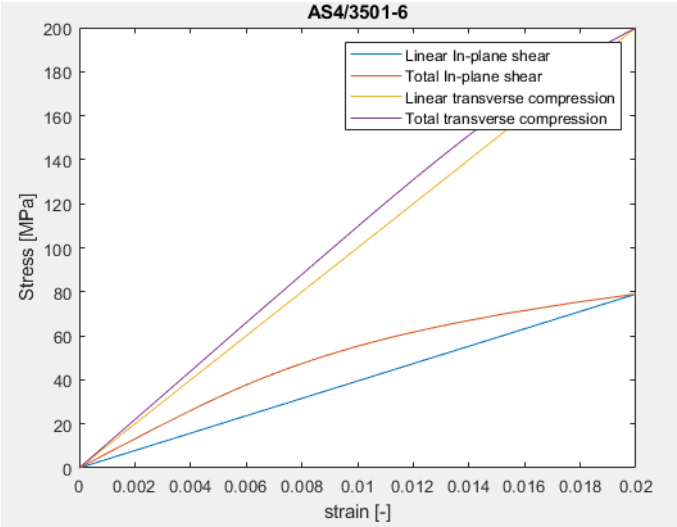

Figure 3.3: Comparison of non-linear and linear stress-strain curves for AS4/3501-6 cfrp. The non-linear data is taken from Kaddour et al. [26]

3.3. PARAMETER SENSITIVITY STUDY

NON-LINEAR STRESS-STRAIN CURVE CORRECTION

Sections 3.2.1 and 3.2.2 show that the fatigue life estimated by the progressive damage model is underestimating the results from the experiments quite drastically. One of the potential reasons is that in the fatigue life estimation model from equation C.1 it is assumed that the stress-strain curve for the longitudinal, transverse and shear direction are linear-elastic. This affects the predicted strain energy density (i.e. the area underneath the stress-strain curve) slightly. For longitudinal compression, transverse tension/compression and shear the stress strain curve is non-linear so the area underneath the stress-strain curve is slightly larger than for a linear stress-strain curve. Figure 3.3 shows that for transverse compression the non-linear behaviour is less than that of the shear stress-strain curve. The linear elastic strain energy density is 0.8 of the total for the in-plane shear and 0.93 for the transverse compression case. The higher the non-linearity of the stress-strain curve, the area difference tends more towards a difference of 0.5 for the linear area with respect to the total. According to the model the increase in lifetime of the $[0/90_2]_s$ laminate is just a few percent. Even if the area underneath the curve is increased by a factor of 2, the lifetime only increases by around 30%. This can be seen in figure 3.4. for this specific laminate the increase in lifetime of the specimen is relatively small because the failure is mainly dominated by the longitudinal 0 degree plies and because these have a roughly linear stress strain curve there is no correction required for the area underneath the curve.

It is in general difficult to find all of the required material parameters including stress-strain curve data for the materials that have been tested for fatigue. Especially considering that each time a batch of specimen is manufactured, the material properties will

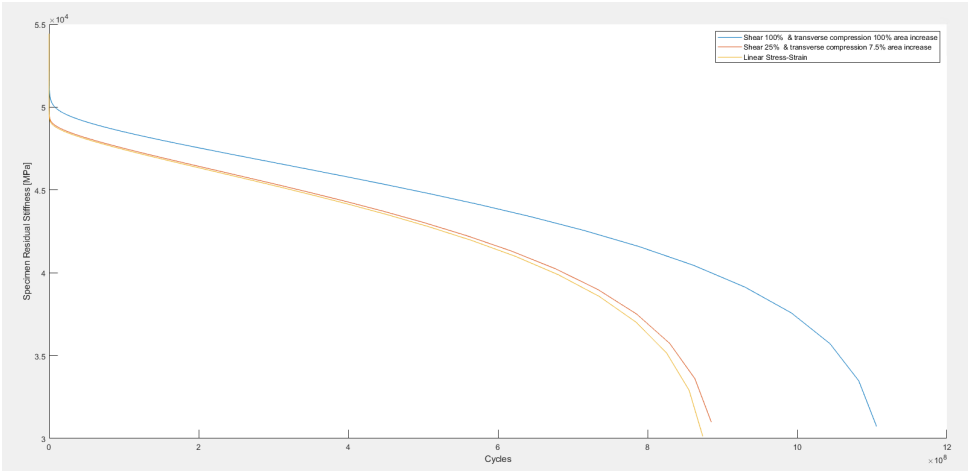

Figure 3.4: Comparison of the effect of the non-linearity correction on the degradation of the AS4/3501-6 $[0/90_2]_s$ laminate subjected to a 360 MPa fatigue load.

differ even if all production methods and environmental variables stay the same. Since for almost all fatigue specimens it is possible to find the initial stiffness and strength, it is required to assume the curve is linear and apply a correction. Since for most specimens it is also unknown what the ultimate strains are, there is also another way to correct for this non-linearity. The, ultimate strain is estimated by equation 3.1. In figure 3.5, the area underneath the linear curve generated with the calculated ultimate strain is compared with the non-linear stress-strain curve acquired from Chen et al. [27]. If the actual stress strain curve is almost linear the area ratio will tend to 1, however for a highly non-linear stress strain curve such as the one for the in-plane shear curve shown below this ratio can get a lot higher. For the curves below the area fraction of linear/non-linear stress strain curves is around 0.2, 0.9 and 0.9 for the in-plane shear, transverse compression and transverse compression respectively. If this difference fraction is used to compensate for this non-linear behaviour in the stress-strain curve the estimated fatigue lifetime will increase.The increase in ultimate strain energy density in the denominator will increase the expected fatigue lifetime to come out of the equation. Figure 3.6 shows the difference in fatigue lifetime prediction between the corrected and the non-corrected fatigue life estimate. The difference between the corrected and non-corrected life estimates is only marginal. This can again be attributed to the fact that failure is mainly dominated by the longitudinal 0 degree plies and because these have a roughly linear stress strain curve there is no correction required for the area underneath the curve.

$$\epsilon_u = \frac{\sigma_u}{E} \tag{3.1}$$

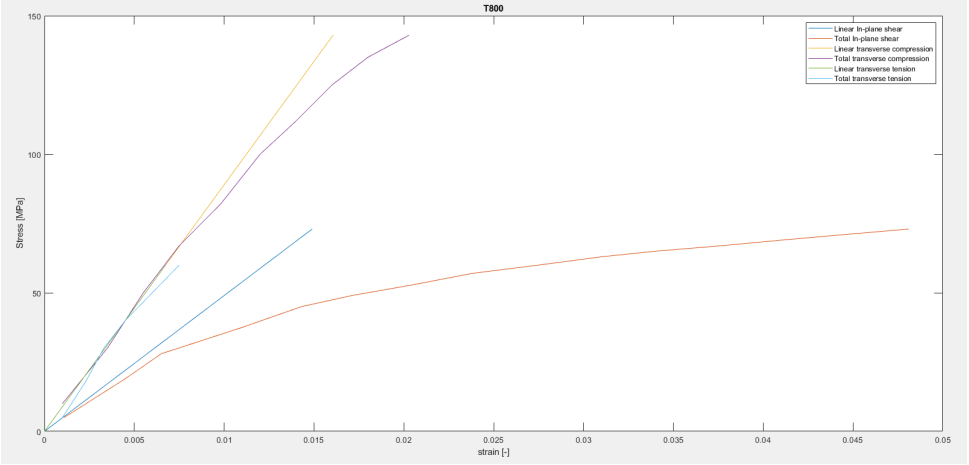

Figure 3.5: Comparison of non-linear and linear stress-strain curves for T800h/3631 cfrp. The non-linear data is taken from Chen et al. [27]

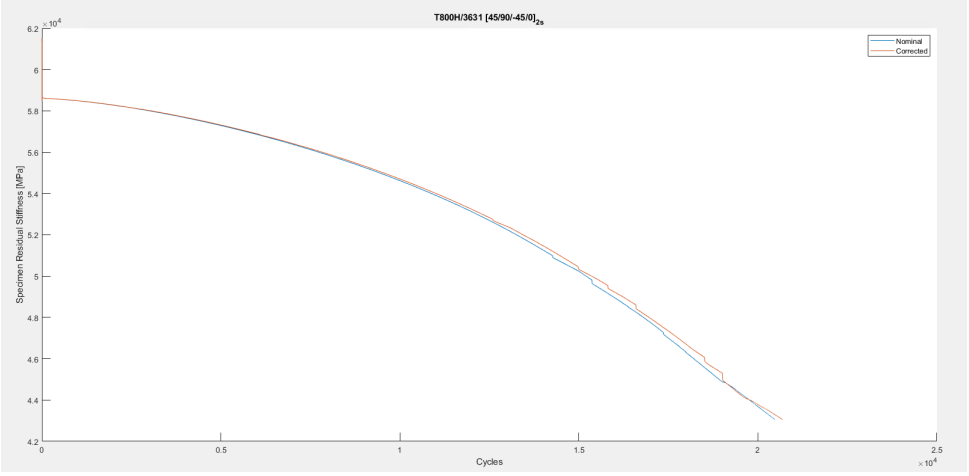

Figure 3.6: Comparison of the effect of the non-linearity correction on the degradation of the T800h/3631 $[45/90/-45/0]_{2s}$ laminate subjected to an arbitrary fatigue load.

Parameters	Tension	Compression
α_{11}	0.473	0.025
α_{22}	0.1255	0.0011
α_{12}	9.11	9.11
β_{11}	10.03	49.03
β_{22}	9.6287	67.36
β_{12}	0.16	0.16
λ_{11}	14.57	14.57
λ_{22}	14.77	14.77
λ_{12}	0.7	0.7
γ_{11}	0.3024	0.3024
γ_{22}	0.1155	0.1155
γ_{12}	11.0	11.0
a	-0.0971	-0.026
K	1.028	1.028

Table 3.7: Nominal set of curve fitting parameters taken from [28] and [29] for the degradation model parameters and fatigue life model parameters respectively.

MODEL PARAMETER SENSITIVITY

In this section the sensitivity of the progressive damage model with respect to the degradation and fatigue life parameters is studied. Since the fatigue life function and the degradation function both use sets of empirically determined parameters, it is critical to understand the influence these have on the prediction given by the model. For the degradation model λ, γ, α and β are the experimental curve fitting parameters. They are given in equations D.2 and D.3. The nominal values are taken from the paper by Shokrieh et al. [28]. This paper determines these parameters by fitting the curves to experimental data for the same AS4/3501-6 graphite epoxy laminate. For the fatigue life model K and a are the experimental parameters given in equations C.16, C.17 and C.18. The nominal values are taken from paper by Meljej et al. [29].

The way this parameter sensitivity study is performed is by differentiating the final results (i.e. the failure cycle of the specimen) with respect to the curve fitting parameters displayed in table 3.7. Since this is a numerical analysis instead the difference is taken between results with the nominal parameters used as input and the results with the changed parameters as input. If this difference is divided by the difference in parameter values this will give the linearized slope of the results with respect to the parameter value. This gives the sensitivity of the results with respect to this parameter. To determine sensitivity to each parameter separately, the parameters are individually increased by 10% whilst the other parameters are kept constant and equal to their nominal values. The equations to determine the sensitivity numerically with respect to a change in parameters is given in equations 3.2, 3.3 and 3.4. Where $f(a*1.1)$ is the failure cycle as a function of the increased parameter a and $f(a)$ is the failure cycle as a function of nominal parameter a.

$$\Delta_{Fail} = f(a*1.1) - f(a) \tag{3.2}$$

$$\Delta_{Parameter} = a * 1.1 - a \tag{3.3}$$

$$slope = \frac{\Delta_{Fail}}{\Delta_{Parameter}} \tag{3.4}$$

This laminate was chosen because similar to the propeller it has a quasi-isotropic layup, there is fatigue life data available [25] and stress-strain curve data was available to test non-linear stress-strain curve correction as was discussed above. Table 3.8 gives the sensitivity of all of the progressive damage model fitting parameters with respect to the failure cycle of a T800h/3631 quasi-isotropic $[45/0/-45/90]_s$ laminate subjected to a 540 MPa fatigue load, with R = 0.1. It shows that the sensitivity of failure cycle with respect to the parameters is 2 and 3 orders of magnitude higher for the a and K parameters respectively compared to the other parameters. This is because these parameters directly influence the predicted residual fatigue life using equations C.16, C.17 and C.18. The way these parameters are used in the equations mean that the K parameter shifts the S-N curve vertically and the a parameter gives the slope of this curve. The sensitivity of some of the parameters are negative, one of the reasons for this is due to the interaction between the different elements and plies. If one ply is has a reduced stiffness then a neighbouring ply will be subjected to increased stress. Vice versa if the stiffness remains higher for longer (i.e. the λ values are increased) then plies will have a delayed but more sudden degradation of the stiffness, leading to increased stresses in that ply over a longer period. This in turn decreases the material more quickly for these plies. Due to the complex nature of this interaction it is difficult to determine what causes the positive sensitivity for some parameters and a negative sensitivity for others. It is recommended for future research to focus on the interaction between the models and different failure modes to get a better picture of the underlying damage mechanics at play. Tables 3.9 and 3.10 show the parameter sensitivity at stress levels of 585 and at 625 MPa respectively. It shows that for a decrease in fatigue life progressive damage model becomes less sensitive to a change in parameters. The sensitivities with respect to the degradation model parameters were not determined at these higher stress levels because the initial analysis already showed that the sensitivity for the fatigue lifetime model parameters was several orders of magnitude higher. However it is important to note that for increased stress levels the sensitivity for the degradation model parameters might increase respectively to the fatigue lifetime model parameters. In other words, the assumption that the model is most sensitive to the fatigue lifetime parameters might not be entirely correct and should be investigated in further research.

Table 3.8: Sensitivity study of failure cycle with respect to experimental parameters for T800h/3631 quasi-isotropic $[45/0/-45/90]_s$ laminate subjected to a 540 MPa fatigue load with R = 0.1

	Failure Cycle	Δ_{Fail}	$\Delta_{Paramater}$	$\Delta_{Fail}/\Delta_{Paramater}$
Nominal	6007	-	-	-
α_{11}	5997	-10	0.0473	$-2.1*10^2$
α_{22}	6029	22	0.01255	$1.8*10^3$
α_{12}	6015	8	0.911	$8.8*10^0$
β_{11}	5980	-27	1.003	$-2.7*10^1$
β_{22}	5807	-200	0.963	$-2.1*10^2$
β_{12}	5998	-9	0.016	$-5.6*10^2$
λ_{11}	6648	641	1.457	$4.4*10^2$
λ_{22}	5994	-3	1.477	$-2.0*10^0$
λ_{12}	5820	-187	0.07	$-2.7*10^3$
γ_{11}	6213	206	0.03024	$6.8*10^3$
γ_{22}	5941	66	0.01155	$4.3*10^3$
γ_{12}	6025	18	1.1	$1.6*10^1$
a	2670	-3337	-0.00971	$3.4*10^5$
K	15798	9791	0.1028	$9.5*10^4$

Table 3.9: Sensitivity study of failure cycle with respect to experimental parameters for T800h/3631 quasi-isotropic $[45/0/-45/90]_s$ laminate subjected to a 585 MPa fatigue load with R = 0.1

	Failure Cycle	Δ_{Fail}	$\Delta_{Paramater}$	$\Delta_{Fail}/\Delta_{Paramater}$
Nominal	994	-	-	-
a	668	-326	-0.00971	$3.4*10^4$
K	2538	1544	0.1028	$1.5*10^4$

Table 3.10: Sensitivity study of failure cycle with respect to experimental parameters for T800h/3631 quasi-isotropic $[45/0/-45/90]_s$ laminate subjected to a 625 MPa fatigue load with R = 0.1

	Failure Cycle	Δ_{Fail}	$\Delta_{Paramater}$	$\Delta_{Fail}/\Delta_{Paramater}$
Nominal	466	-	-	-
a	268	-198	-0.00971	$2.0*10^4$
K	1205	739	0.1028	$7.1*10^3$

Tables 3.11, 3.12 and 3.13 show the sensitivity of the orthotropic $[-45/0/+45/0]_{2s}$ AS4/APC-2 laminate for the failure cycle with respect to the fatigue life model parameters a and K. Similar to the quasi-isotropic laminate discussed above, this laminate shows a similar increase in sensitivity of the progressive damage model for lower stress levels and a decrease for higher stress levels. What can also be noted is that for a decreasing stress level the sensitivity of the a parameter increases more than the sensitivity of the K value. This is to be expected since the a parameter represents the slope of the estimated S-N curve in the progressive damage model.

Table 3.11: Sensitivity study of failure cycle with respect to experimental parameters for $[-45/0/+45/0]_{2s}$ orthotropic laminate subjected to a 360 MPa fatigue load with R = 0.1

	Failure Cycle	Δ_{Fail}	$\Delta_{Paramater}$	$\Delta_{Fail}/\Delta_{Paramater}$
Nominal	765250000	-	-	-
a	125150000	-640100000	-0.00971	$6,6 * 10^9$
K	1815800000	1050550000	0.1028	$1,0 * 10^9$

Table 3.12: Sensitivity study of failure cycle with respect to experimental parameters for $[-45/0/+45/0]_{2s}$ orthotropic laminate subjected to a 650 MPa fatigue load with R = 0.1

	Failure Cycle	Δ_{Fail}	$\Delta_{Paramater}$	$\Delta_{Fail}/\Delta_{Paramater}$
Nominal	26080	-	-	-
a	10628	-15452	-0.00971	$-1.6 * 10^6$
K	62267	36187	0.1028	$3.5 * 10^5$

Table 3.13: Sensitivity study of failure cycle with respect to experimental parameters for $[-45/0/+45/0]_{2s}$ orthotropic laminate subjected to a 835 MPa fatigue load with R = 0.1

	Failure Cycle	Δ_{Fail}	$\Delta_{Paramater}$	$\Delta_{Fail}/\Delta_{Paramater}$
Nominal	328	-	-	-
a	197	-131	-0.00971	$1.3 * 10^4$
K	807	479	0.1028	$7,9 * 10^3$

The sensitivity of residual stiffness with respect to a change in experimental parameters λ_{11}, λ_{22} and λ_{12} is plotted in figure 3.7. This figure shows that there is a reduction in stiffness drop if the λ_{11} parameter is increased by 10%. This can be explained by looking at equation D.2, an increase in λ raises the power of the normalized applied cycles. This causes a delay in reduction of longitudinal stiffness and causes the reduction to become more sudden towards the end. In the case of this quasi-isotropic laminate this delays the reduction of the load carrying capacity of the 0° plies. Which in turn decreases the reduction in strength of the neighbouring plies, leading to a longer fatigue life. The other parameters did not significantly influence the residual stiffness of the specimen over its life.

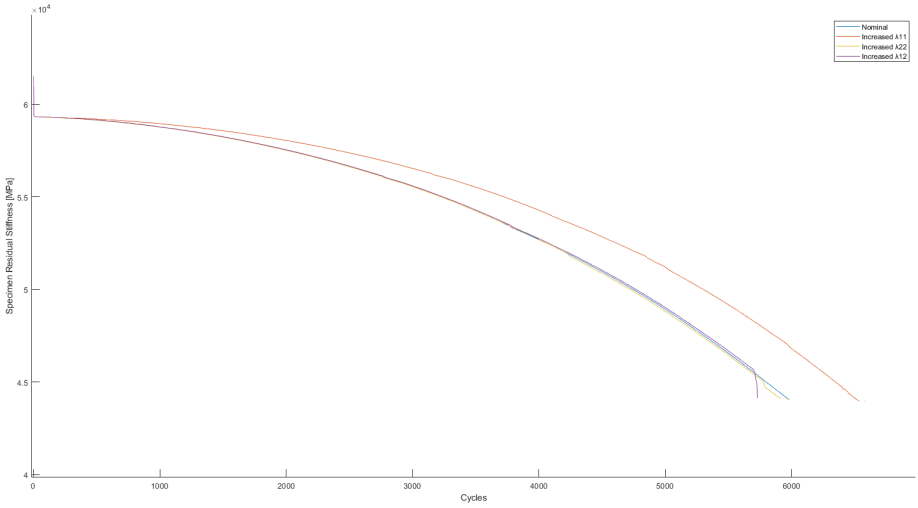

Figure 3.7: Sensitivity of residual stiffness with respect to a change in experimental parameters λ_{11}, λ_{22} and λ_{12} for T800h/3631 quasi-isotropic $[45/0/-45/90]_s$ laminate subjected to a 540 MPa fatigue load with R = 0.1

It can be concluded that in order to get accurate predictions from this model it is of critical importance that the curve fitting parameters included in the progressive damage model should be carefully chosen or determined, especially for fatigue cycles in the high cycle fatigue range (>10^6 cycles). The parameters that are used to determine the shape of the material degradation curves λ, γ, α and β are less important however. Due to their phenomenological nature they give a more realistic shape to the material degradation curves, however the effect this has on the results is only marginal. These parameters effectively only cause the damage creation to be more gradual or more sudden within preset bounds. The initial bounds are represented by the initial undamaged strength and stiffness and the final bounds are set by the applied stress and the expected final stiffness. For a more detailed overview of these material degradation model see appendix D.

4

RESULTS & EVALUATION

This chapter is dedicated to the results of the progressive damage model applied to the composite marine propeller as well as the evaluation of the results. Section 4.1 shows the results of the simulation of the fatigue damage progression throughout propeller blade. This section also describes the increase in propeller blade tip deflection due to formed damage. Section 4.2 gives an evaluation of the results and what they mean for the performance of the propeller.

4.1. RESULTS

Figure 4.1 shows the increase in deflection as a function of applied cycles. Because the applied pressure distribution is assumed to be constant throughout the life of the propeller blade, the increase in deflection is caused by the decrease in blade stiffness. The increase in propeller blade tip deflection can be seen to progress faster for the first few cycles due to matrix cracking in the transverse plies near the stress hot spot locations. After this initial redistribution of stress the deflection remains approximately constant.

To make sure that the model gives a consistent fatigue life prediction for the propeller two different approaches have been tested. The first approach was to run the model from 0 to 10^{10} cycles in one go. The other was to run the model until 10^8 cycles and extract the reduced stiffness and strengths of all the elements and the plies within those elements. These reduced material parameters were then used as an input for the run from 10^8 to 10^{10} cycles to check if the results would overlap. Figure 4.2 indeed shows that the results from the two approaches perfectly overlap. It can therefore be concluded that the progressive damage model is consistent. The reason for this perfect overlap is that a artificial method is used to make the model consistent, this method is called the cumulative damage approach and is explained in more detail in appendix D. This method is a way to fix inconsistencies in the material degradation model, however it does not have any physiological basis in fatigue modelling.

The increase in deflection is caused by the increase in damage created throughout the blade which is represented by figures 4.3 and 4.4 for the damage created on the pressure and suction side of the blade respectively. Care must be taken when analysing the

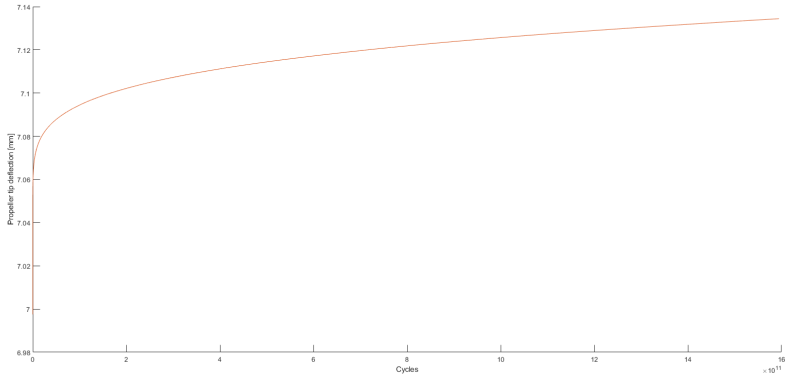

Figure 4.1: Propeller blade tip deflection as a function of applied cycles

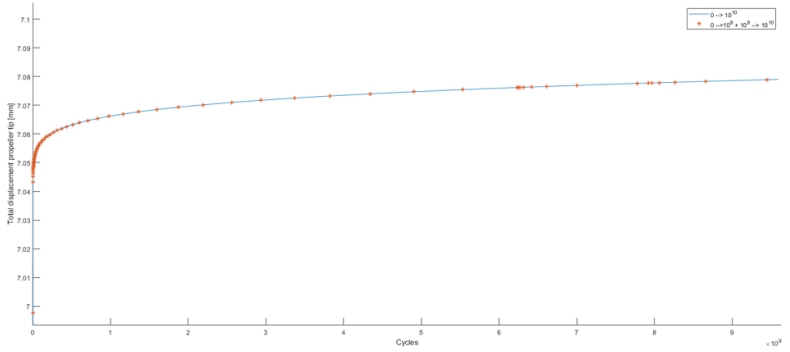

Figure 4.2: Propeller blade tip deflection as a function of applied cycles determined for a continuous run and a split run

figures due to the changing axes. The axes were changed on purpose to get the maximum information out of them. Similar to the hot-spot location mentioned in the thesis by Zhang [8], the damage starts to form near the leading edge of the blade. With an increasing number of cycles the damage starts progressing further outwards from this location and also start initiating throughout the rest of the propeller blade. It can be noted that even for 10^{12} cycles the maximum damage in most parts of the blade are still below 0.1.

The damage progression was shown to be very small for the determined load case of the propeller. So in order to capture more noticeable damage behaviour, the pressure load was increased by a factor of 3. Figures 4.5 and 4.6 show the fatigue damage progression on the propeller after 10^6, 10^7 and 10^8 cycles for this increase in pressure. It is a definitive increase in damage when compared to the normal load case. Already after 10^6 cycles the amount of damage formed on the propeller blade is more than at the 10^{12}

cycles at normal pressure load. The formation of damage is more pronounced on the pressure side of the blade than on the suction side. On the pressure side of the blade most of the elements are loaded in tension-tension fatigue, compared to compression-compression fatigue on the suction side. The damage indicated in the figures is the maximum damage throughout the skin of the propeller blade, that means that the maximum damage indicated in these figures the highest damage of one of the plies on that indicated elements. In this case most of the elements indicate the damage that occurred in plies that are oriented at roughly 90° with respect to the radial direction of the propeller. These plies failed due to the formation of transverse matrix cracks on the plies. Since the matrix has better performance in compression than tension it makes sense that the damage on the suction side is less pronounced than on the pressure side of the blade. Even though the fatigue damage is significantly higher, the increase in deflection with respect to the initial value is only around 0.8 mm after 10^8 cycles.

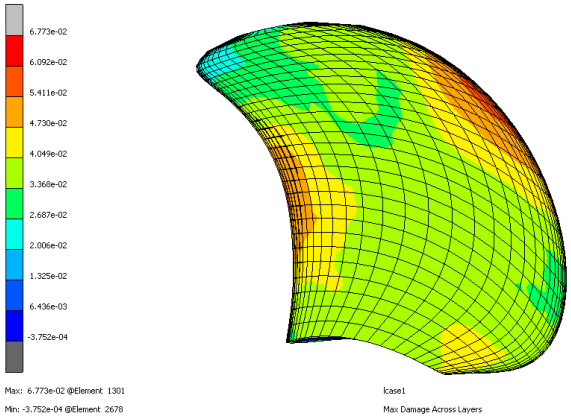

(a)

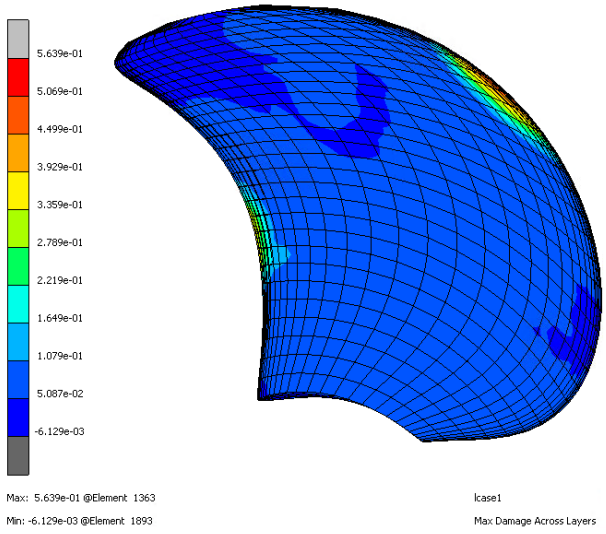

(b)

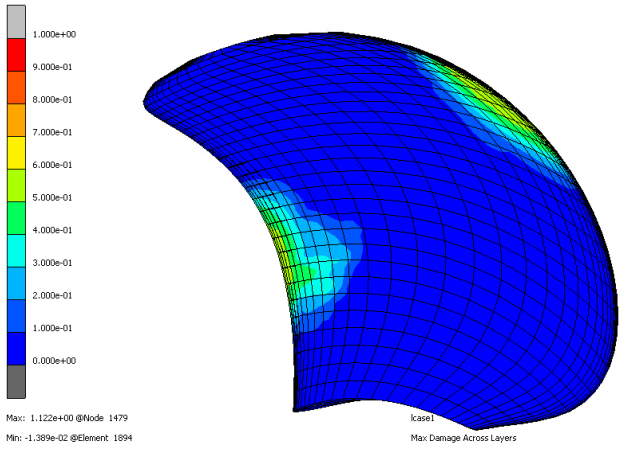

(c)

Figure 4.3: Damage progression on the pressure side of the blade rated from 0 for no damage to 1 for failure after a) 10^6 cycle b) 10^{10} cycle and c) 10^{12} cycles

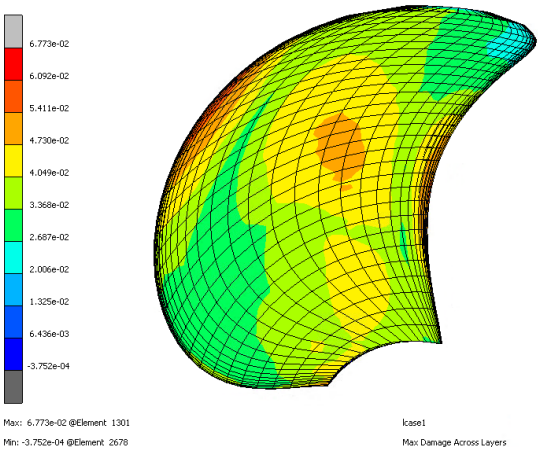

(a)

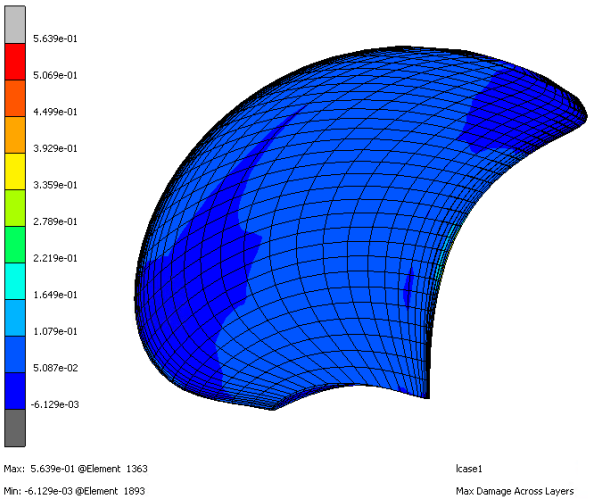

(b)

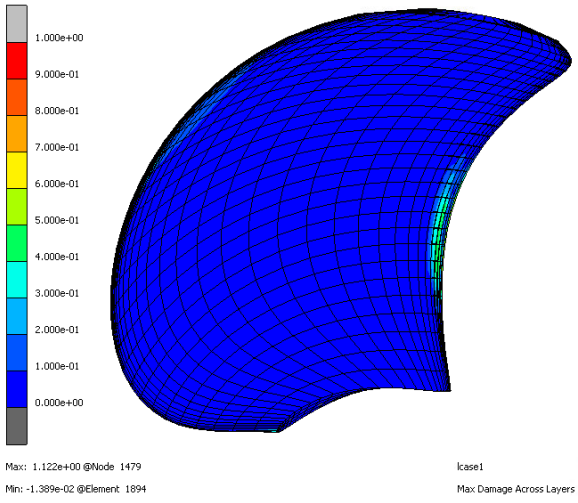

(c)

Figure 4.4: Damage progression on the suction side of the blade rated from 0 for no damage to 1 for failure after a) 10^6 cycle b) 10^{10} cycle and c) 10^{12} cycles

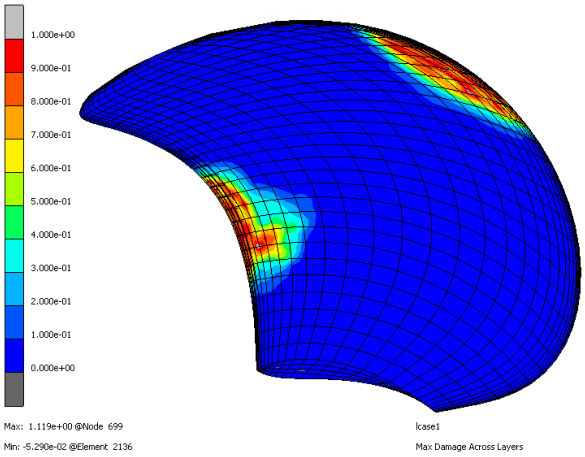

(a)

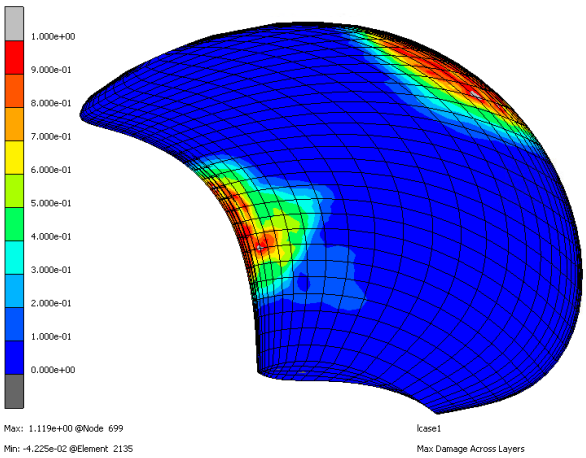

(b)

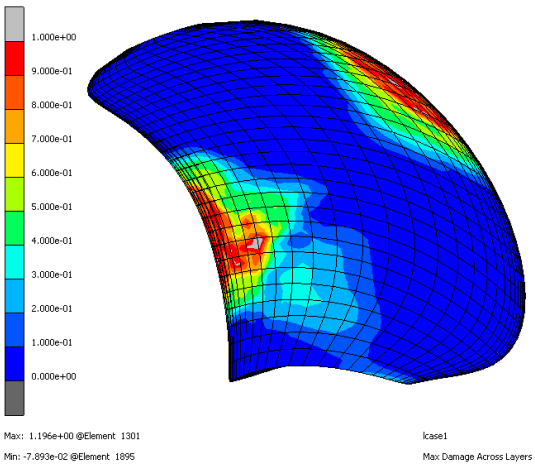

(c)

Figure 4.5: Damage progression on the pressure side of the blade rated from 0 for no damage to 1 for failure after a) 10^6 cycle b) 10^7 cycle and c) 10^8 cycles at 3 times the normal pressure load

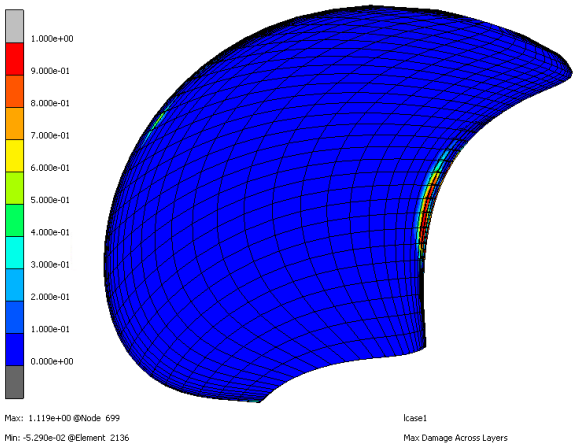

(a)

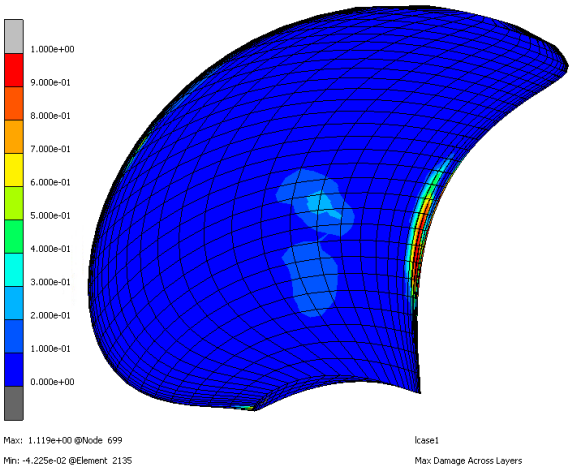

(b)

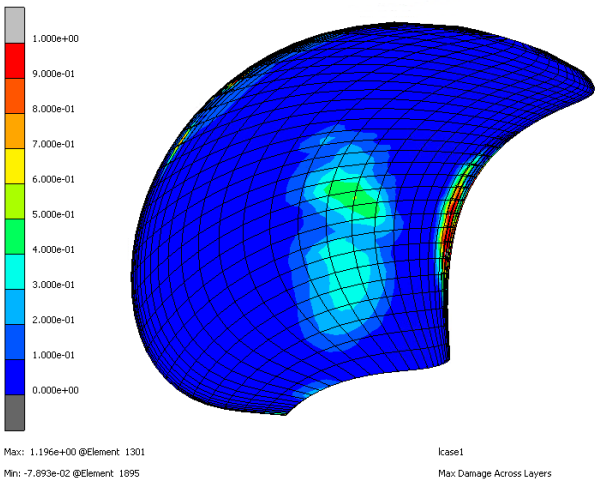

(c)

Figure 4.6: Damage progression on the suction side of the blade rated from 0 for no damage to 1 for failure after a) 10^6 cycle b) 10^7 cycle and c) 10^8 cycles at 3 times the normal pressure load

4.2. EVALUATION

The results show that according to the progressive damage model the damage formed on the propeller blade due to the fatigue loading is small. Even for very high fatigue cycles the damage increase is only marginal. One possible explanation for this is that most of the damage is formed near the leading and trailing edges of the propeller where the stress hot-spots are located. Due to the curved geometry of the element at the leading edge have a much greater length than width, they have a large aspect ratio. The accuracy of the finite element model deteriorates with larger aspect ratios, which possibly influences the results of the progressive damage model as well. It is also important to note that there are also stress concentrations near the root of the blade where the boundary conditions is assumed as fixed due to the high difference in stiffness between the blade and the hub it is attached to. Realistically the stress concentrations might not be as high as predicted by the FEM. Another explanation is that the stresses in the blade are really low. This can be deducted by analyzing figure 2.12, which shows that for the stress hot-spot locations the failure indices are at maximum 0.326. For the areas that carry most of the loads, such as the elements near the root of the blade the failure indices go no higher than 0.06. This means that the plies in these elements are approximately experiencing a stress level that is only 6% of the ultimate stress that the plies should be able to cope with. According to experimental data from literature if the applied maximum stress percentage is this low, the fatigue life of the specimen is really high. One example of this is displayed in figure 4.7. It shows the S-N diagram of a T800H/3631 $[45/0/-45/90]_{2s}$ quasi-isotropic laminate subjected to up to 10^9 cycles. The figure shows that no failure is expected to occur at a stress level of 0.3 well above 10^9 cycles. It also shows that at this stress level there is more than likely no damage initiation at all. Similar patterns in S-N diagrams can be found for other laminates subjected to high cycle fatigue in [24][25][30].

At 10^{12} cycles the composite propeller rotating at 600 rpm could theoretically last more than 3000 years even if it runs continuously for that time span. It is important to not that this only considering structural failure of the propeller blade and not considering the loss in hydrodynamic efficiency. Even slight changes in the stiffness create a difference in the pressure distribution on the blade leading to a difference in hydrodynamic performance. So it could be that even though the propeller structurally would last over 10^{12} cycles, it fails earlier due to the loss of its hydrodynamic performance.

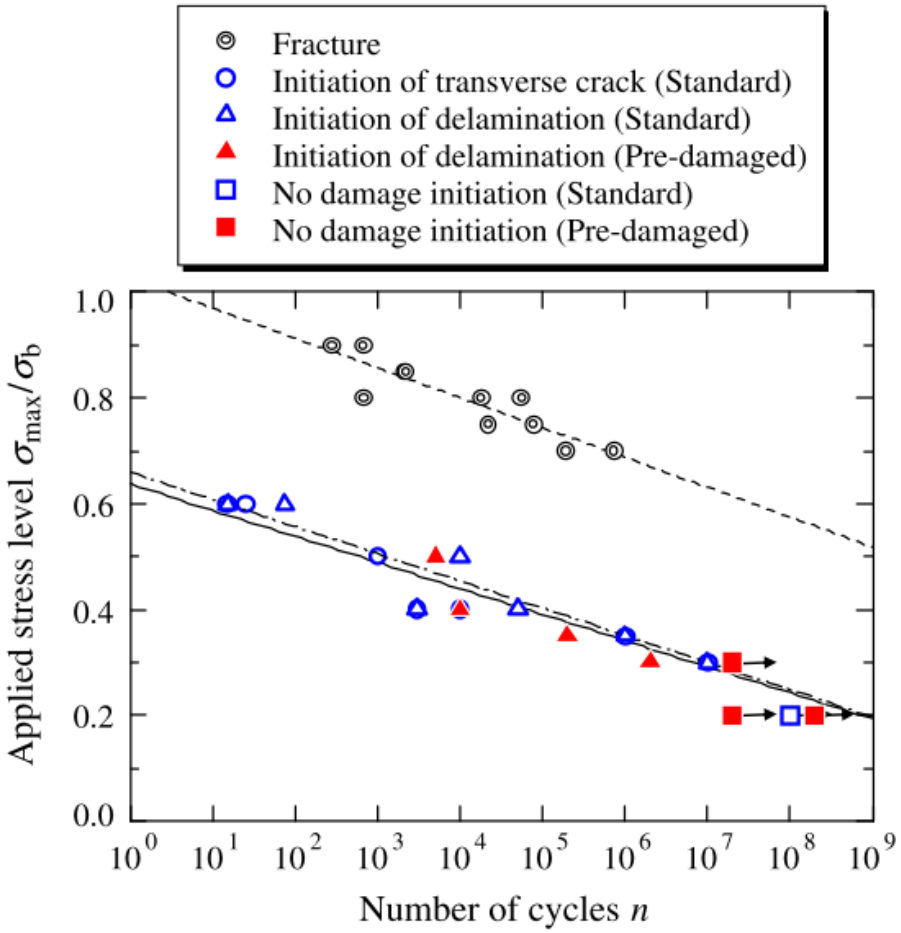

Figure 4.7: S-N diagram for specimen failure, crack initiation of transverse cracks and delamination up to 10^9 cycles for T800H/3631 $[45/0/-45/90]_{2s}$ quasi-isotropic laminate [25]

5

Conclusion & Recommendations

5.1. Conclusion

'What is the estimated fatigue lifetime of a composite marine propeller subjected to a predefined pressure load?', The answer to this question is according to the results at least 10^{12} cycles under the considered loading condition. If the propeller would rotate at 600 rpm for 24 hours per day it would last over 3000 years. The reason behind this is that the combination of the applied pressure load and the strength of the carbon fiber propeller is such that the stresses in each ply are really low. These low stresses create almost no damage throughout the propeller blade even for ultra high cycles. In order to capture more noticeable damage behaviour, the pressure load was increased by a factor of 3. In this case, the damage in the propeller became more pronounced below 10^{12} cycles. Even in the first few cycles elements started to fail due to the higher stress levels. The damage initiated due to transverse matrix cracks in the plies near the stress hot-spot locations on the blade near the leading and trailing edge. From there, matrix cracks start to form in neighbouring plies, spreading outwards. The effect on the propeller blade tip deflection remains limited since the affected plies are oriented at roughly 90° to the main radial direction and the highest loads are carried by the plies at a 0° orientation. The highest loads are carried by the elements near the root of the propeller. However they remain largely unaffected by the fatigue loads.

Additionally there are some important points to note on the results. Firstly, the validation study of the progressive damage model shows that for these high fatigue cycles the results become more sensitive to the curve fitting parameters of the material degradation and the fatigue life models. And since these parameters are not determined for the exact laminate used in the analysis it can lead to an overestimation of the results. Secondly, the model does not include the delamination as a failure mechanism. This can also lead to an overestimation in expected fatigue life. Thirdly, the model does not include salt water intrusion into the composite propeller. If this is incorporated in the

progressive damage model, it will probably lead to a decrease in predicted fatigue life. Furthermore, the applied pressure distribution remains constant throughout the entire fatigue life of the blade whereas normally the pressure distribution would change due to a change in blade stiffness and different operating conditions. This pressure distribution was imported from previous research, though it is not stated if this is the most critical loading condition. Lastly, the blade to hub connection is now modelled as an infinitely stiff boundary condition at the root of the blade. This is not realistic since real life structures will always have a finite stiffness.

5.2. RECOMMENDATIONS

5.2.1. PRESSURE DISTRIBUTION

Studying other loading conditions of the propeller is recommended. In current research the propeller is considered to work in a non-uniform wakefield, which was generated from the straight path sailing of the considered vessel in calm water at constant speed of 10.4 knots. The other manoeuvres and sailing conditions would result in more complex loads that can influence the fatigue lifetime of the composite propeller. One critical loading condition to be considered is when reverse thrust is applied. Since the propeller design is optimized for forward sailing. Furthermore, the pressure distribution will also change due to a loss in stiffness of the propeller blade. So over the propellers lifetime the pressure distribution will change and this is not incorporated into the model.

5.2.2. EFFECT OF SEAWATER ON FATIGUE OF THE PROPELLER BLADE

It is recommended to take into account the effect of seawater intrusion on the fatigue life performance of the blade. This model does not take this into account, but the expectation is that seawater intrusion negatively affects the fatigue performance of the propeller. This can lead to an overestimation of the fatigue performance of the blade. One of the methods that can be used to do this is by reducing the material properties by a certain factor determined from static fatigue tests. If the fatigue failure stresses are normalized with respect to the ultimate stress of the material in a quasi-static test, the S-N curves overlap for different types of water saturation and dry specimens. This indicates that for different types of saturation, the damage mechanisms remain approximately constant [31][32]. It also indicates that if the dry S-N curve is known, together with the ratio between ultimate tensile strengths of dry versus wet specimens, a pretty good estimate can be made of the S-N curve for a saturated specimen. This could save a significant amount of time since one does not need to artificially increase the seawater content for a considerable amount of specimens to gain the required fatigue performance curves.

5.2.3. CURVE FITTING OF EXPERIMENTAL PARAMETERS

In the parameter sensitivity study it was shown that the fatigue results are sensitive to the a and K parameters from the fatigue life model. This sensitivity is also shown to increase with an increasing number of cycles. It is therefore recommended to fit these parameters for the material used in the marine propeller in order to get a more accurate prediction.

5.2.4. PROGRESSIVE DAMAGE MODEL VALIDATION

It is recommended to perform extra model validation studies on the material used in the propeller blade. Even though this is a time consuming and expensive process it will give more relevant and accurate results. Especially considering that most of the fatigue data misses a part of the required data to correctly apply the model.

5.2.5. FULL SCALE VALIDATION

In order to validate the model on full scale, a full scale experiment should be performed. Using in-situ measurements by acoustic emission sensors the damage type and location can be validated. The blade deflection measurements with optical sensors can be used to validate the reduction in stiffness of the blade and the predicted damage initiation locations.

5.2.6. HUB INTERACTION

Lastly it is recommended to put some effort in modelling the propeller blade to hub connection. Due to the sudden change in stiffness this is a source of high stress concentrations. Currently it is modelled as an infinitely stiff boundary condition at the root of the blade however this is not entirely realistic.

BIBLIOGRAPHY

[1] P. Maljaars. "Hydro-Elastic analysis of flexible marine propellers". PhD thesis. 2019, p. 165. ISBN: 9789055841745. DOI: 10.4233/uuid.

[2] J. Degrieck and W. Van Paepegem. "Fatigue damage modeling of fibre-reinforced composite materials: Review". In: *Applied Mechanics Reviews* 54.4 (2001), pp. 279–300. ISSN: 00036900. DOI: 10.1115/1.1381395.

[3] I.M. Daniel and A. Charewicz. "Fatigue damage mechanisms and residual properties of graphite/epoxy laminates". In: *Engineering Fracture Mechanics* 25.5 (1986), pp. 793–808. ISSN: 0013-7944. DOI: https://doi.org/10.1016/0013-7944(86)90042-1. URL: https://www.sciencedirect.com/science/article/pii/0013794486900421.

[4] P. M. Barnard, R. J. Butler, and P. T. Curtis. "Fatigue Scatter of UD Glass Epoxy, a Fact or Fiction?" In: 1985.

[5] W. Hwang and K.S. Han. "Cumulative Damage Models and Multi-Stress Fatigue Life Prediction". In: *Journal of Composite Materials* 20.2 (1986), pp. 125–153. DOI: 10.1177/002199838602000202.

[6] I.R. Farrow. "Fatigue of Composite Materials under Aircraft Service Loading". In: *Proceedings of the Institution of Mechanical Engineers, Part G: Journal of Aerospace Engineering* 210.1 (1996), pp. 101–107. DOI: 10.1243/PIME_PROC_1996_210_348_02.

[7] C. Peyrac, T. Jollivet, and N. Leray. "Self-heating Method for Fatigue Limit Determination on Thermoplastic Composites". In: *Procedia Engineering* 133 (2015). Fatigue Design 2015, International Conference Proceedings, 6th Edition, pp. 129–135. ISSN: 1877-7058. DOI: https://doi.org/10.1016/j.proeng.2015.12.639. URL: https://www.sciencedirect.com/science/article/pii/S1877705815045580.

[8] X. Zhang. *Short-term Structural Performance of Self-monitoring Composite Marine Propellers*. 2021. ISBN: 9789463842730. URL: https://repository.tudelft.nl/..

[9] Z. Hashin and A. Rotem. "A Fatigue Failure Criterion for Fiber Reinforced Materials". In: *Journal of Composite Materials* 7.4 (1973), pp. 448–464. ISSN: 1530793x. DOI: 10.1177/002199837300700404.

[10] M. M. Shokrieh and L. B. Lessard. *Progressive fatigue damage modeling of composite materials, Part I: Modeling*. 1998.

[11] Anastasios P. Vassilopoulos. *Fatigue life prediction of composites and composite structures*. 2010, pp. 1–552. ISBN: 9781845695255. DOI: 10.1533/9781845699796.

[12] Jt Fong. “What Is Fatigue Damage?” In: *ASTM special technical publications* (1982), pp. 243–266.

[13] E. N Eliopoulos and T. P Philippidis. “A progressive damage simulation algorithm for GFRP composites under cyclic loading . Part II : FE implementation and model validation”. In: *Composites Science and Technology* 71.5 (2011), pp. 750–757. ISSN: 0266-3538. DOI: 10.1016/j.compscitech.2011.01.025. URL: http://dx.doi.org/10.1016/j.compscitech.2011.01.025.

[14] A. I. Khan, S. Venkataraman, and I. Miller. “Predicting fatigue damage of composites using strength degradation and cumulative damage model”. In: *Journal of Composites Science* 2.1 (2018). ISSN: 2504477X. DOI: 10.3390/jcs2010009.

[15] C. Stens and P. Middendorf. “Computationally efficient modelling of the fatigue behaviour of composite materials”. In: *International Journal of Fatigue* 80 (2015), pp. 69–75. ISSN: 01421123. DOI: 10.1016/j.ijfatigue.2015.05.001. URL: http://dx.doi.org/10.1016/j.ijfatigue.2015.05.001.

[16] M. M. Shokrieh and F. Taheri-Behrooz. “Progressive fatigue damage modeling of cross-ply laminates, I: Modeling strategy”. In: *Journal of Composite Materials* 44.10 (2010), pp. 1217–1231. ISSN: 00219983. DOI: 10.1177/0021998309351604.

[17] K. I. Tserpes, P. Papanikos, G. Labeas, and S. Pantelakis. “Fatigue damage accumulation and residual strength assessment of CFRP laminates”. In: *Composite Structures* 63.2 (2004), pp. 219–230. ISSN: 02638223. DOI: 10.1016/S0263-8223(03)00169-7.

[18] E. N Eliopoulos and T. P Philippidis. “A progressive damage simulation algorithm for GFRP composites under cyclic loading . Part I : Material constitutive model”. In: *Composites Science and Technology* 71.5 (2011), pp. 742–749. ISSN: 0266-3538. DOI: 10.1016/j.compscitech.2011.01.023. URL: http://dx.doi.org/10.1016/j.compscitech.2011.01.023.

[19] Zia Javanbakht. *Advanced Finite Element Simulation with MSC Marc*. ISBN: 9783319476674.

[20] W Van Paepegem. “The cycle jump concept for modelling high-cycle fatigue in composite materials”. In: *Fatigue of Textile Composites*. Elsevier Ltd, 2015, pp. 29–55. ISBN: 9781782422815.

[21] I. M. Daniel, J. W. Lee, and G. Yaniv. “Damage mechanisms and stiffness degradation in graphite/epoxy composites”. In: *Sixth International Conference on Composite Materials and Second European Conference on Composite Materials*. 1987, pp. 4129–4138.

[22] J. W. Lee, I. M. Daniel, and G. Yaniv. “Fatigue Life Prediction of Cross-Ply Composite Laminates”. In: *Composite Materials: Fatigue and Fracture* 2nd (1989), pp. 19–28.

[23] I. M. Daniel and J. W. Lee. “Damage Development in Composite Laminates Under Monotonic Loading”. In: *Journal of Composites Technology Research* 12.2 (1990), pp. 98–102.

[24] S. A. Michel, R. Kieselbach, and H. J. Martens. “Fatigue strength of carbon fibre composites up to the gigacycle regime (gigacycle-composites)”. In: *International Journal of Fatigue* 28.3 (2006), pp. 261–270. ISSN: 01421123. DOI: 10.1016/j.ijfatigue.2005.05.005.

[25] A. Hosoi, J. Shi, N. Sato, and H. Kawada. “Variations of Fatigue Damage Growth in Cross-Ply and Quasi-Isotropic laminates Under High-Cycle Fatigue Loading *”. In: *Journal of Solid Mechanics and Materials Engineering* 3.2 (2009), pp. 138–149. DOI: 10.1299/jmmp.3.138.

[26] A S Kaddour, M J Hinton, P A Smith, and S Li. “Mechanical properties and details of composite laminates for the test cases used in the third world-wide failure exercise”. In: *Journal of Composite Materials* 47.20-21 (2013), pp. 2427–2442. DOI: 10.1177/0021998313499477. URL: https://doi.org/10.1177/0021998313499477.

[27] G. Chen and X. Suo. “Constitutive modeling of nonlinear compressive behavior of fiber reinforced polymer composites”. In: *Polymer Composites* 41.February 2019 (2020), pp. 182–190. DOI: 10.1002/pc.25358.

[28] M. M. Shokrieh and L. B. Lessard. “Progressive Fatigue Damage Modeling of Composite Materials, Part II: Material Characterization and Model Verification”. In: *Journal of Composite Materials* 34.13 (2000), pp. 1081–1116.

[29] V. G. Mejlej, D. Osorio, and T. Vietor. “An Improved Fatigue Failure Model for Multidirectional Fiber-reinforced Composite Laminates under any Stress Ratios of Cyclic Loading”. In: *Procedia CIRP* 66 (2017), pp. 27–32. ISSN: 22128271. DOI: 10.1016/j.procir.2017.03.303. URL: http://dx.doi.org/10.1016/j.procir.2017.03.303.

[30] P. Shabani, F. Taheri-Behrooz, S. S. Samareh-Mousavi, and M. M. Shokrieh. “Very high cycle and gigacycle fatigue of fiber-reinforced composites: A review on experimental approaches and fatigue damage mechanisms”. In: *Progress in Materials Science* 118.September 2020 (2021), p. 100762. URL: https://doi.org/10.1016/j.pmatsci.2020.100762.

[31] H. C. Tang, T. Nguyen, T. Chuang, J. Chin, J. Lesko, and H. F. Wu. “Fatigue Model for Fiber-Reinforced Polymeric Composites for Offshore Applications”. In: *NIST Tehcnical Note* 1434 (2000). ISSN: 0899-1561. DOI: 10.1061/(asce)0899-1561(2000)12:2(97). URL: http://www.csa.com/partners/viewrecord.php?requester=gs&collection=TRD&recid=200123000005CE.

[32] F. McBagonluri, K. Garcia, M. Hayes, K.N.E. Verghese, and J.J. Lesko. “Characteristics of fatigue and combined environments on durability performance of glass/vinylester composites for infrastructure.” In: *International Journal of Fatigue* 22 (2000), pp. 53–64.

[33] J. W. Weeton, D. M. Peters, and K. L. Thomas. “Engineer’s guide to composite materials”. In: *American Society for Metals* 3 (1990).

[34] M Kaminski, F Laurin, J.F. Maire, C Rakotoarisoa, and E Hémon. “Fatigue Damage Modeling of Composite Structures : the ONERA Viewpoint”. 2015.

[35] C. Kassapoglou and M. Kaminski. “Modeling damage and load redistribution in composites under tension-tension fatigue loading”. In: *Composites Part A: Applied Science and Manufacturing* 42.11 (2011), pp. 1783–1792. ISSN: 1359835X. DOI: 10.1016/j.compositesa.2011.08.001. URL: http://dx.doi.org/10.1016/j.compositesa.2011.08.001.

[36] K. L. Reifsnider, K. Schulte, and J. C. Duke. “Long-Term Fatigue Behavior of Composite Materials.” In: *ASTM Special Technical Publication* ASTM STP 8 (1983), pp. 136–159. ISSN: 10403094. DOI: 10.1520/stp31820s.

[37] S. Aghajani, M. Hemati, and S. Torabnia. “Life prediction of wind turbine blades using multi-scale damage model”. In: *Journal of Reinforced Plastics and Composites* 40.17-18 (2021), pp. 644–653. ISSN: 15307964. DOI: 10.1177/0731684421995886.

[38] K. L. Reifsnider. “Damage and Damage Mechanics”. In: *Composite Materials Series* 4.C (1991), pp. 11–77. ISSN: 09270108. DOI: 10.1016/B978-0-444-70507-5.50006-8.

[39] S. D. Pandita, G. Huysmans, M. Wevers, and I. Verpoest. “Tensile fatigue behaviour of glass plain-weave fabric composites in on- and off-axis directions”. In: *Composites - Part A: Applied Science and Manufacturing* 32.10 (2001), pp. 1533–1539. ISSN: 1359835X. DOI: 10.1016/S1359-835X(01)00053-7.

[40] P. L. Chevalier, C. Kassapoglou, and Z. Gürdal. “Fatigue behavior of composite laminates with automated fiber placement induced defects- a review”. In: *International Journal of Fatigue* 140.June (2020), p. 105775. ISSN: 0142-1123. URL: https://doi.org/10.1016/j.ijfatigue.2020.105775.

[41] M. M. Shokrieh and F. Taheri-Behrooz. “A unified fatigue life model based on energy method”. In: *Composite Structures* 75.1-4 (2006), pp. 444–450. ISSN: 02638223. DOI: 10.1016/j.compstruct.2006.04.041.

[42] H E L Kadi and F Ellyin. “Effect of stress ratio on the fatigue of unidirectional glass fibre / epoxy composite laminae”. In: 25.10 (1994), pp. 917–924.

[43] S. Mandegarian and F. Taheri-Behrooz. “A general energy based fatigue failure criterion for the carbon epoxy composites”. In: *Composite Structures* 235.June 2019 (2020). ISSN: 02638223. DOI: 10.1016/j.compstruct.2019.111804. URL: https://doi.org/10.1016/j.compstruct.2019.111804.

[44] M Kawai. “A phenomenological model for off-axis fatigue behavior of unidirectional polymer matrix composites under different stress ratios”. In: *Composites Part A: Applied Science and Manufacturing* 35.35 (2004), pp. 955–963. DOI: 10.1016/j.compositesa.2004.01.004.

[45] J. Awerbuch and H. T. Hahn. “Off-Axis Fatigue of Graphite / Epoxy Composite”. In: *Fatigue of Fibrous Composite Materials* ASTM STP 7 (1981), pp. 243–273.

[46] M Kawai and T Teranuma. “A multiaxial fatigue failure criterion based on the principal constant life diagrams for unidirectional carbon / epoxy laminates”. In: *COMPOSITES PART A* 43.8 (2012), pp. 1252–1266. ISSN: 1359-835X. DOI: 10.1016/j.compositesa.2012.03.003. URL: http://dx.doi.org/10.1016/j.compositesa.2012.03.003.

[47] T K. O'Brien and K. L Reifsnider. "Fatigue damage evaluation through stiffness measurements in Boron-Epoxy Laminates". In: *Journal of Composite Materials* 15.January (1981), pp. 55–70.

[48] S. G. Pantelakis and E. C. Kyriakakis. "Fatigue damage of APC-2 composite assessed from material degradation and non-destructive evaluation data". In: *Theoretical and Applied Fracture Mechanics* 32.1 (1999), pp. 37–46. ISSN: 0167-8442. DOI: https://doi.org/10.1016/S0167-8442(99)00024-5. URL: https://www.sciencedirect.com/science/article/pii/S0167844299000245.

[49] S. G. Pantelakis*, E. C. Kyriakakis, and P. Papanikos. "Non-destructive fatigue damage characterization of laminated thermosetting fibrous composites". In: *Fatigue & Fracture of Engineering Materials & Structures* 24.10 (2001), pp. 651–662. DOI: https://doi.org/10.1046/j.1460-2695.2001.00445.x. URL: https://onlinelibrary.wiley.com/doi/abs/10.1046/j.1460-2695.2001.00445.x.

[50] P Papanikos, K. I. Tserpes, and S. Pantelakis. "Modelling of fatigue damage progression and life of CFRP laminates". In: *Fatigue Fracture of Engineering Materials Structures* 26.1 (2003), pp. 37–47.

[51] N. Stojković, R. Folić, and H. Pasternak. "Mathematical model for the prediction of strength degradation of composites subjected to constant amplitude fatigue". In: *International Journal of Fatigue* 103 (2017), pp. 478–487. ISSN: 0142-1123. DOI: https://doi.org/10.1016/j.ijfatigue.2017.06.032. URL: https://www.sciencedirect.com/science/article/pii/S0142112317302815.

[52] C. Kassapoglou. *Modeling the Effect of Damage in Composite Structures*. 2013, p. 248.

[53] N. Stojković, R. Folić, and H. Pasternak. "Mathematical model for the prediction of strength degradation of composites subjected to constant amplitude fatigue". In: *International Journal of Fatigue* 103 (2017), pp. 478–487. ISSN: 01421123. DOI: 10.1016/j.ijfatigue.2017.06.032.

[54] W. Lian and W. Yao. "Fatigue life prediction of composite laminates by FEA simulation method". In: *International Journal of Fatigue* 32.1 (2010), pp. 123–133. ISSN: 0142-1123. DOI: 10.1016/j.ijfatigue.2009.01.015. URL: http://dx.doi.org/10.1016/j.ijfatigue.2009.01.015.

A

FATIGUE FAILURE MECHANISMS

A.1. MICROSCOPIC SCALE APPROACH

On microscopic scale the mechanisms of damage accumulation, are sometimes occurring independently and other times interactively. Figure A.1 shows the effect on fatigue performance for various types of fiber architectures for the same material under uniaxial loading. It shows that continuous fibers and unidirectional fibers are better in dealing with fatigue loads than short fibers and woven fabrics. Especially in the case where the fibers align with the loading direction.

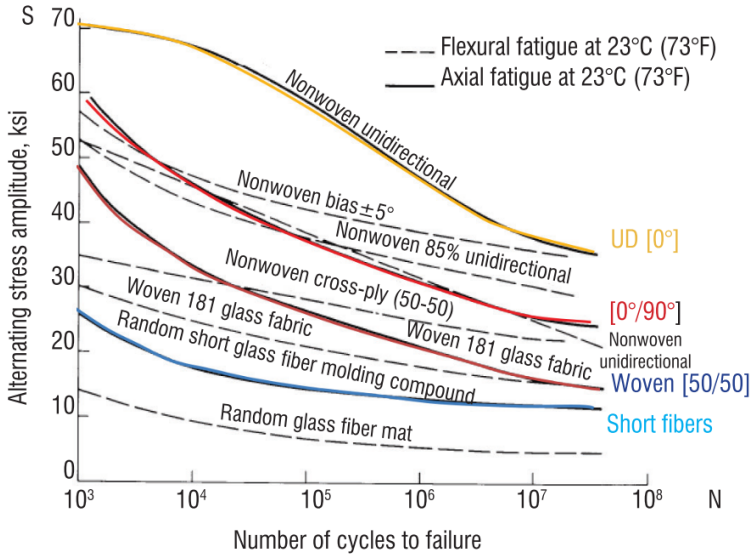

Figure A.1: Comparison of fatigue strengths of different layups and fiber configurations, with the same material. [33]

Since unidirectional and woven (fabrics created by weaving the longitudinal yarns and transverse yarns, patterns include plain, twill or satin) continuous fibers will be used in the design of the composite marine propeller, the focus will be narrowed down to only those types of fibers. To get a better understanding of the micro mechanics governing the material deterioration over the lifetime for these fiber architectures and how they compare, the tension-tension fatigue life of both will be discussed below. According to [34] the damage mechanisms are comparable for both static and fatigue loading.

UNIDIRECTIONAL FIBER LAMINATES

For unidirectional fiber laminates, a schematic representation of fatigue damage over the lifetime is given in figure A.2. During the first stage of fatigue of the cross ply laminate, damage is mostly characterized by the creation of transverse matrix cracks (90°with respect to loading direction) inside the cross-ply lamina, which increase in density in stage 2. The increase in crack density leads to coupling between these transverse cracks, eventually leading to inter-facial debonding between the fibers and matrix in the longitudinal direction of the fibers in 0°direction. However for strain values exceeding 3000 microstrain, the 0°plies develop cracks in some of the fibers. The increase in crack density in the 90°plies, creates an increase in local stresses in the neighbouring 0° plies [35]. Together with the strength reduction of the matrix in the 0° plies, radial cracks can start to initiate from the location of the fiber crack. As fatigue cycling continues these matrix cracks grow and multiply until they reach adjacent fibers. This second type of degradation is more common for laminae with angles other than 90°next to the 0° plies. In the second stage the reduction in residual stiffness and strength is gradual due to the slow and linear increase in damage. In stage 3 these debonded interfaces and transverse matrix cracks accumulate and lead to delamination. The matrix cracks and delaminations cause stress concentration factors in the 0°plies. This causes localized fiber failures, which eventually leads to final fracture of the laminate [35]. During these later stages the damage increases exponentially in the plies that are oriented in parallel or close to parallel with respect to the applied load (so-called on-axis plies), causing an accelerated decline in the residual material properties. This is because laminate's the residual material properties are governed by the state of damage in the on-axis plies as they carry most of the load [36][37].

WOVEN FIBER LAMINATES

For continuous fibers in a woven configuration the fatigue development is quite different to that of unidirectional cross-ply laminates. However similar to unidirectional laminates the fatigue performance in off-axis directions is worse than the on-axis directions. Unlike unidirectional cross-ply laminates, woven on-axis laminates fatigue life can be classified into four stages. During the initial stage no reduction in stiffness can be observed. This is because the matrix cracks start appearing in the transverse fiber yarns, which carry almost no loads and have a low influence on the stiffness. After a third of the total lifetime further cracks start to form in the matrix of the transverse fiber yarn including debonding on the fibers and matrix interface of that yarn. This accumulates into continuous transverse cracks through the yarn. Leading to a delimitation between the transverse yarn and longitudinal yarn in the next stage, called meta-delamination.

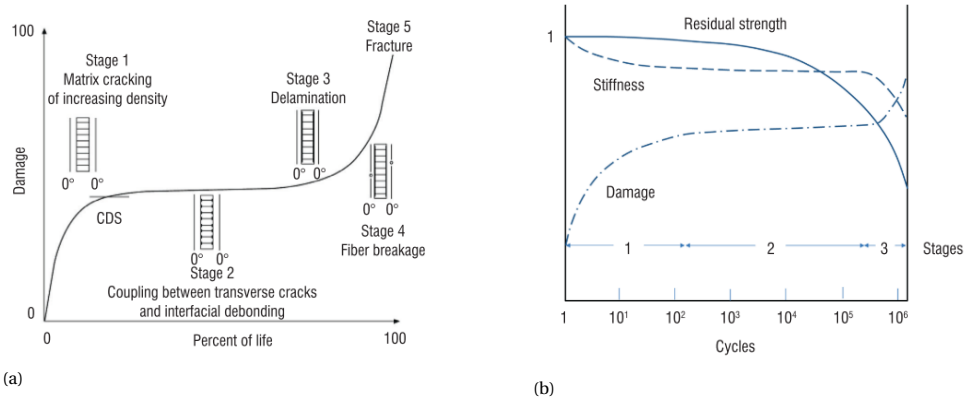

Figure A.2: a) Fatigue damage growth over lifetime of a cross-ply laminate, b) Effect of damage evolution on residual stiffness and strength. [38]

Since the residual strength and stiffness are almost completely governed by the damage in the longitudinal fiber bundles, there is almost no loss in properties up until this stage. The final stage is governed by the separation and the fracture of the fibers in the longitudinal yarns, causing a rapid degradation in the residual material properties. Until the residual properties are deteriorated enough to cause complete fracture of the longitudinal fiber bundles. This indicates the failure of the complete laminate [39]. The off-axis fatigue behaviour of woven fiber laminates shows a similar 3 stage reduction trend as that of the unidirectional cross-ply laminates. Figure A.4 indicates similar trends to that of a cross-ply unidirectional laminate subjected to higher and lower frequencies.

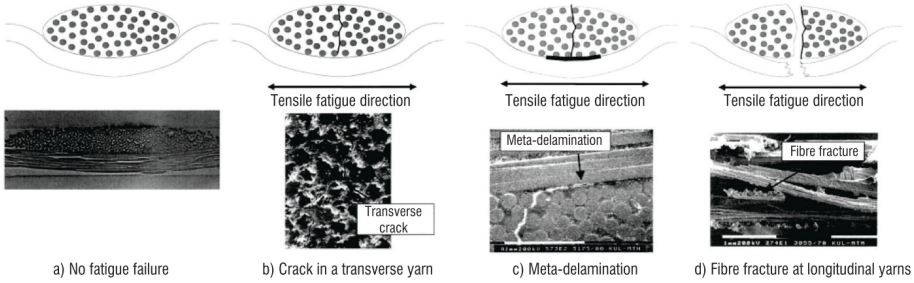

Figure A.3: Scheme of fatigue damage development in woven fabric composite, subjeted to tension-tension fatigue in on-axis direction. [39]

A.2. MACROSCOPIC SCALE APPROACH

Unlike the microscopic scale, the macroscopic scale models quantify fatigue damage by the loading conditions and is specific for a certain type of laminate and material combination. Usually they require a large amount of experimental data and are therefore

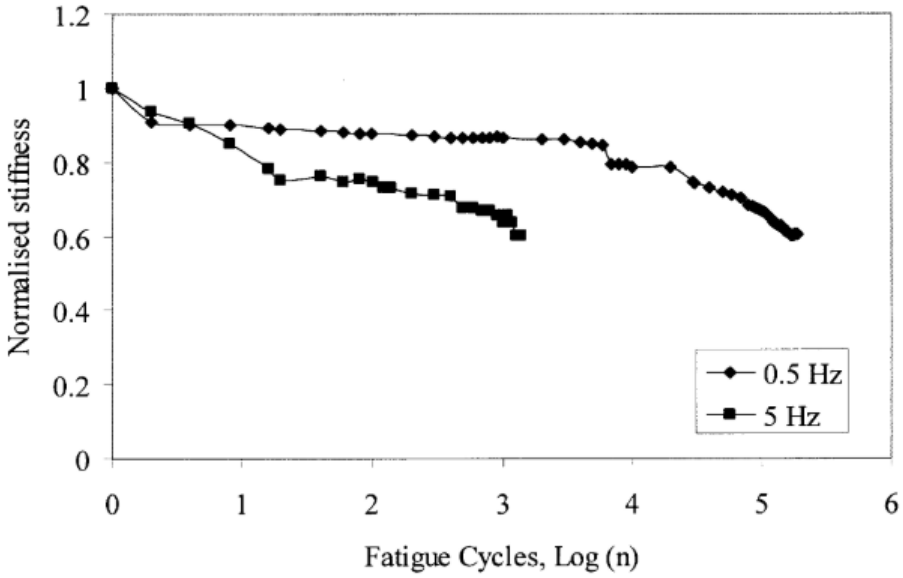

Figure A.4: Stiffness reduction of off-axis woven fiber composite for 2 different frequencies. [39]

expensive to apply to an arbitrary composite subjected to an arbitrary loadcase. Macroscopic models are categorized into two groups empirical models and phenomenological models. Empirical do not take the previously mentioned material degradation mechanisms into account, but use Goodman diagrams or S-N curves and usually introduce a fatigue failure criterion. The phenomenological models describe fatigue damage evolution by the evolution of the stiffness and strength of the composite structure in terms of macroscopic variables [3][10][35]. Similar to the empirical model the phenomenological models also require a considerable amount of experimental data to get a more accurate model.

The benefit of the macroscopic scale models compared to the microscopic scale models is that they are significantly easier to implement and take a lot less time to run. Because these models do not require knowledge of the changing local properties on such a small scale, which are sometimes impossible to validate, such as fracture energies of individual fiber/matrix interfaces. Also the fatigue behaviour on microscopic scale can change due to resin rich and resin poor regions and the models still require some kind of strength reduction model on the required scale in order for the model to work. Even though the microscopic models are a lot more detailed and give a better understanding of the degradation mechanisms in the fatigue life of a composite, the extra time and effort it takes to solve them might not be worth it. An effort has been made, by Chevalier et al [40], to estimate the amount of hours a simulation is allowed to run per specimen before it is cheaper to experimentally test the specimens. It states that if the cost of simulation is less than 5.5 hrs per specimen it is better to simulate than to test for a batch

of 18 specimens. If the batch size is reduced the the level at which it pays of to do simulation increases to between 6-9 hrs. It argues that for simpler coupons with simulation could be beneficial but also points out that even at this relatively simple level it might still not be possible to replace testing completely [40].

B

SPECIMEN SIZED FEM MODEL

B.1. LOAD CONTROLLED MODEL

To be able to compare the progressive damage model to experimentally gathered data from literature another FEM model has been made. The FEM model consists of a rectangular specimen that is clamped at both sides. On one side it is completely clamped and has no degrees of freedom, while on the other side the specimen is clamped in every degree of freedom except displacement in X. A line load is applied to this edge with a direction perpendicular to the edge. The specimen is discretised using quadrilateral shell elements. The shell elements are able to efficiently determine the stress state in the in plane direction. Which is sufficient able to capture the real stress states due to the unidirectional loading applied to these specimens. A convergency study to find the required number of elements in both X and Y direction still needs to be performed probably leading to more accurate results. For now the specimen consits of 5 elements in the width direction and 30 elements in the length direction.

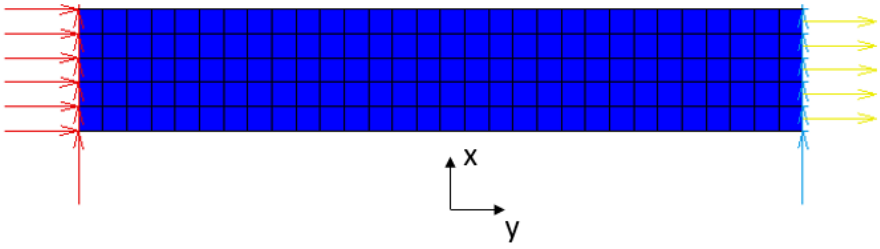

Figure B.1: The boundary conditions and line load applied to the propeller blade

To apply the correct stresses to the FEM model, an equivalent line load is applied to the free edge in X direction perpendicular to the edge. The material is applied to the

FEM model by using a composite layup, with the orientations, thicknesses and number of layers corresponding to that laminate, The same modelling approach is used as is discussed in section 2.4.4 and depicted in 2.3. The benefit of using the same software package is that the same subroutines can also be applied. This gives the ability to validate the modelling approach on a specimen scale, before applying it to the full propeller blade.

B.2. DISPLACEMENT CONTROLLED MODEL

In the situation where the experiments are done using displacement control instead of load control, there is a different FEM model to determine the fatigue behaviour. X. Zhang for example used a displacement controlled test to gather stiffness and strength degradation data of the a specimen that contained the hot-spot stress state and layup. The models is similar to the load controlled model but instead of applying an edge load in x direction, a displacement in x direction is applied.

B.3. STRESS SINGULARITY

The fixed boundary conditions on the specimen introduces a stress singularity at the corners of the specimen where this boundary condition is applied. A fixed boundary condition represents the clamp at the boundary, however because the boundary is fixed the stiffness of this clamp is infinite which is not physically possible. The stiffness of the clamp should have a finite value to give a more realistic load introduction into the specimen. However imposing such an elastic boundary condition comes with its own challenges and inconsistencies. The figures below show the damage that is created throughout the specimen at the top and bottom and middle layer after a certain amount of cycles. They show that the top layer does not experience its most critical stress at the stress singularity location when the mesh size is still at 5mm for figures B.2, B.3 and B.4. However when the mesh size is decreased, the location of maximum damage in the top layer has also moved to the stress singularity location. This is because when the mesh size is decreased, the stresses at the singularity location tend to infinity. This increased stress then also increases the amount of damage created each cycle at that location, leading to premature failure. See figures B.5, B.6 and B.7 for the fatigue analysis with the decreased mesh size of 1mm.

The way this is fixed by excluding the elements within a 5 mm distance from the fixed boundary condition from the fatigue analysis. Even though some information on the fatigue life of a specimen might be overlooked in this scenario it is assumed that the results are still relevant because in the case of static failure the specimens from X. Zhang did not fail at this boundary either, see figures B.8 and B.9.

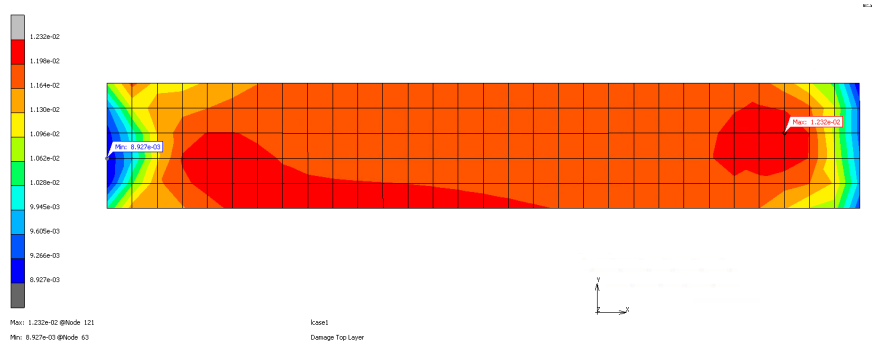

(a)

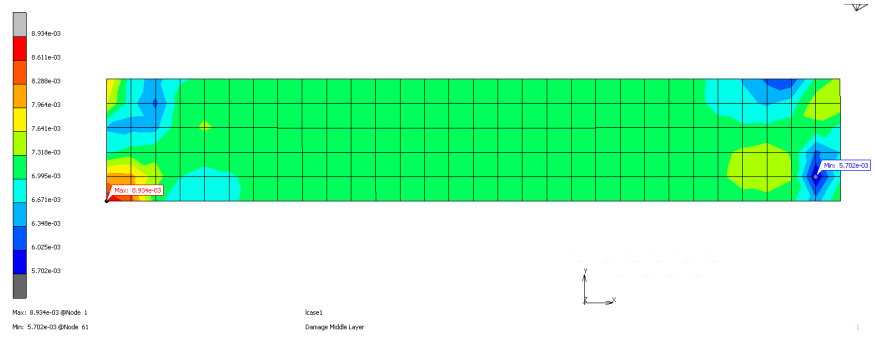

(b)

Figure B.2: a) Degradation of the top 38° layer after 1 cycle b) Degradation of the middle −7° layer after 1 cycle

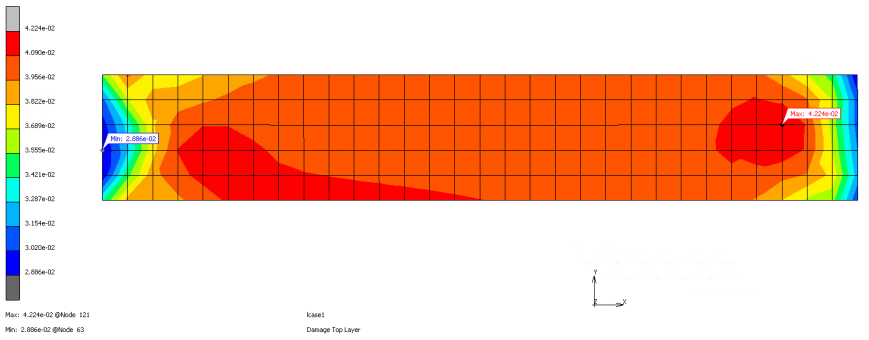

(a)

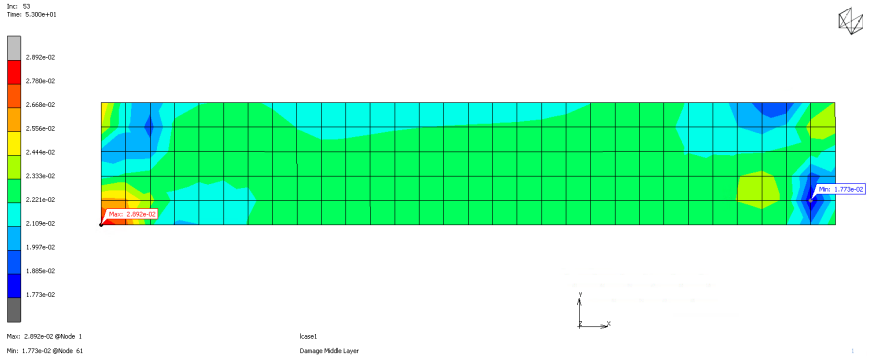

(b)

Figure B.3: a) Degradation of the top 38° layer after 10^4 cycle b) Degradation of the middle −7° layer after 10^4 cycle

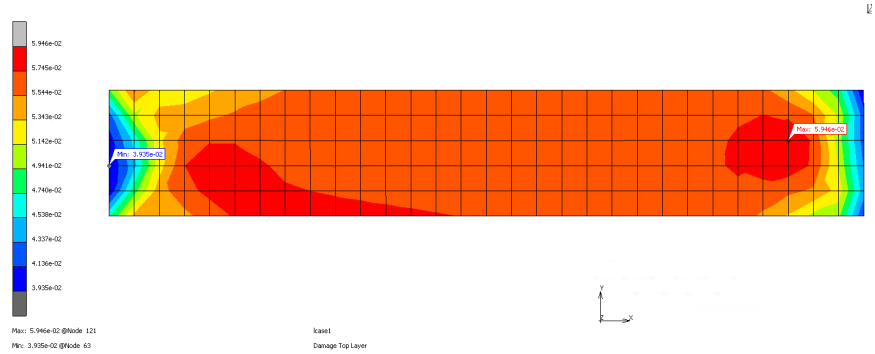

(a)

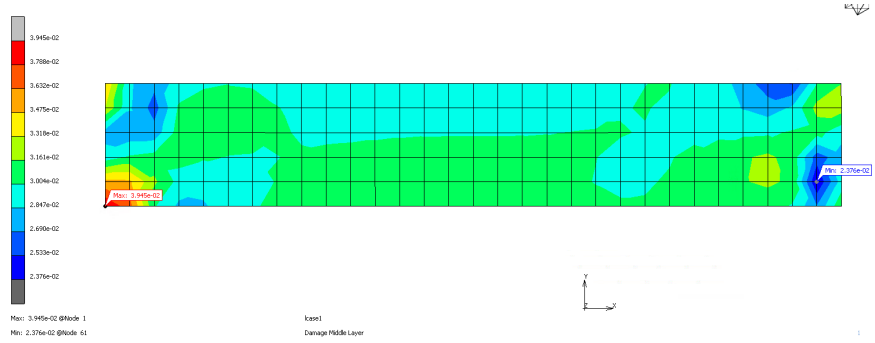

(b)

Figure B.4: a) Degradation of the top 38° layer after 10^6 cycle b) Degradation of the middle $-7°$ layer after 10^6 cycle

B

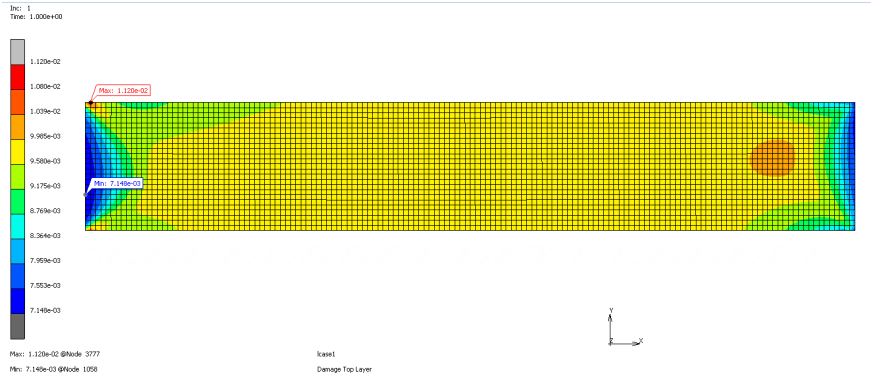

(a)

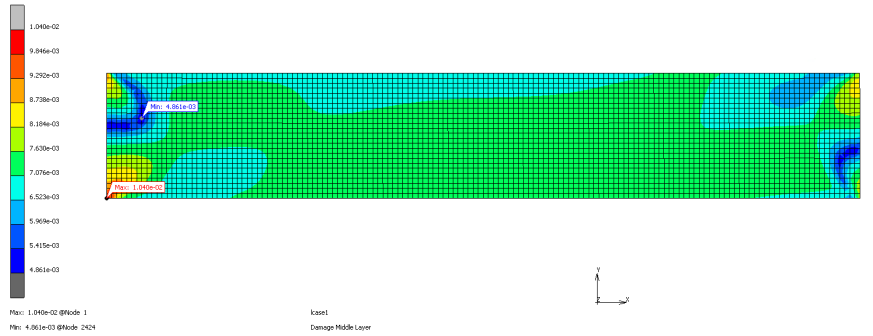

(b)

Figure B.5: a) Degradation of the top 38° layer after 1 cycle b) Degradation of the middle −7° layer after 1 cycle for a mesh size of 1mm

(a)

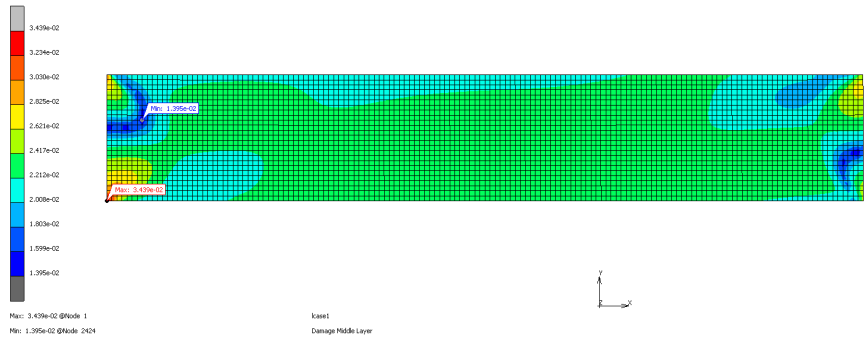

(b)

Figure B.6: a) Degradation of the top 38° layer after 10^4 cycle b) Degradation of the middle $-7°$ layer after 10^4 cycle for a mesh size of 1mm

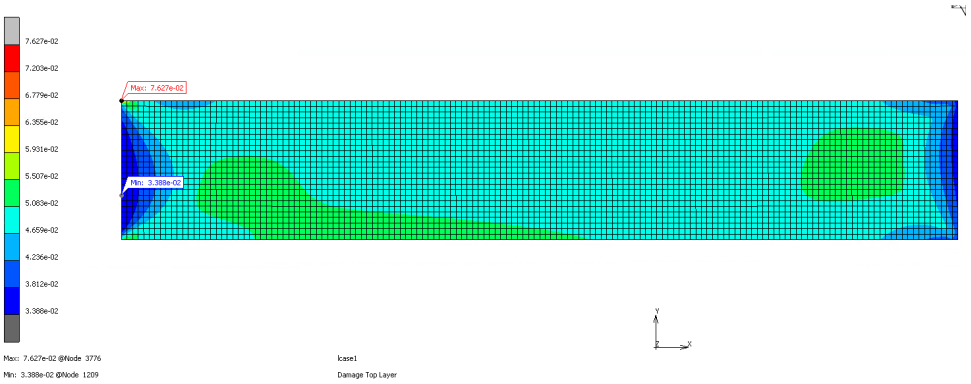

(a)

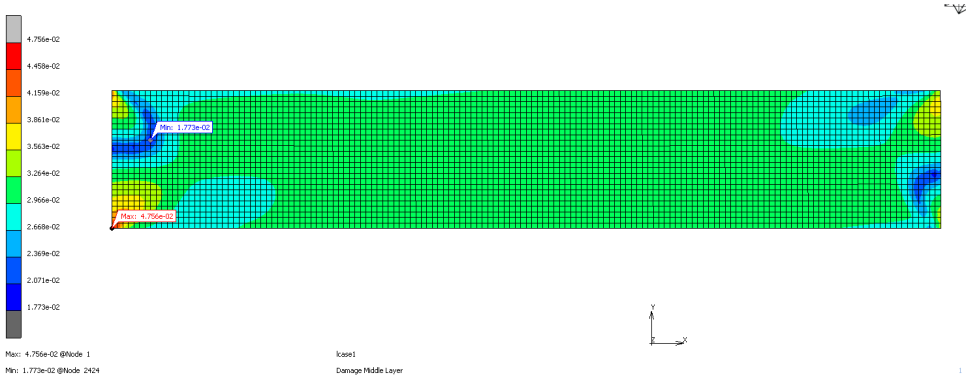

(b)

Figure B.7: a) Degradation of the top 38° layer after 10^6 cycle b) Degradation of the middle −7° layer after 10^6 cycle for a mesh size of 1mm

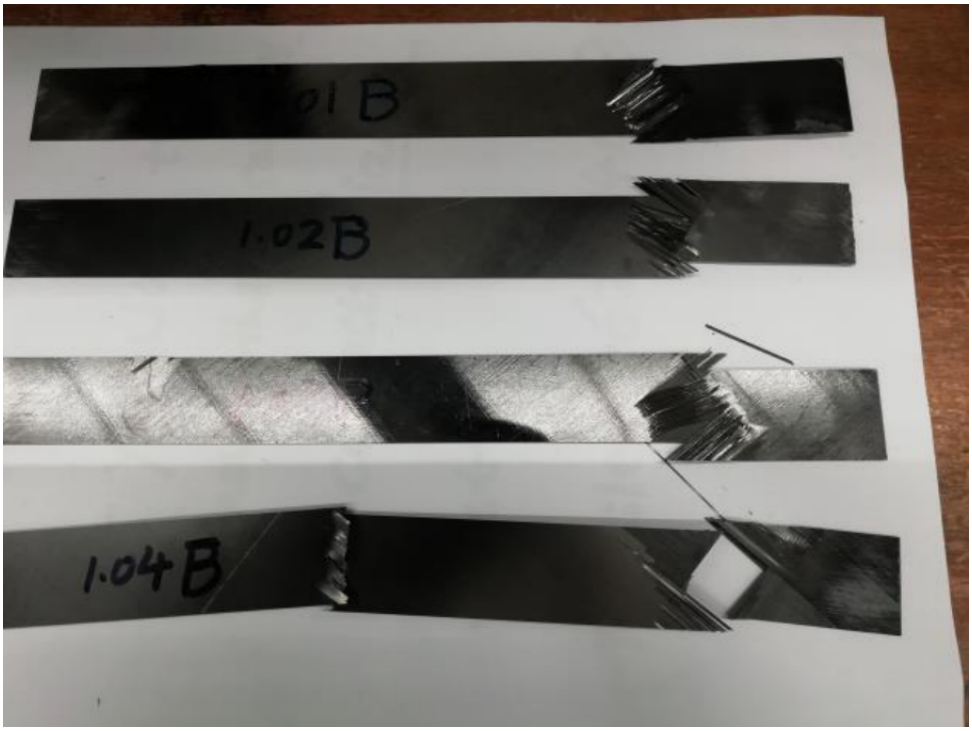

Figure B.8: Ultimate tensile failure tests of intact specimens [8]

B

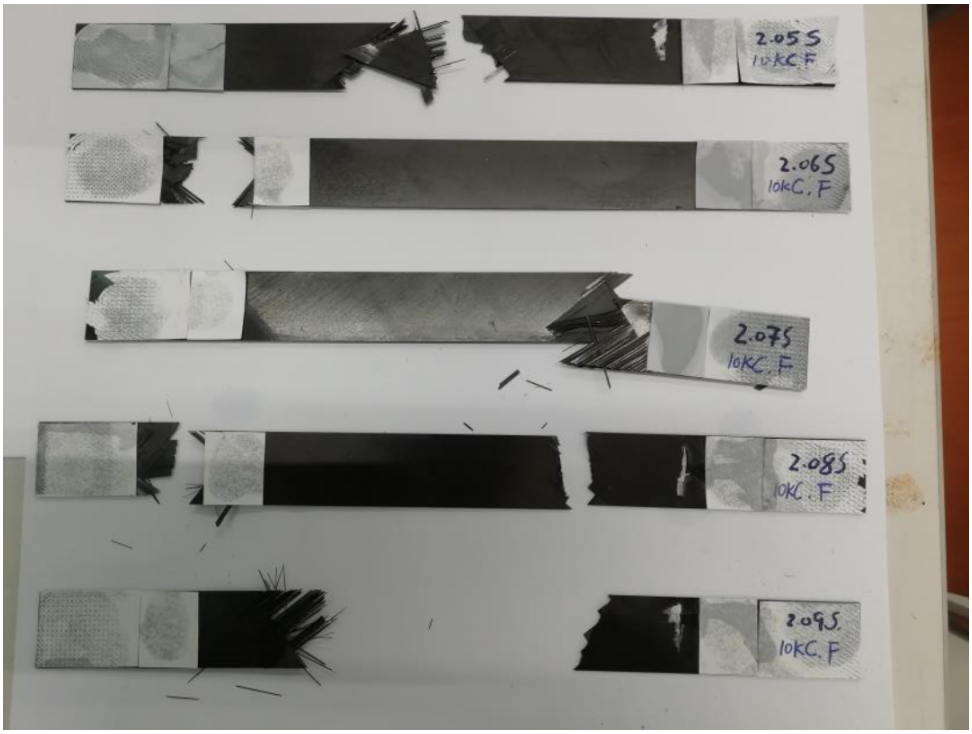

Figure B.9: Ultimate tensile failure tests of specimens after 10k cycles[8]

C

DETAILED DESCRIPTION OF THE FATIGUE LIFE MODELS

C.1. BACKGROUND OF FATIGUE LIFE MODELS

Fatigue life models use S-N curves or Goodman diagrams to extract fatigue information about the composite and base a fatigue failure criteria on that information. It does not include damage accumulation but rather predicts failure by the number of cycles at which it occurs under a given loading condition. Another commonly used approach is to use constant life diagrams (CLD). This diagram depicts the number of cycles to failure as a function of mean stress on the x-axis and alternating stress on the y-axis. They show the sensitivity of the composite fatigue with respect to stress ratio and amplitude. CLD's of composites are asymmetric due to their an-isotropic nature, where the peaks of the diagrams are shifted to the right of the alternating stress axis because of the reason that composites fare better under tensions than compression. The main benefit of using these CLD's over using S-N curves is that they are able to estimate the fatigue life of stress ratio's and amplitudes that were not experimentally acquired due to the a simple piecewise linear interpolation between data points. A typical example of what a CLD looks like is depicted in figure C.1.

Fatigue life models are easy to use and require no knowledge of the actual damage mechanisms that degrade the material. The main reason for not using a fatigue life model is that they depend on large quantities of experimental data for each material, layup and loading condition. This makes them impossible to use in more general cases with multi-axial stress states. They also require a significant experimental effort to be able to fit the fatigue life models correctly.

C.2. FATIGUE LIFE MODEL 1

The fatigue life models give an estimation of the fatigue life of a ply subjected to a fixed constant amplitude loading by using curve fitting parameters. On of these models is given in the journal paper "*A unified fatigue life model based on energy method*" by

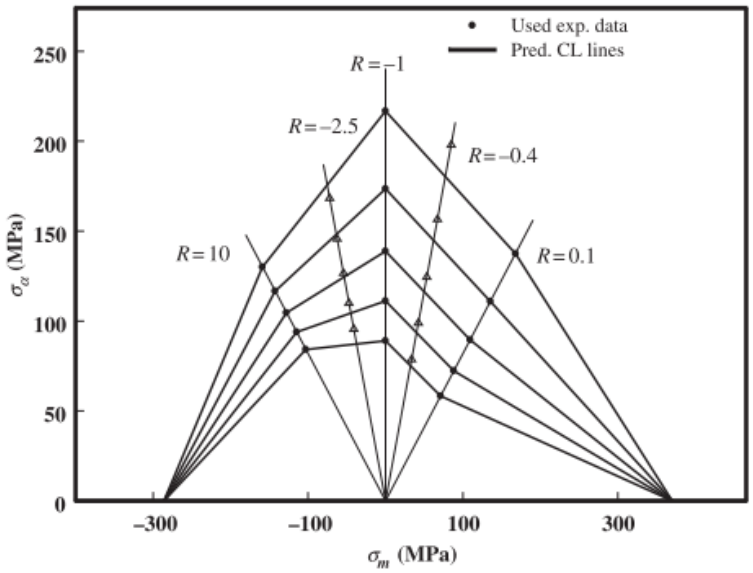

Figure C.1: Typical CLD with linear interpolation between data points [11]. The CLD shows a range between 10^4 cycles (top line) to 10^8 cycles (bottom line) with factor 10 increments

Shokrieh and Taheri-Behrooz [41]. The writers introduce a way to determine the fatigue life of a composite with an energy based method. This method reduces the amount of fatigue tests required to determine the fatigue life for arbitrary stress ratio and fiber orientations. The fatigue life is expressed in cycles until failure and is defined by equation C.1.

$$N_f = \left(\frac{K}{\Delta W^*}\right)^{\frac{1}{a}} \tag{C.1}$$

Here N_f is the fatigue life given in the amount of cycles at certain stress ratio R and stress level. K and α are experimentally fitted parameters. ΔW^* is the normalized strain energy density. The normalized strain energy density can be divided into 3 distinctly different contributions, see C.2. In this equation ΔW_1^*, ΔW_2^* and ΔW_3^* denote the local in-plane longitudinal, transverse and shear contributions to the normalized strain energy density. The longitudinal, transverse and shear contributions are defined below for different load ratios. The equation for the stress ratio is given in 2.3.

$$\Delta W^* = \Delta W_1^* + \Delta W_2^* + \Delta W_3^* \tag{C.2}$$

For 0 < R < 1:

$$\Delta W_1^* = \frac{(\sigma_{1max}\epsilon_{1max} - \sigma_{1min}\epsilon_{1min})}{X_t \epsilon_{u1}} \tag{C.3}$$

$$\Delta W_2^* = \frac{(\sigma_{2max}\epsilon_{2max} - \sigma_{2min}\epsilon_{2min})}{Y_t \epsilon_{u2}} \tag{C.4}$$

$$\Delta W_3^* = \frac{(\sigma_{12max}\epsilon_{12max} - \sigma_{12min}\epsilon_{12min})}{S_{12}\epsilon_{u12}} \tag{C.5}$$

For 1 < R :

$$\Delta W_1^* = \frac{(\sigma_{1max}\epsilon_{1max} - \sigma_{1min}\epsilon_{1min})}{X_c\epsilon_{u1}} \tag{C.6}$$

$$\Delta W_2^* = \frac{(\sigma_{2max}\epsilon_{2max} - \sigma_{2min}\epsilon_{2min})}{Y_c\epsilon_{u2}} \tag{C.7}$$

$$\Delta W_3^* = \frac{(\sigma_{12max}\epsilon_{12max} - \sigma_{12min}\epsilon_{12min})}{S_{12}\epsilon_{u12}} \tag{C.8}$$

For R < 0 :

$$\Delta W_1^* = \frac{(\sigma_{1max}\epsilon_{1max} + \sigma_{1min}\epsilon_{1min})}{(X_t^2 + X_c^2)^{0.5}\epsilon_{u1}} \tag{C.9}$$

$$\Delta W_2^* = \frac{(\sigma_{2max}\epsilon_{2max} + \sigma_{2min}\epsilon_{2min})}{(Y_t^2 + Y_c^2)^{0.5}\epsilon_{u2}} \tag{C.10}$$

$$\Delta W_3^* = \frac{(\sigma_{12max}\epsilon_{12max} + \sigma_{12min}\epsilon_{12min})}{S_{12}\epsilon_{u12}} \tag{C.11}$$

Where the X, Y, S are the maximum static strengths in longitudinal, transverse and shear direction. ϵ_u are the maximum static strains in the material directions. Furthermore, σ_{max},ϵ_{max},σ_{min},ϵ_{min} denote the maximum applied stress and strain and the minimum applied stress and strain respectively.

This method is used to predict the fatigue life of unidirectional composites with acceptable accuracy however it also has some limitations [41][42]. For example, since the fatigue life prediction is a power- law type equation, the fitted power constant α has a large influence on the predictions. Even small changes in α can negatively impact the fatigue life predictions especially at the higher cycles. Furthermore, because the constants α and K are determined by fitting to experimental data which are logarithmic scaled, a small error in the data can lead to large errors in the model. On the other hand the major advantage of using this method is that it negates the effect of the fiber orientation and stress ratio on the constants α and K. [43].

C.3. FATIGUE LIFE MODEL 3

Another fatigue life model is given in the paper "*A phenomenological model for off-axis fatigue behavior of unidirectional polymer matrix composites under different stress ratios*" [44] by M. Kawai. In this paper the author comes up with a new way to determine the fatigue life of a composite with a method based on the failure criteria. This method reduces the amount of fatigue tests required to determine the fatigue life for arbitrary stress ratio and fiber orientations. The fatigue life is expressed in cycles until failure and is defined by the following equation.

$$N_f = \frac{1}{(\sum)^{n^*}} \tag{C.12}$$

Here N_f is the amount of cycles as a function of a "*modified non-dimensional effective stress*" $\sum^*$ and a $n*$ which is an experimentally fitted parameter. The modified non-dimensional effective stress, $\sum^*$ is a function of the failure index f_i and the stress ratio R of the ply, the equation to acquire it is given below. This equation is used to remove the dependence of the modified effective stress ratio on the stress ratio. Giving a fatigue life formulation that is more widely applicable for a single set of experimental parameters.

$$\sum = \frac{\frac{1}{2}(1-R)f_i}{1-\frac{1}{2}(1+R)f_i} for R < 1 \tag{C.13}$$

$$\sum = \frac{\frac{1}{2}(R-1)f_i}{1-\frac{1}{2}(1+R)f_i} for R > 1 \tag{C.14}$$

To determine the failure indices one can use a variety of failure criteria. The one used in the aforementioned literature is the Tsai-Hill static failure criteria. The failure index predicted by the Tsai-Hill failure criteria for plane stress is given in equation C.15.

$$f_i = \sqrt{\left(\frac{\sigma_{11}}{X}\right)^2 - \left(\frac{\sigma_{11}\sigma_{22}}{X^2}\right) + \left(\frac{\sigma_{22}}{Y}\right)^2 + \left(\frac{\sigma_{12}}{S}\right)^2} \tag{C.15}$$

where σ_{11}, σ_{22} and σ_{12} are the stress components along the principal material axes. Furthermore X, Y and S are the longitudinal, transverse and shear strengths, respectively.

CHANGES MADE TO FATIGUE LIFETIME MODELS

Fatigue life models predict the overall fatigue life of a ply. This fatigue life estimate can subsequently be used to determine the degradation of stiffness and strength of the ply in longitudinal, transverse and shear direction. However it is important to note that the fatigue life calculated is for the specimen when it fails completely, it does not discriminate whether the applied stress is longitudinal, transverse or shear. The problem this causes will be explained with the following example, a unidirectional 10° ply loaded in an axial load will give a fatigue life estimate of 10 million cycles. Due to the small angle of the unidirectional ply with respect to the loading direction, most of the stress will be carried by the fibers in longitudinal direction. Only small stresses will be experienced in transverse and shear. However due to the singular estimate for the fatigue life of the ply, all of the properties will be degraded to failure at 10 million cycles. This means that the degradation of the transverse and shear strengths will be a lot more severe than could be expected from the only small amount of stress experienced in those directions. Leading to a conservative estimate of the lifetime of a structure and an increased rate of reduction in the residual stiffness and strength properties. It also causes a loss in information on the distinction on when what type of failure would occur, because now the ply will fail both in fiber, matrix and fiber-matrix shear at the same time. To counteract this problem new fatigue life models have been developed based on the models described above.

C.4. FATIGUE LIFE MODEL 2

The second model is based on the unified fatigue life model by Shokrieh and Taheri-Behrooz. Instead of combining the normalized strain energy densities from the 3 different contributions into a single entity as is done in equation C.1, they are used separately to determine their own respective contributions to the fatigue life. The equations that express the fatigue life for the longitudinal, transverse and shear direction are given by equation C.16, C.17 and C.18 respectively. The downside is that instead of one set of experimentally determined parameters, now 3 sets are required.

$$N_{f11} = \left(\frac{K}{\Delta W_1^*}\right)^{\frac{1}{a}} \tag{C.16}$$

$$N_{f22} = \left(\frac{K}{\Delta W_2^*}\right)^{\frac{1}{a}} \tag{C.17}$$

$$N_{f12} = \left(\frac{K}{\Delta W_3^*}\right)^{\frac{1}{a}} \tag{C.18}$$

C.5. FATIGUE LIFE MODEL 4

The fourth model is a different approach to the theory introduced by Kawai, where the failure index calculated with the Tsai-Hill failure criteria is normalized with respect to the applied stress ratio. Instead of using the multi-axial Tsai-Hill criteria another failure criteria by Hashin can be used. To determine the contributions of the longitudinal, transverse and shear stresses separately. To determine the failure stress in the fiber direction Hashin presented equation C.19.

$$\frac{\sigma_{11}^2}{X_R^2} + \frac{\sigma_{12}^2}{S_R^2} = f_{1i} \tag{C.19}$$

In this equation σ_{11} is the stress component in fiber direction, σ_{12} is the in-plane shear stress component. Furthermore, X_R is the residual strength in fiber direction and S_R is the residual in-plane shear strength. The residual strength of the lamina are determined using a set gradual and immediate degradation rules given in sections. Which will be explained in more detail in appendix D. Depending on whether the loading is tensile or compressive, the tensile or compressive strength is used respectively. However, according to research fiber breakage seldom happens except in the 0°plies. The failure of fibers only happens when the longitudinal stress exceeds the fiber strength [45][42] Equation C.19 can therefore be modified to equation C.20.

$$\frac{\sigma_{11}^2}{X_R^2} = f_{1i} \tag{C.20}$$

Hashin presented equation C.21 to predict failure in transverse direction due to a combination of transverse and shear stress.

$$\frac{\sigma_{22}^2}{Y_R^2} + \frac{\sigma_{12}^2}{S_R^2} = f_{2i} \tag{C.21}$$

Where σ_{22} is the stress component in transverse direction and Y_R is the residual strength in transverse direction. The in-plane shear failure criteria is given by equation C.22. In the case of a mainly longitudinal load, the fatigue life using the Hashin criteria match that of the Tsai-Hill criterion. This is because when the stress state is dominated by the longitudinal stress, Tsai-Hill matches equation C.19, due to the other terms being closer to zero. The same goes for the other loading directions. This makes it able use the same parameters as were determined for the Tsai-Hill criterion.

$$\frac{\sigma_{12}^2}{S_R^2} + \frac{\sigma_{22}^2}{Y_R^2} - \frac{\sigma_{11}\sigma_{22}}{X_R^2} = f_{12i} \tag{C.22}$$

C.6. MODEL COMPARISON

In this section the four different fatigue life models explained above will be compared against each other and against experimental data gathered from literature. Using classical laminate theory the applied unidirectional stresses are transformed into a longitudinal, transverse and a shear stress for each ply in the laminate. Then using the fatigue life models an estimation is made for the lifetime of the plies under those stress states. In this case the laminates used are unidirectional as well thus giving the same stress state and fatigue life for each ply.

Figure C.2 displays the predicted fatigue life compared against the experimental data for a T800h/2500 laminate for 3 different stress ratios. For the positive stress ratios all models give a reasonable prediction for the all the angles except at 10 and 15 degrees. Where the predicted fatigue life underestimates the performance of the laminate by about 2-3 orders of magnitude depending on the model selected. The expectations is that this is due to the higher interaction between the longitudinal transverse and shear stresses. For the 0 and 90 degree plies all of the models are able to predict the fatigue life to within the experimental scatter. This is because that at these ply orientations the stresses in the plies are mainly unidirectional and thus there is almost no interaction between longitudinal or transverse and shear stress. For the stress ratio of -1 the models 3,4 match the experimental results accurately including the correct first cycle failure stress level and the slope of the curve. However for models 1 and 2 both the slope and the first cycle failure stress level show significant differences. This shows that for the models 1 and 2 the slope and first cycle failure stress level are not independent of the stress ratio R.

For the Eglass/epoxy glass fiber laminate C.3 and positive stress ratios we can find similar results with excellent prediction capabilities for the 0 and 90 degree plies, however the models now also are able to predict the fatigue life of the off-axis angles to an acceptable degree that lies within the experimental scatter. Similar to the prediction for the T800H cfrp, the models 1 and 2 have a larger error for predicting the S-N curve than that of model 3 and 4. As stated above this is probably due to the not completely independent behaviour of the S-N curves with respect to the stress ratios and thus other slope and first cycle failure stress parameters need to be picked for a more accurate representation at positive and negative stress ratios. The difference is increased for the ply angles near 90 degrees with respect to the applied stress.

Figure C.4 shows the predicted fatigue life of the S4/3501-6 carbon fiber laminate for

a stress ratio of 0.1. Similar to the predicted fatigue lives of the carbon and glass fiber samples discussed above, the predictions are accurate for the 0° and 90° plies and less accurate for the other directions. Also, the second model overestimates the fatigue life of the samples with angles between 10 and 60 degrees and especially at 30 degrees. This can be explained by looking at equations C.3,C.4,C.5. If these equations are used separately as is done in model 2, the interaction between normalized strain energy densities is neglected. The decomposed strain energy densities are lower and thus give a higher fatigue life for a specific stress level.

Lastly, figure C.5 shows the predicted fatigue life of the T700s/2592 carbon fiber specimens and the experimentally determined values for stress ratio's of 2 and 10. This is when the samples are loaded in compression-compression, Only the models 1 and 2 are shown because the models 3 and 4 are not able to predict the fatigue life in compression compression loading. This is because of how the failure criteria is made independent with respect to the stress ratio R. Models 1 and 2 give an accurate prediction for the 0°, 10° and 20° plies. For angles in between the predictions are matching the experiments. The models underestimate the performance considerably for the angles 30° and 45°.

Even though the difference between the predicted and the experimental results can be significant, it is often conservative. The model with the best fit in most of the cases is model 3, however because this study also tries to determine the type of failure at the end of life to the lamina in an element. Model 4 should be chosen with the separate fatigue life estimates for the longitudinal, transverse and shear directions. However because the propeller is a sandwich structure and the orientation of the loading on the propeller blade is assumed to be constant. The elements on the suction side are always in compression-compression R >1 and the elements on the pressure side are always in tension-tension 0>R>1 it is assumed that these are the most important ratios to look at. Since models 3 and 4 are unable to properly predict the fatigue life performance of the elements on the suction side of the blade, model 2 is picked. Because this also allows for separate fatigue life estimates for the longitudinal, transverse and shear directions. The first cycle failure stress and slope of the S-N curve can be changed by varying the K and alpha parameters respectively. Even though this takes more time and money, it will make the predictions more accurate. For the stress ratios ranges R<1, R>1 and 0>R>1 a different set of K and alpha value should be determined for the most accurate fit. However since this study is merely used to get a first order estimate of the fatigue life of the blade more generalized parameters are chosen that underestimate the fatigue life performance.

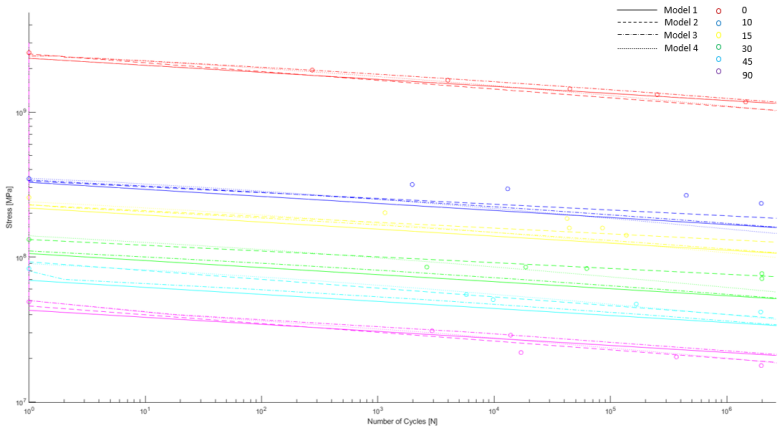

(a) R = 0.1

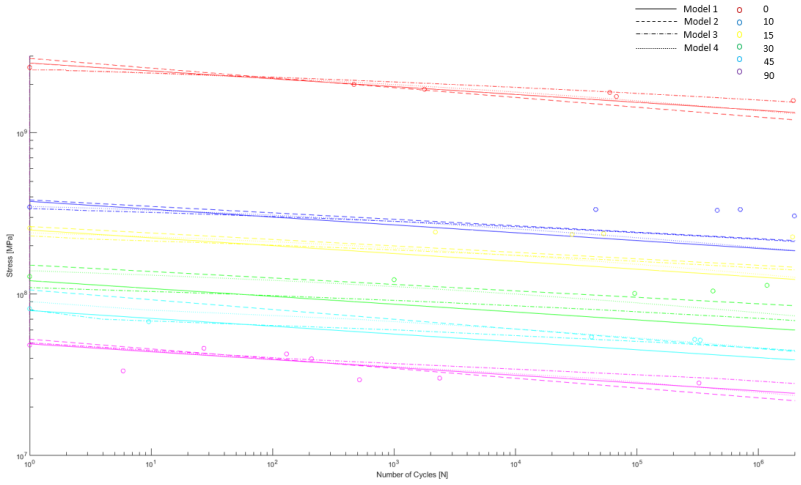

(b) R = 0.5

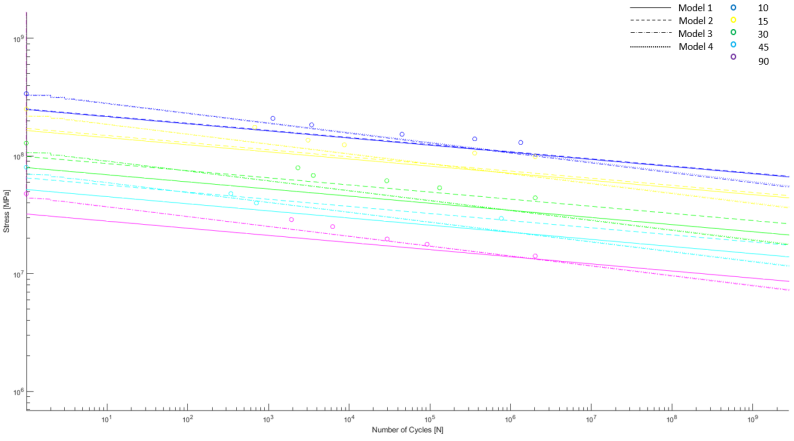

(c) R = -1.0

Figure C.2: Predicted fatigue life from the 4 different models compared against a experimental data for unidirectional T800h/2500 carbon fiber laminate with angles 0° up to 90° at 3 different stress ratios [42]

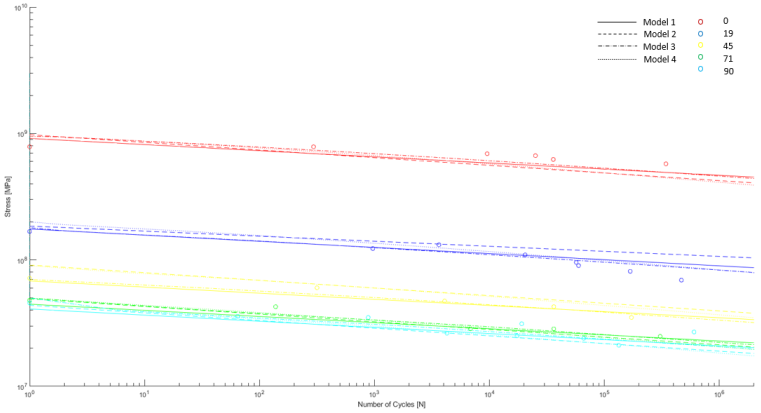

(a) R = 0

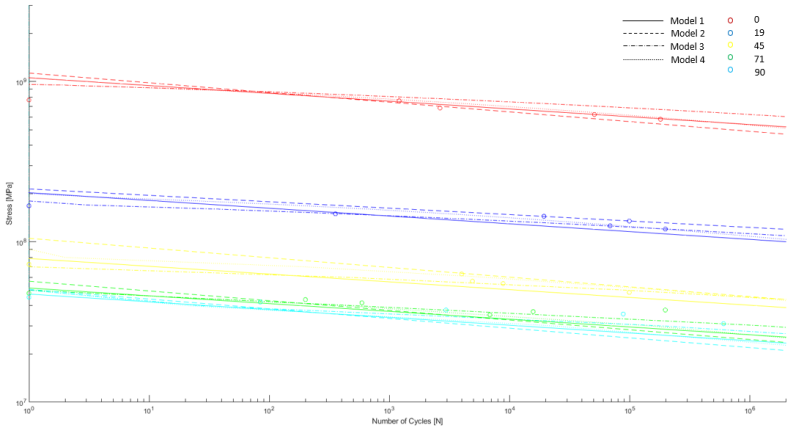

(b) R = 0.5

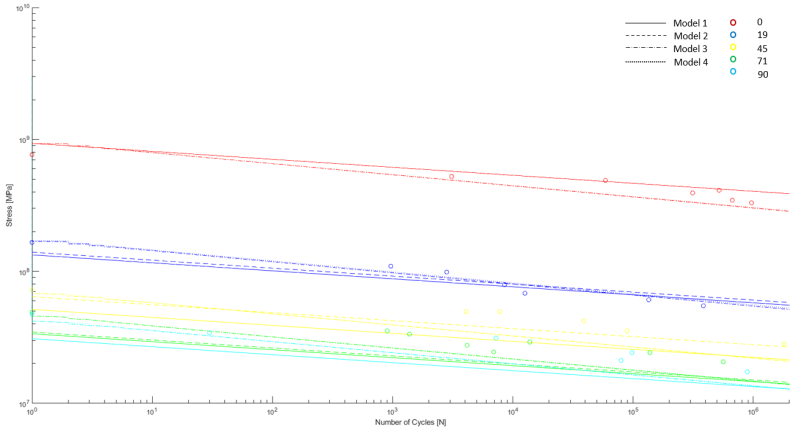

(c) R = -1.0

Figure C.3: Predicted fatigue life from the 4 different models compared against a experimental data for unidirectional E-glass/Epoxy fiber laminate with angles 0° up to 90° at 3 different stress ratios [9]

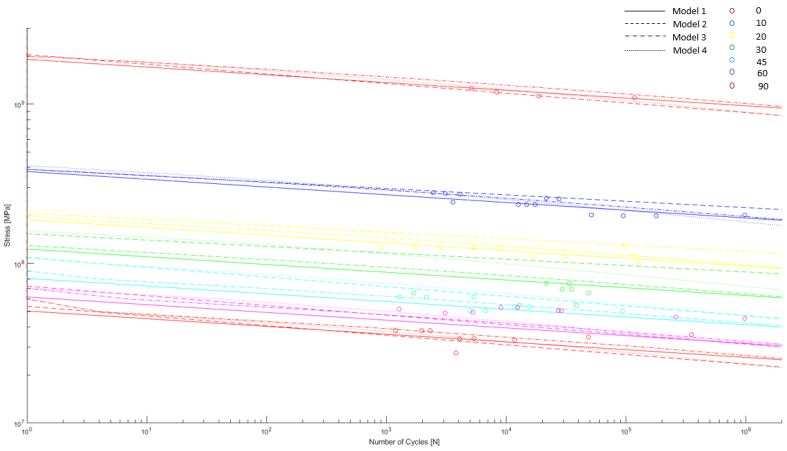

Figure C.4: Predicted fatigue life from the 4 different models compared against a experimental data for unidirectional AS4/3501-6 carbon fiber laminate with angles 0° up to 90° at R = 0.1 [45]

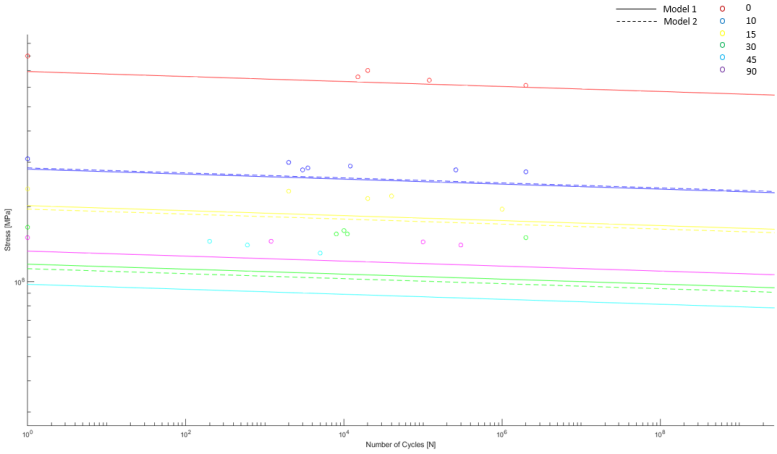

(a) R = 10

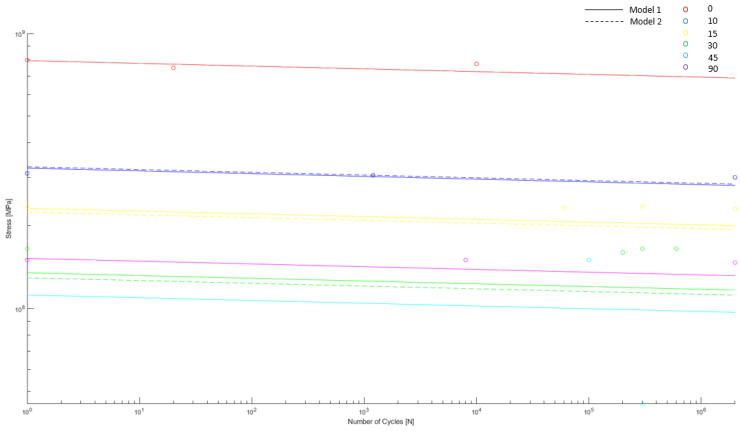

(b) R = 2

Figure C.5: Predicted fatigue life from the first 2 models compared against a experimental data for unidirectional T700s/2592 carbon fiber laminate with angles 0° up to 90° at 2 different stress ratios[46]

D

DETAILED DESCRIPTION OF THE MATERIAL DEGRADATION MODELS

D.1. BACKGROUND OF DEGRADATION MODELS

BACKGROUND STIFFNESS DEGRADATION MODELS

The stiffness of the laminate degrades as the damage to the matrix and fibers increases. The residual stiffness of the laminate is an important parameter in determining the fatigue life of a composite structure, because it allows one to predict the deformation and the the resulting stress redistribution. Most of these residual stiffness models use experimental data fitting parameters to determine the loss in stiffness over a certain amount of cycles. The values of these parameters are different for stresses in different directions and different lamina. The final failure of the composite is assumed to occur when the stiffness has degraded to a critical level [47] or when the resultant strain reaches the ultimate static strain [5]. Multiple studies have shown a similar trend in residual stiffness degradation of a quasi-isotropic composite subjected to fatigue loading [48][49]. The stiffness degraded almost linearly with respect to the number of cycles. Figure D.1 shows the normalized residual stiffness of two quasi-isotropic laminates subjected to a tension-compression fatigue load for varying stress levels. Although the effect of stress level on the degradation of stiffness is small, it can be noted that for increasing stresses the drop in stiffness over the lifetime becomes smaller [50]. This is because at lower stress levels the amount of cycles to which the laminate is subjected is higher, leading to an increased amount of time in which damage can form. Since the residual strength of the material is directly influenced by the amount of damage present, it makes sense that for lower stress levels the residual strength needs to decrease further to reach the applied cyclic max load D.2. Hence there is more damage present [36]. This is considering that the frequency and load ratio remain constant.

$$E(n) = [A(n/N_f) + 1]E_s \tag{D.1}$$

Figure D.1 appears to show a linear relation between normalized residual stiffness

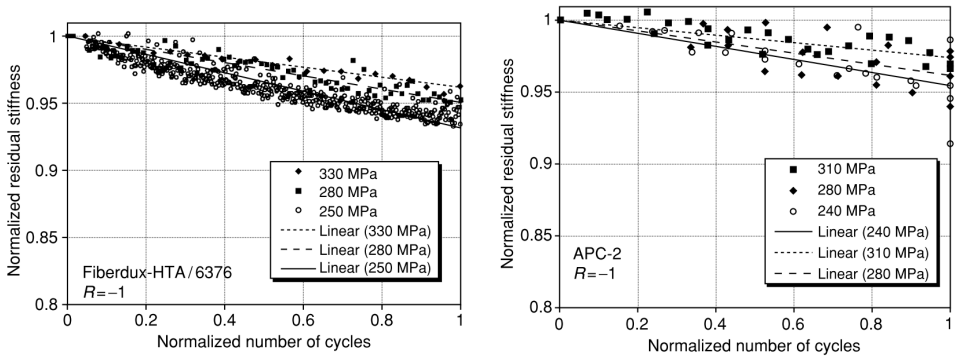

Figure D.1: Normalized residual stiffness plotted over the normalized cycles for different stress levels for an a) Fiberdux-HTA/6376 laminate [49] and b) APC-2 laminate [48]

over the normalized cycles. A possible formulation for this is given in equation D.1. Here E and E_s are the residual and initial stiffness respectively,n is the number of cycles, N_f is the amount of cycles to failure and A is the experimental curve fitting parameter. Another non-linear residual stiffness model which is widely used is written in the paper by Shokrieh et al [10]. The equation is depicted in D.2. The equation uses a relation between the normalized stiffness and cycles however the relation is now non-linear and the stiffness degradation looks more similar to the curve found in figure A.2, which is more accurate for uni-directional laminates.

There are a few drawbacks of using these more complicated non-linear degradation models. To get these models tuned for a given laminate and loading condition experimental data is required to determine the model parameters. Also these models are not inherently consistent. This means that after a certain amount of cycles n_1 the residual stiffness is E_1 and the strength is σ_1. Adding n_2 cycles on top of that will give a residual stiffness and strength of E_2 and σ_2. Now applying the same equation starting from n_1 with the E_1, σ_1 and $N_f - n_1$ as starting conditions E_s, σ_s and N_f respectively. The solution for E_2 and σ_2 will be different. However, beneficial for the stiffness models is that measuring the residual stiffness of a composite can be done non-destructively. It also varies less due to statistical scatter compared to residual strength models, however the scatter is big and the drop in stiffness relatively small.

BACKGROUND STRENGTH DEGRADATION MODELS

The residual strength models describe the degradation of the residual strength during fatigue loading. This means the stress bearing capacity of the composite as a function of the amount of load cycles over it's entire fatigue life. These models assume that the residual strength is a continuously decreasing function of amount of cycles. Furthermore they assume that the residual strength at failure is equal to the applied amplitude load and that the initial residual strength is equal to the static strength. Residual strength models do not give the extent of the damage present in the structure, such as the loca-

tion, size and orientation of the cracks. But they do quantify the effect the damage has on the residual strength over the fatigue life. The main benefit of using a residual strength model is that they have a natural failure criteria built in, if the applied stress is greater than the residual strength at a certain cycle, the specimen will break. This philosophy is represented in figure D.2 for a tensile-tensile loaded structure. However to gain the required information to build the residual strength models one does need to destroy the specimens, which does not allow you compare the differences in damage states between these specimens. The main drawback of a residual strength models is the that they are not able to predict the stiffness degradation, this makes the models unable to predict the deformation of the composite and the stress redistribution throughout their life.

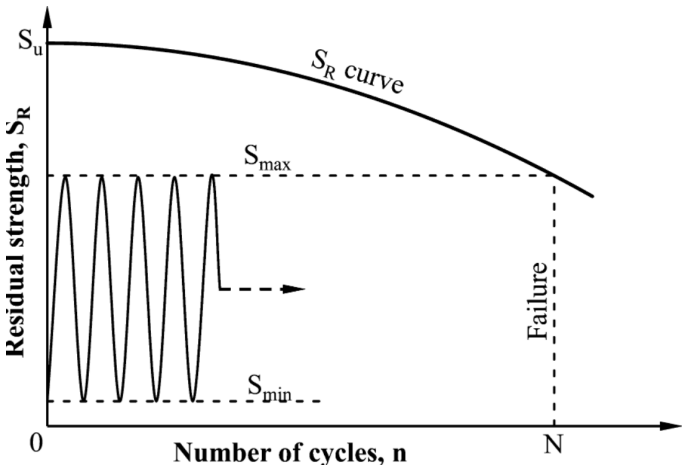

Figure D.2: Residual strength degradation philosophy [51]

In general the problem with these "phenomenological" models is that there is no connection and the actual damage phenomena taking place at microscopic scale. The only characteristics that relates these models to reality are that the rate of change of the residual strength is a function of cycles and that the boundary conditions of the residual strength being equal to the starting strength at the beginning of life and the applied stress at the end of life [52][53].

D.2. IMMEDIATE DEGRADATION

If the stresses and strains are sufficiently high during a cycle, it can trigger damage to form. For correct quantification and qualification of the damage it is necesarry to be able to individually detect every failure mode. This is done with certain failure criteria, a failure criterion to state that the matrix or fiber will fail under compression, tension, shear or delamination at ply level. The failure criteria vary with the authors of the numerous papers, using Tsai-Wu, Hashin 2D/3D or Puck failure criteria depending on their preference. The failure criteria for 3 different sources are given in table D.1. Here X_t, Y_t, Z_t, X_c, Y_c and Z_c are the longitudinal, transverse and orthogonal tensile and compressive strengths respectively. The applied stresses in all directions are given by σ_{11}, σ_{22},

σ_{33}, σ_{12}, σ_{23}, σ_{31}. The failure indices for matrix failure fiber failure and fiber-matrix failure are given by g_M, g_F, $g_F M$ respectively. If they reach unity, they indicate that the material will fail in the respective failure mode. If the failure criteria described above indicate failure, material stiffness properties are degraded by the so called immediate degradation rules. A few of these immediate material property degradation schemes are shown in table D.2. Here E, E^d ,ν and ν^d indicate the stiffness and Poisson ratio from before and after failure respectively.

Table D.1: Failure criteria for immediate degradation of material properties from 3 different sources

Failure mode	Failure criterion	Source
Matrix tensile cracking	$\left(\frac{\sigma_{22}}{Y_t}\right)^2 + \left(\frac{\frac{\sigma_{12}^2}{2E_{12}} + \frac{3}{4}\delta\sigma_{12}^4}{\frac{S_{12}^2}{2E_{12}} + \frac{3}{4}\delta S_{12}^4}\right) + \left(\frac{\sigma_{23}}{S_{23}}\right)^2 = -g_{M^+}^2$	
Matrix compressive cracking	$\left(\frac{\sigma_{22}}{Y_c}\right)^2 + \left(\frac{\frac{\sigma_{12}^2}{2E_{12}} + \frac{3}{4}\delta\sigma_{12}^4}{\frac{S_{12}^2}{2E_{12}} + \frac{3}{4}\delta S_{12}^4}\right) + \left(\frac{\sigma_{23}}{S_{23}}\right)^2 = -g_{M^-}^2$	
Fiber tensile failure	$(\frac{\sigma_{11}}{X_t})^2 + \left(\frac{\frac{\sigma_{12}^2}{2E_{12}} + \frac{3}{4}\delta\sigma_{12}^4}{\frac{S_{12}^2}{2E_{12}} + \frac{3}{4}\delta S_{12}^4}\right) + \left(\frac{\frac{\sigma_{13}^2}{2E_{13}} + \frac{3}{4}\delta\sigma_{13}^4}{\frac{S_{13}^2}{2E_{13}} + \frac{3}{4}\delta S_{13}^4}\right) = g_{F^+}^2$	[10]
Fiber compressive failure	$\left(\frac{\sigma_{11}}{X_c}\right) = g_{F^-}$	
Fiber-matrix shear-out	$(\frac{\sigma_{11}}{X_c})^2 + \left(\frac{\frac{\sigma_{12}^2}{2E_{12}} + \frac{3}{4}\delta\sigma_{12}^4}{\frac{S_{12}^2}{2E_{12}} + \frac{3}{4}\delta S_{12}^4}\right) + \left(\frac{\frac{\sigma_{13}^2}{2E_{13}} + \frac{3}{4}\delta\sigma_{13}^4}{\frac{S_{13}^2}{2E_{13}} + \frac{3}{4}\delta S_{13}^4}\right) = g_{FM}^2$	
Matrix tensile cracking	$\left(\frac{\sigma_{22}}{Y_t}\right)^2 + \left(\frac{\sigma_{12}}{S_{12}}\right)^2 + \left(\frac{\sigma_{23}}{S_{23}}\right)^2 = -g_{M^+}$	
Matrix compressive cracking	$\left(\frac{\sigma_{22}}{Y_c}\right)^2 + \left(\frac{\sigma_{12}}{S_{12}}\right)^2 + \left(\frac{\sigma_{23}}{S_{23}}\right)^2 = -g_{M^-}$	
Fiber tensile failure	$\left(\frac{\sigma_{11}}{X_t}\right) = g_{F^+}$	[17]
Fiber compressive failure	$\left(\frac{\sigma_{11}}{X_c}\right) = g_{F^-}$	
Fiber-matrix shear-out	$\left(\frac{\sigma_{11}}{X_c}\right)^2 + \left(\frac{\sigma_{12}}{S_{12}}\right)^2 + \left(\frac{\sigma_{13}}{S_{13}}\right)^2 = g_{FM}$	
Delamination in tension	$\left(\frac{\sigma_{33}}{Z_t}\right)^2 + \left(\frac{\sigma_{13}}{S_{13}}\right)^2 + \left(\frac{\sigma_{23}}{S_{23}}\right)^2 = g_D^+$	
Delamination in compression	$\left(\frac{\sigma_{33}}{Z_c}\right)^2 + \left(\frac{\sigma_{13}}{S_{13}}\right)^2 + \left(\frac{\sigma_{23}}{S_{23}}\right)^2 = g_D^-$	
Matrix tensile cracking	$\left(\frac{\sigma_{22}}{Y_t}\right)^2 + \left(\frac{\sigma_{12}}{S_{12}}\right)^2 = g_{M^+}$	
Matrix compressive cracking	$\left(\frac{\sigma_{22}}{Y_c}\right)^2 + \left(\frac{\sigma_{12}}{S_{12}}\right)^2 = g_{M^+}$	
Fiber tensile failure	$\left(\frac{\sigma_{11}}{X_t}\right) = g_{F^+}$	[29]
Fiber compressive failure	$\left(\frac{\sigma_{11}}{X_c}\right) = -g_{F^-}$	
Fiber-matrix shear-out	$\left(\frac{\sigma_{11}}{X_c}\right)^2 + \left(\frac{\sigma_{12}}{S_{12}}\right)^2 = g_{FM}$	

Table D.2: Immediate degradation schemes of material properties from 3 different sources

Failure mode	immediate degradation rule	Source
Matrix tensile cracking	$E_{22}^d = \nu_{23}^d = \nu_{21}^d = 0$	
Matrix compressive cracking	$E_{22}^d = \nu_{23}^d = \nu_{21}^d = 0$	
Fiber tensile failure	$E_{11}^d = E_{22}^d = E_{33}^d = E_{12}^d = E_{23}^d = E_{31}^d = \nu_{12}^d = \nu_{23}^d = \nu_{31}^d = 0$	[10]
Fiber compressive failure	$E_{11}^d = E_{22}^d = E_{33}^d = E_{12}^d\ E_{23}^d = E_{31}^d = \nu_{12}^d = \nu_{23}^d = \nu_{31}^d = 0$	
Fiber-matrix shear-out	$E_{12}^d = \nu_{12}^d = \nu_{21}^d = 0$	
Matrix tensile cracking	$E_{22}^d = 0.2\ E_{22}$, $E_{12}^d = 0.2\ E_{xy}$, $E_{zy}^d = 0.2\ E_{zy}$	
Matrix compressive cracking	$E_{22}^d = 0.4\ E_{22}$, $E_{12}^d = 0.4\ E_{xy}$, $E_{zy}^d = 0.4\ E_{zy}$	
Fiber tensile failure	$E_{11}^d = 0.07\ E_{11}$	[17]
Fiber compressive failure	$E_{11}^d = 0.14\ E_{11}$	
Fiber-matrix shear-out	$E_{12}^d = 0$	
Delamination in tension and compression	$E_{33}^d = E_{23}^d = E_{13}^d = 0$	
Matrix tensile cracking	$E_{22}^d = \nu_{12}^d = 0$	
Matrix compressive cracking	$E_{22}^d = \nu_{12}^d = 0$	
Fiber tensile failure	$E_{11}^d = E_{22}^d = E_{33}^d = E_{12}^d\ E_{23}^d = E_{31}^d = \nu_{12}^d = \nu_{23}^d = \nu_{31}^d = 0$	[29]
Fiber compressive failure	$E_{11}^d = E_{22}^d = E_{33}^d = E_{12}^d\ E_{23}^d = E_{31}^d = \nu_{12}^d = \nu_{23}^d = \nu_{31}^d = 0$	
Fiber-matrix shear-out	$\nu_{12}^d = 0$	

Due to the fact that the progressive damage model is solved numerically with the use of finite element software, the residual stiffness properties of the elements cannot be degraded to 0. This will lead to numerical errors, stopping the progressive damage analysis prematurely. Hence to make sure this does not happen all stiffness properties are degraded to a minimum of 1% of their initial static values.

D.3. GRADUAL DEGRADATION

In the situation where the failure criteria described by the immediate degradation scheme, do not indicate failure, the material properties are still degraded due to the cyclic load that is applied. The speed with which the material properties degrade is investigated both experimentally and mathematically. The benefit of the experimental approach is that it gives an accurate picture of the degradation of the material properties throughout its life. However these experiments are setup for a specific material under a known stress ratio and material orientations in certain manufacturing conditions. This makes them inapplicable for other materials, stress ratio's and orientations. The mathematical model uses limited amounts of experimental data to describe in a more generalized manner, material property degradation as a function of the amount of applied cycles, applied stress and stress ratio [10]. A more generalized approach of these gradual material property degradation schemes, leads to less accurate but they are more widely applicable. Mathematical models have been put forth by many authors, almost all of them need experimentally determined parameters to fit the degradation curves correctly. The more parameters the better the fit will be to experimental data, however also more tests are required to get their values and it will be less generally applicable. A mathematical model has been introduced by Shokrieh and Lessard [10], this has been used by many

researchers in past and present as a basis for the material degradation model.

Using these type of gradual degradation models takes away from the pure physics based damage mechanics and makes the analysis a more statistical approach. This can lead to models that work well for the laminates it has been fit for but it will most likely give a wrong fatigue lifetime for other laminates.

D.3.1. MODEL 1

A gradual degradation model has been introduced by Shokrieh and Lessard [10]. This has been used by many researchers in past and present as a basis for the material degradation model. The general form of the gradual degradation model of the stiffness is given in equation D.2 and the strength degradation model is given in equation D.3.

$$E_R = \left[1 - \left(\frac{log(n) - log(0.25)}{log(N_f) - log(0.25)}\right)^{\lambda}\right]^{\frac{1}{\gamma}} \left(E_s - \frac{\sigma_{max}}{\epsilon_f}\right) + \frac{\sigma_{max}}{\epsilon_f} \tag{D.2}$$

$$S_R = \left[1 - \left(\frac{log(n) - log(0.25)}{log(N_f) - log(0.25)}\right)^{\beta}\right]^{\frac{1}{\alpha}} (S_s - \sigma_{max}) + \sigma_{max} \tag{D.3}$$

Here E_R is the residual stiffness, E_S is the initial stiffness, S_R is the residual strength, S_S is the initial strength. σ_{max} is the applied maximum stress, ϵ_f is the average strain to failure, n and N_f are the amount of cycles applied and the cycles to failure respectively. Furthermore, λ, γ, α and β are the experimental curve fitting parameters.

D.3.2. MODEL 2

A more simplified version of the stiffness and strength degradation are given in equations D.4 and D.5.

$$E_R = \left(1 - \frac{n}{N_f}\right)\left(E_s - \frac{\sigma}{\epsilon_f}\right) + \frac{\sigma}{\epsilon_f} \tag{D.4}$$

$$S_R = \left(1 - \frac{n}{N_f}\right)(S_s - \sigma_{max}) + \sigma_{max} \tag{D.5}$$

D.3.3. CHANGES MADE TO GRADUAL DEGRADATION MODELS

In simulation, since the stresses and strengths of the elements are changing cycle-by-cycle due to the redistribution of the stress within the laminates and the degradation of the material's properties, each element was subjected a variable-amplitude cyclic loading process. However, the stiffness/strength degradation rule applied in the simulation was obtained under constant-amplitude cyclic loading in the experiment. This problem is solved below in 2 different ways.

First, the amount of cycles applied at a certain stress level can be divided by the expected fatigue lifetime of the ply at that stress level to determine the fatigue life fraction. The expected fatigue lifetime is then added to the life fraction of the ply from previous cycles and stress levels [54]. This is also known as the Miner's theory, for which the equation is displayed below.

$$\frac{n}{N} = \sum_{i=1}^{j} \frac{n_i}{N_i} \tag{D.6}$$

In the equation above, ni is the stepping number at ith simulation (stepping strategy was adopted to save the computing time). Ni is the fatigue life under constant-amplitude loading at condition of ith cycle. This equation is altered slightly to better fit the gradual degradation model proposed by Shokrieh and Lessard to equation D.7.

$$\frac{log(n) - log(0.25)}{log(N) - log(0.25)} = \sum_{i=1}^{j} \frac{log(n_i) - log(0.25)}{log(N_i) - log(0.25)} \tag{D.7}$$

Equation D.7 can be substituted into equations D.2 and D.3 to give the total stiffness and strength degradation.

It is important to note that the Miner's rule does in general not apply to composites. At least, it does not apply all the time. The Miner's rule can be conservative or un-conservative depending on the on the order of loading because it implies that the order of loading does not matter. High loads followed by low loads would give the same fatigue life if low loads are followed by high loads. However this is not the case if one looks at the degradation curves for both stiffness and strength.

The second way to solve this is to use a cumulative damage model that introduces a damage variable that is able to track damage accumulation over the cycles. Maintaining continuity even if the stress levels change cycle to cycle. The damage accumulated in a cycle is accounted for as well as the already sustained damage from previous cycles. Figure D.3 provides a schematic of the cumulative damage approach. The curves represent the residual strength degradation as a function of the number of cycles for different constant amplitude fatigue loading stress levels. Where $\sigma_{applied1} > \sigma_{applied2} > \sigma_{applied3}$. When the amount of cycles reach the maximum fatigue cycles of that stress level, the plies fail because the applied stress level equals the residual strength. Connecting these endpoints together gives the S-N curve. In the cumulative damage approach, the amount of damage between fatigue cycles is maintained when there is a stress level change. First, at $\sigma_{applied1}$ n_1 cycles are applied leading to a damage D_1. When the stress level changes to $\sigma_{applied2}$ the damage at the start of this new loading block must be equal to D_1. Using equation D.12 one can now calculate the amount of cycles that need to be applied at $\sigma_{applied2}$ to match this damage quantity. This amount of cycles is called the equivalent number of cycles n_{2s} and should be added to the cycles applied at $\sigma_{applied2}$ to acquire the damage at the end of this loading block.

The damage can be defined as the reduction in material strength with respect to the initial static strength. The damage variable is given in equation D.10. In the case of the model from Shokrieh and Lessard, the damage variable can be given by equation D.12 and in case of the linear degradation model the damage variable can be given as D.14.

$$\frac{S_R - \sigma_{max}}{S_s - \sigma_{max}} = \left[1 - \left(\frac{log(n) - log(0.25)}{log(N_f) - log(0.25)}\right)^{\beta}\right]^{\frac{1}{\alpha}} \tag{D.8}$$

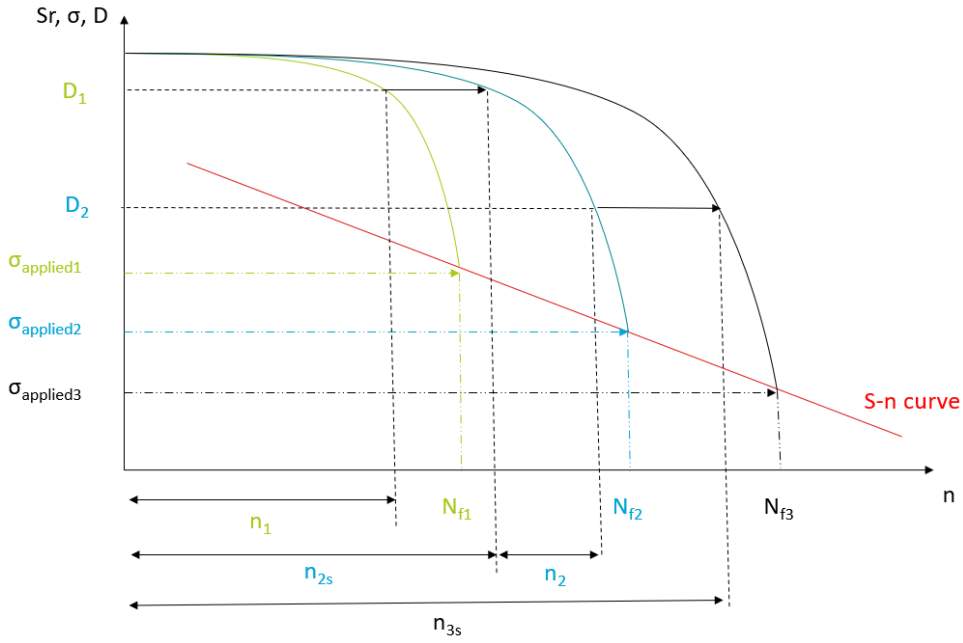

Figure D.3: Schematic showing the cumulative damage approach

$$\frac{E_R - \frac{\sigma_{max}}{\epsilon_f}}{E_s - \frac{\sigma_{max}}{\epsilon_f}} = \left[1 - \left(\frac{log(n) - log(0.25)}{log(N_f) - log(0.25)}\right)^{\lambda}\right]^{\frac{1}{\gamma}} \tag{D.9}$$

$$D_s = 1 - \frac{S_R - \sigma_{max}}{S_s - \sigma_{max}} \tag{D.10}$$

$$D_e = 1 - \frac{E_R - \frac{\sigma_{max}}{\epsilon_f}}{E_s - \frac{\sigma_{max}}{\epsilon_f}} \tag{D.11}$$

$$D_s = 1 - \left(1 - \left(\frac{log(4n)}{log(4N_f)}\right)^{\beta}\right)^{\frac{1}{\alpha}} \tag{D.12}$$

$$D_e = 1 - \left(1 - \left(\frac{log(4n)}{log(4N_f)}\right)^{\lambda}\right)^{\frac{1}{\gamma}} \tag{D.13}$$

$$D = 1 - \left(1 - \frac{n}{N_f}\right) \tag{D.14}$$

These equations state that the damage is a starting from 0 when the residual strength is equal to the static strength before the load is applied and the damage is equal to 1 when the residual strength is equal to the applied stress. Furthermore the stiffness degrades

from static stiffness at D = 0 to the failure stiffness at D = 1. The failure stiffness is given as a ratio between the maximum applied stress σ_{max} and the ultimate failure strain ϵ_f. The equations D.15 and D.15 show that the damage variable at the beginning of one loading block $i2s$ is equal to the damage caused over the previous loading block $i1$. Which can be rewritten to find the amount of cycles n^{i2s} that need to be added to the next loading block $i2$ to get to the accumulated damage level at the start of that loading block, see equation D.17. Substituting equation D.17 into equations D.2 and D.3 results in equations D.19 and D.18. These equations give the loss of stiffness and strength respectively for loading block $i2$.

$$D_s^{i2s} = D_s^{i1} = \frac{log(4n^{i2s})}{log(4N_f^{i2s})} = \frac{log(4n^{i1})}{log(4N_f^{i1})} \tag{D.15}$$

$$D_e^{i2s} = D_e^{i1} = \frac{log(4n^{i2s})}{log(4N_f^{i2s})} = \frac{log(4n^{i1})}{log(4N_f^{i1})} \tag{D.16}$$

$$n^{i2s} = 0.25e^{\left(\frac{log(4n^{i1})}{log(4N_f^{i1})} * log(4N_f^{i2s})\right)} \tag{D.17}$$

$$S_R^{i2} = \left[1 - \left(\frac{log(n^{i2} + n^{i2s}) - log(0.25)}{log(N_f^{i2}) - log(0.25)}\right)^{\beta}\right]^{\frac{1}{\alpha}} \left(S_s - \sigma_{max}^{i2}\right) + \sigma_{max}^{i2} \tag{D.18}$$

$$E_R^{i2} = \left[1 - \left(\frac{log(n^{i2} + n^{i2s}) - log(0.25)}{log(N_f^{i2}) - log(0.25)}\right)^{\lambda}\right]^{\frac{1}{\gamma}} \left(E_s - \frac{\sigma_{max}^{i2}}{\epsilon_f}\right) + \frac{\sigma_{max}^{i2}}{\epsilon_f} \tag{D.19}$$

The smaller the step size of the constant amplitude loading blocks n^{i2} are chosen the more accurate the results will become, because it will update the material properties and thus the applied stresses more frequently. However the time it takes to solve the equation will also increase.

It is important to note that this cumulative damage approach is used to make sure that the model is consistent and the material degradation models are used in the way that they are intended to be used. Also, the material degradation models are not based on a micro-mechanics model that monitor the increase in crack and or delamination length. Thus the progressive damage model needs a cumulative damage approach otherwise all of the information would be lost. However, the model has no physiological bases in fatigue modelling and should therefore be used with this in mind.